



ulm university universität
uulm

**Compensatory T-type calcium channel activity alters the dopamine
D2-autoreceptor response of dopaminergic substantia nigra neurons
from juvenile Cav1.3 KO mice**

Dissertation zur Erlangung des Doktorgrades Dr. rer. nat.
der Fakultät für Naturwissenschaften der Universität Ulm

vorgelegt von
Christina Pötschke (M. Sc.)

aus Bautzen

Ulm 2014

Die vorliegende Arbeit wurde im Institut für Angewandte Physiologie der Universität Ulm durchgeführt (Betreuer: Prof. Dr. Birgit Liss, Institutsleiter).

Amtierender Dekan: Prof. Dr. Joachim Ankerhold

Erstgutachter: Prof. Dr. Günter Ehret

Zweitgutachter: Prof. Dr. Birgit Liss

Tag der Promotionsprüfung: 08.07.2014

CONTENTS

CONTENTS	II
LIST OF ABBREVIATIONS	V
LIST OF FIGURES	VII
LIST OF TABLES	IX
LIST OF SUPPLEMENTAL TABLES	IX
1 INTRODUCTION	1
1.1 The dopaminergic midbrain system.....	1
1.2 Ion channels and receptors define distinct <i>in vitro</i> activity patterns of SN DA neurons	3
1.2.1 Dopamine D2-autoreceptors.....	4
1.2.2 Voltage-gated Nav, HCN and A-type Kv channels.....	6
1.2.3 Ligand gated SK and K _{ATP} channels	7
1.2.4 Voltage-gated T-type calcium channels	7
1.3 Cav1.3 L-type calcium channels.....	10
1.3.1 Role of Cav1.3 channels in SN DA neurons and PD	14
1.4 The aim of this work	16
2 MATERIALS AND METHODS.....	17
2.1 Materials	17
2.1.1 Animals.....	17
2.1.2 Chemicals, gases and stock solutions.....	17
2.1.3 Electrophysiology hardware, instruments, accessories and software	20
2.2 Methods.....	23
2.2.1 Preparation of solutions.....	23
2.2.2 Preparation of coronal vital brain slices.....	24
2.2.3 Patch-clamp recordings.....	25
2.2.4 Data analysis and statistics.....	27
	II

2.2.5	Genotyping	30
3	RESULTS	32
3.1	Whole-cell characterisation – basal electrophysiological parameters.....	32
3.1.1	Whole-cell comparison of SN DA neurons from juvenile WT and Cav1.3 KO mice	32
3.1.2	Whole-cell comparison of SN DA neurons from adult WT and Cav1.3 KO mice	38
3.1.3	Age-dependent differences between SN DA neurons from juvenile and adult mice	41
3.2	Pacemaker characterisation in perforated-patch patch-clamp recordings: Basal pacemaker frequency and its precision	45
3.3	Analysis of the Ca²⁺ dependent dopamine D2-autoreceptor response in SN DA neurons.....	47
3.3.1	Kinetics of D2-AR responses in SN DA neurons from WT and Cav1.3 KO mice	47
3.3.2	The D2-AR response from juvenile WT mice displays prominent dopamine-dependent desensitisation, whereas juvenile Cav1.3 KO mice display adult-like, non-desensitising D2-AR responses	48
3.3.3	Isradipine has no effect on the D2-AR response of juvenile WT or Cav1.3 KO mice	50
3.3.4	Buffering internal Ca ²⁺ with 10 mM EGTA induces WT-like, rapidly desensitising D2-AR responses in SN DA neurons from juvenile Cav1.3 KO mice	50
3.3.5	The T-type blocker Z941 induces WT-like, desensitising D2-AR responses in SN DA neurons of juvenile Cav1.3 KO mice	51
3.3.6	Adult-like, non-desensitising D2-AR responses of SN DA neurons from juvenile Cav1.3 KO mice depend on interaction of NCS-1 with D2-ARs	51
4	DISCUSSION	54
4.1	Methodical aspects and minor findings	54
4.1.1	Patch-clamp configurations: whole-cell vs. perforated-patch/on-cell recordings.....	54
4.1.2	Use of 100 μ M dopamine	54
4.1.3	Comparing of SN DA neurons from C57BL/6 vs. Cav1.3 ^{+/+} and Cav1.3 KO mice: strain differences?.....	55
4.1.4	Comparison of SN DA neurons from juvenile WT and Cav1.3 KO mice at different temperatures: full compensation at 36°C?	57
4.1.5	Capacitance difference between SN DA neurons from juvenile versus adult mice	58
4.1.6	Action potential threshold and width at threshold	59
4.1.7	Differences in sag-component and overshoot	59
4.1.8	Side effects of the functional DNIP peptide	60

4.2	Main findings: differences between SN DA neurons from juvenile and adult WT and Cav1.3 KO mice	61
4.2.1	Buffering internal Ca ²⁺ with 10 mM high EGTA disables the depolarisation block in SN DA neurons of juvenile mice	61
4.2.2	Pacemaking of SN DA neurons is extremely robust	61
4.2.3	Whole-cell data indicate that loss of Cav1.3 is differently compensated in SN DA neurons from juvenile and adult mice	62
4.2.4	The non-desensitising adult-like D2-AR response of SN DA neurons from juvenile Cav1.3 KO mice cannot be induced in the WT by acute block of LTCCs	63
4.2.5	The non-desensitising D2-AR response in SN DA neurons of juvenile Cav1.3 KO mice depends on free internal Ca ²⁺ levels	63
4.2.6	Loss of Cav1.3 is compensated by T-type calcium channels in SN DA neurons of juvenile Cav1.3 KO mice	64
4.2.7	Interaction of NCS-1 with D2-AR is necessary for the non-desensitising, adult-like D2-AR response of SN DA neurons from juvenile Cav1.3 KO mice.....	65
4.3	Outlook	65
5	SUMMARY: GENERAL KO OF Cav1.3 CAUSES COMPENSATORY T-TYPE CHANNEL ACTIVITY, WHICH ENHANCES Ca²⁺ MEDIATED NCS-1/D2-AR INTERACTION, AND THUS PREVENTION OF D2-AR DESENSITISATION IN SN DA NEURONS FROM JUVENILE Cav1.3 KO MICE	68
	LITERATURE.....	70
	APPENDIX.....	i
	Supplemental tables	i
	ACKNOWLEDGEMENT/DANKSAGUNG	xv
	STATUTORY DECLARATION	xvii
	CURRICULUM VITAE.....	xviii

LIST OF ABBREVIATIONS

ACSF	artificial cerebrospinal fluid
ADHD	attention deficit hyperactivity disorder
AHP	afterhyperpolarisation
AMPA	α -amino-3-hydroxy-5-methyl-4-isoxazolepropionic acid; the AMPA receptor is a glutamate receptor
ATP	adenosine triphosphate
bp	base pair
Ca ²⁺	calcium
Cav	voltage-gated calcium channel
CDI	calcium-dependent inhibition
CV ISI	coefficient of variation of the interspike interval
D2-AR	dopamine D2-autoreceptor
D2-R	dopamine D2-receptor
DA	dopaminergic
DHP	dihydropyridine (L-type calcium channel antagonists)
DNIP/srDNIP	D2-receptor/NCS-1 interfering peptide or its scrambled version
DNQX	6,7-dinitroquinoxaline-2,3-dione; AMPA and Kainate receptor antagonist
EGTA	ethylene glycol tetraacetic acid; a calcium chelator
GABA	γ -aminobutyric acid
GIRK	G-protein-coupled inwardly-rectifying potassium channel
GTP	guanosine triphosphate
HCN	hyperpolarisation activated cyclic nucleotide gated cation channel
HEPES	4-(2-hydroxyethyl)-1-piperazineethanesulfonic acid; a chemical buffering agent
HVA	high voltage activated
I.D.	inner diameter
I _h	HCN channel current
K _{ATP}	ATP-dependent potassium channel
KChIP	Kv channel-interacting protein
KO	knockout
K _v	voltage-gated potassium channel
LTCC	L-type calcium channel
LVA	low voltage activated
Nav	voltage-gated sodium channel
NCS-1	neuronal calcium sensor 1
O.D.	outer diameter

LIST OF ABBREVIATIONS

PBS	phosphate buffered saline
PCR	polymerase chain reaction
PD	Parkinson's disease
PFA	paraformaldehyde
PN	(here) post-natal (day)
RNA	ribonucleic acid; mRNA: messenger ribonucleic acid
RRF	retrotranslational field
R_s	series resistance
RyR	ryanodine receptor
SANDD	synatrial node dysfunction and deafness (syndrome)
SEM	standard error of the mean
SK	apamine-sensitive small conductance potassium channel
SN	substantia nigra
SOP	slow oscillatory potential
SUR	sulfonylurea receptor; SUR1 is a K_{ATP} subunit
TH	tyrosine hydroxylase, a marker gene for dopaminergic neurons
TK	thymidine kinase
TRP	transient receptor potential channel
ttx	tetrodotoxin
V_{max}	peak voltage
VTA	ventral tegmental area
WT	wildtype
Z941	T-type calcium channel blocker
ZD7288	HCN channel blocker

LIST OF FIGURES

Figure 1-1: Projections of dopaminergic midbrain neurons	2
Figure 1-2: Ion channels and receptors important for this work, and their role for SN DA neuron activity.....	4
Figure 1-3: Schematic build of LTCCs and schematic of Cav1.3 splice variants	11
Figure 2-1: Vibratomes for preparing acute brain slices	25
Figure 2-2: Electrophysiological recording setup.....	26
Figure 2-3: Analysis of action potential parameters and sag-component of SN DA neurons.....	29
Figure 3-1: Sample traces of spontaneous activity from whole-cell recordings of SN DA neurons from juvenile mice.....	33
Figure 3-2: The HCN channel blocker ZD7288 dramatically changes the proportion of active/inactive SN DA neurons of juvenile WT and Cav1.3 KO mice.....	34
Figure 3-3: Afterhyperpolarisation and threshold of action potentials from SN DA neurons of juvenile WT and Cav1.3 KO mice	36
Figure 3-4: Input resistance and maximal inducible frequency of SN DA neurons from juvenile WT and Cav1.3 KO mice.....	37
Figure 3-5: Sample traces of spontaneous activity from whole-cell recordings of SN DA neurons from adult mice	38
Figure 3-6: Block of HCN channels dramatically affects pacemaker activity of SN DA neurons from both adult WT and Cav1.3 KO mice; LTCC block affects Cav1.3 KO	39
Figure 3-7: AHP and threshold of action potentials of SN DA neurons from adult WT and Cav1.3 KO mice.....	40
Figure 3-8: Input resistance and maximal frequency of SN DA neurons from adult WT and Cav1.3 KO mice.....	41
Figure 3-9: The pacemaker of SN DA neurons from adult mice is less stable compared to juvenile mice and depends particularly on HCN channel activity.....	42
Figure 3-10: The afterhyperpolarisation and action potential width of SN DA neurons from juvenile and adult mice under control conditions and in isradipine	44
Figure 3-11: pacemaker frequency and its precision (CV ISI) of SN DA neurons from SN DA neurons of WT and Cav1.3 KO mice.....	46

LIST OF FIGURES

Figure 3-12: Sample traces of SN DA neurons from juvenile and adult WT and Cav1.3 KO mice show prominent desensitisation of D2-AR in juvenile WT mice, that is absent in adult mice, as well as juvenile Cav1.3 KO	47
Figure 3-13: Non-desensitising D2-AR responses in SN DA neurons from juvenile Cav1.3 KO mice depend on T-type calcium channel function	48
Figure 3-14: The D2-autoreceptor response from juvenile WT mice shows prominent receptor desensitisation, whereas juvenile Cav1.3 KO mimics those from adult mice	49
Figure 3-15: Non-desensitising D2-AR responses in SN DA neurons from juvenile Cav1.3 KO mice depend on internal Ca ²⁺ , T-type calcium channels, and calcium-dependent NCS-1/D2-AR interaction	52
Figure 4-1: Comparison of D2-AR, basal frequency and CV ISI of SN DA neurons from juvenile Cav1.3 ^{+/+} and C57BL/6 mice	56
Figure 4-2: Comparison of D2-AR, basal frequency and CV ISI of SN DA neurons from WT and Cav1.3 KO mice under control conditions and at 36°C.....	58

LIST OF TABLES

LIST OF TABLES

Table 1-1: Biophysical properties of Cav1.3 $\alpha 1$ splice variants.....	13
Table 2-1: Overview over used chemicals and gases	19
Table 2-2: Overview over used stock solutions	20
Table 2-3: Comparison of the used electrophysiological recording setups and used software	21
Table 2-4: Detailed description of Puller Program P10	22

LIST OF SUPPLEMENTAL TABLES

Supplemental Table 1: Spontaneous activity overview of all analysed neurons for basal electrophysiological characterisation	i
Supplemental Table 2: Overview over data from juvenile and adult C57BL/6, Cav1.3 ^{+/+} and Cav1.3 KO mice	v
Supplemental Table 3: Comparison matrixes for parameters from whole-cell recordings...	xii
Supplemental Table 4: Comparison matrixes for parameters from 40 minute recordings...	xiv

1 INTRODUCTION

1.1 The dopaminergic midbrain system

Various complex neurological processes, like motor function, cognition and emotion are dependent on the dopaminergic midbrain system. Best known is probably the contribution of the dopaminergic system to voluntary movement (Obeso and Lanciego, 2011), but it is also important for associative learning (updates to the working memory, (D'Ardenne et al., 2012)) and reinforcement learning (Maia and Frank, 2011). Furthermore, emotion, concentration, attention and goal-directed behaviour, as well as reward and motivation (Gerfen and Surmeier, 2011; Grace et al., 2007; Schultz, 2010) and therefore probabilistic decision making (Chowdhury et al., 2013), are not properly working either without the dopaminergic midbrain system. And the gooseflesh sometimes experienced while listening to a piece of music is also mediated by the dopaminergic midbrain system since it is involved in the anticipation and experience of peak-emotion while listening to music (Salimpoor et al., 2011). With the dopaminergic midbrain's system involvement in such varying processes, it is not surprising that disturbances of it play a critical role in a diversity of disorders, such as Parkinson's disease (PD), schizophrenia, attention deficit hyperactivity disorders (ADHD) or drug abuse (Abi-Dargham et al., 2010; Arnsten and Pliszka, 2011; Everitt et al., 2010; Grace, 2012; Maia and Frank, 2011).

The somata of most dopaminergic (DA) midbrain neurons are arranged in three nuclei: the substantia nigra pars compacta (SN, A9), the ventral tegmental area (VTA, A10) and the retrorubral field (RRF, A8) (Bjorklund and Dunnett, 2007).

The phenotypically well-described dopaminergic neurons of the SN (SN DA), which are the focus of this work, form the so-called mesostriatal axonal projection to the striatum. They are defined by electrophysiological hallmark features such as a low action potential frequency (2-6 Hz), a low maximal inducible firing frequency (~10 Hz) and a small or non-existent rebound spike delay after hyperpolarisations (Ford and Williams, 2008; Lammel et al., 2008). They also display a pronounced sag-component in response to hyperpolarisation through the opening of slowly activating, hyperpolarisation activated cyclic nucleotide gated cation (HCN) channels, which causes a depolarising "sag" of the membrane in response to hyperpolarisation (Ford and Williams, 2008; Lammel et al., 2008). SN DA neurons also show a dopamine D2-autoreceptor (D2-AR) mediated autoinhibition of their activity in

response to dopamine (see 1.2.1 for more details on the D2-AR response). SN DA neurons are a part of the motoric basal ganglia circuit and essential for voluntary movement (Obeso and Lanciego, 2011). The loss of these mesostrially projecting SN DA neurons in the course of PD in particular causes the typical movement related symptoms (akinesia, rigor, resting tremor and postural instability) that are observed in the patients (Hindle, 2010).

Axons of VTA DA neurons form the mesolimbic projection, e.g. to the ventral striatum and the basolateral amygdala (Lammel et al., 2008) and belong to the brain's motivation and reward system (Salomone, 2010; Tobler, 2010). Another projection of VTA DA neurons is the mesocortical one, targeting areas in the neocortex (mainly the prefrontal and cingulate cortex), which plays a role in the working memory and cognition (Schultz, 1998, 2002; Surmeier, 2007b).

The DA neurons of the RRF haven't been studied as extensively as VTA DA or SN DA neurons. They have projections to the striatum, are thought to be important for orofacial movement, and their loss might contribute to the stiff facial expression of PD patients (Mai and Paxinos, 2011). Neurons from the RRF also form connections to VTA and SN DA neurons and may therefore play a role in coordinating and modulating cognitive and motor functions (Mai and Paxinos, 2011).

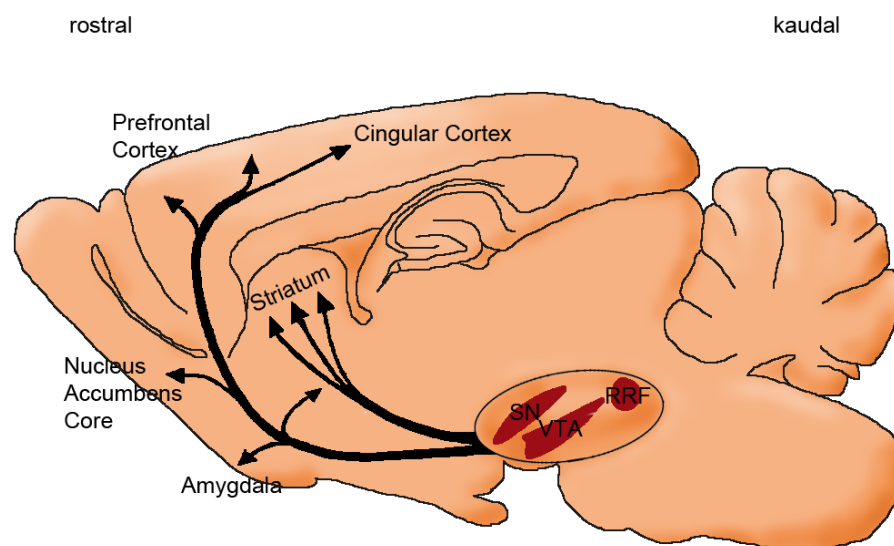


Figure 1-1: Projections of dopaminergic midbrain neurons

Schematic drawing of a rodent brain (sagittal cut). Substantia nigra (SN), ventral tegmental area (VTA) and retrorubral field are marked in red, with dopaminergic projections in black. Modified after (Bjorklund and Dunnett, 2007; Smidt and Burbach, 2007).

It is still unclear why SN DA neurons are particularly vulnerable to degeneration in PD in comparison to other neurons, including neighbouring VTA DA neurons. The cause of most (idiopathic) PD cases is still unclear as well, even though trigger factors have been identified, in particular mitochondrial and proteasomal dysfunction, as well as calcium (Ca^{2+}) overload and oxidative stress (Sulzer, 2007; Surmeier et al., 2011b; Surmeier and Schumacker, 2013).

1.2 Ion channels and receptors define distinct *in vitro* activity patterns of SN DA neurons

SN DA neurons *in vitro*, as well as *in vivo*, have distinctive activity modes, which are generated and mediated by an orchestra of ion channels (Liss and Roeper, 2010). In the following only SN DA neurons *in vitro* are considered. Most prominent (and the focus of this work) is their regular pacemaker activity: an intrinsic, spontaneous activity, independent of synaptic inputs, which is physiologically associated with tonic low-level dopamine release. SN DA neurons can also switch into a so-called burst activity, which is generally not observed under control conditions in *in vitro* brain slice preparations, but can be pharmacologically induced. Burst activity (as well as irregular firing) is predominantly observed *in vivo* and is associated with a phasic release of dopamine (Blythe et al., 2009), which is of behavioural importance, particularly concerning rewards (reward prediction error coding, (Schultz, 2007, 2010)). Frequency of bursts, as well as pacemaker activity, is modulated by various ion channels.

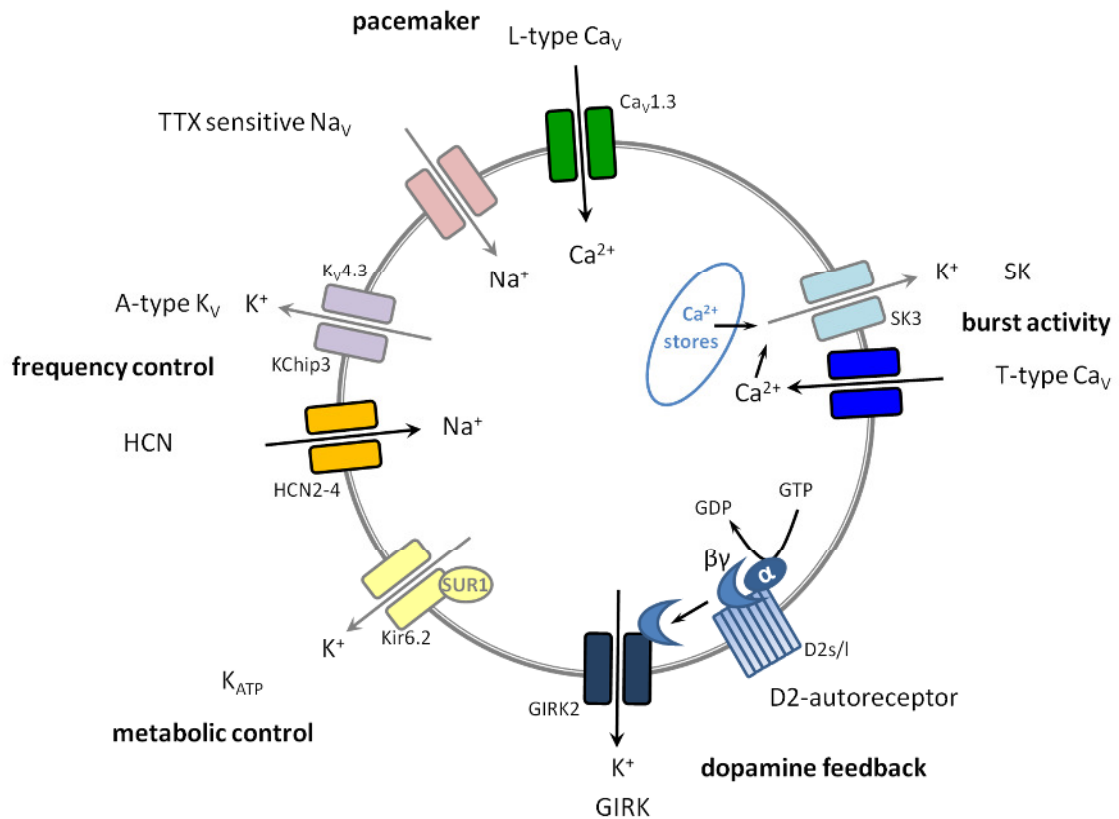


Figure 1-2: Ion channels and receptors important for this work, and their role for SN DA neuron activity

Shown are ion channels that are involved in creating or modulating different activity patterns of SN DA neurons. Tetrodotoxin-(tx)-sensitive voltage-gated sodium (Na_V) channels, voltage-gated A-type potassium (K_V) channels, hyperpolarisation activated cyclic nucleotide gated cation (HCN) channels, ATP dependent potassium (K_{ATP}) channels, the dopamine D2-autoreceptor coupled to the G-protein-coupled inwardly-rectifying potassium channel (GIRK2), small conductance potassium (SK) channels, and voltage-gated L-type and T-type calcium channels (Ca_V s). Channels/receptors in brighter colours are particularly important for this work and are described in greater detail in the text. Modified after (Liss and Roeper, 2010).

Figure 1-2 shows a cartoon with a selection of ion channels (including the dopamine D2-AR) in SN DA neurons that are important for this work. Their specific contributions to pacemaker or burst activity and thus dopamine release are described in more detail in the following paragraphs.

1.2.1 Dopamine D2-autoreceptors

Dopamine itself is released pre-synaptically, as well as somatodendritically (Beckstead et al., 2007; Ford et al., 2010) and is mediating its actions through binding to dopamine receptors. Dopamine receptors belong to the family of G-protein-coupled 7-transmembrane receptors and are subdivided, based on their excitatory or inhibitory effects, into two

families: D1-like receptors (D1 and D5, with excitatory effects) and D2-like receptors (D2, D3 and D4, with inhibitory effects) (Beaulieu and Gainetdinov, 2011). Dopamine displays a significantly higher affinity for D2-like receptors (Marcellino et al., 2012) which therefore predominantly contribute to signal transduction upon tonic release of dopamine.

Dopamine D2-autoreceptors (D2-AR) are expressed presynaptically and somatodendritically on DA midbrain neurons (Beaulieu and Gainetdinov, 2011; Ford, 2014). This work focuses only on somatodendritically D2-ARs expressed on the DA cell body, which are able to shape SN DA activity in a negative feedback loop in response to locally released dopamine within the midbrain (Ford et al., 2010).

Activation of D2-ARs in response to dopamine binding causes direct activation of the GIRK2 channel (G-protein-coupled inwardly-rectifying potassium channel, Kir3.2) via the G $\beta\gamma$ -subunit of the D2-receptor, leading to hyperpolarisation of the membrane potential and reduction or complete inhibition of pacemaker activity (Beaulieu and Gainetdinov, 2011; Luscher and Slesinger, 2010). In contrast to adult mice (Lammel et al., 2008), SN DA neurons from juvenile mice display prominent desensitisation of the D2-AR response *in vitro* (see Figure 3-13 and (Dragicevic et al., 2014)).

Besides GIRK2 activation, a variety of other D2-AR activated pathways have been described (De Mei et al., 2009). Postsynaptic D2-receptor (D2-R) desensitisation for example is mediated by the neuronal calcium sensor 1 (NCS-1) (Kabbani et al., 2002), which, as we have recently shown, is important for the D2-AR response of SN DA neurons from juvenile mice (Dragicevic et al., 2014). The additional signalling mechanisms of D2-ARs however remain poorly understood (Beaulieu and Gainetdinov, 2011).

Mouse models with mutations in PARK-genes (PARK-genes are loci identified to cause monogenic familial forms of PD when mutated (Gasser et al., 2011)) show altered D2-AR responses (Goldberg et al., 2005; Tong et al., 2009). SN DA neurons from adult DJ-1 KO mice show a rapid desensitisation of the D2-AR response (Goldberg et al., 2005), and they also display increased oxidative stress levels during pacemaker activity, caused by L-type calcium (LTCC) channel activity (Guzman et al., 2010). Together these findings suggest a possible link between LTCCs and D2-AR function.

1.2.2 Voltage-gated Nav, HCN and A-type Kv channels

Most important for the generation of the action potential itself in SN DA neurons are voltage-gated tetrodotoxin-(ttx)-sensitive sodium (Nav) channels that display rapid activation and inactivation, and are responsible for the fast rising phase of the action potential (Bean, 2007). Somatic Navs have also been implicated to mediate the susceptibility to the so-called depolarisation block of SN DA neurons that is thought to limit their maximal firing frequency; the higher the somatic density of Navs, the more delayed the depolarisation block ((Tucker et al., 2012); see also 4.2.1).

To reach that threshold where Nav channels are activated, so-called slow oscillatory potentials (SOPs) are needed. In SN DA neurons those oscillations of the membrane potential are still visible in the presence of ttx (Chan et al., 2007). One channel that might be creating those SOPs is the voltage-gated LTCC Cav1.3 ((Puopolo et al., 2007); see 1.3 for details). Another channel that has the electrophysiological features to create SOPs (and is expressed in SN DA neurons) is the HCN channel (Chan et al., 2007).

HCN channels mediate the slowly activating I_h , a non-selective cation current that contains Na^+ and K^+ ions, responsible for the sag-component in SN DA neurons. The permeability ratio of the channel is about 1:4 for these ions, but opening of HCN channels under physiological conditions produces a net sodium influx (Wahl-Schott and Biel, 2009). HCN channels are activated upon hyperpolarisation and via cyclic nucleotides, and display differences in their – very slow – gating speed depending on their subunit composition (Franz et al., 2000).

Murine SN DA neurons express the genes HCN2-4 (not HCN1, mediating faster activation kinetics; (Franz et al., 2000)). In SN DA neurons, HCN channels regulate the pacemaker frequency by modulating the interspike interval (ISI). Block of HCN channels with 30 μ M ZD7288 was shown to reduce frequency of SN DA neurons of juvenile C57BL/6 by about 40 % (Neuhoff et al., 2002).

Negative pacemaker frequency control of SN DA neurons is mediated by A-type potassium channels (Kv4.3 with KChIP3 β -subunits (Liss et al., 2001)), also by modulating the ISI. The more functional A-type potassium channels the slower is the frequency; a complete block of the channel causes an about 2.7 increase in pacemaker frequency (Liss et al., 2001; Liss and Roeper, 2010).

1.2.3 Ligand gated SK and K_{ATP} channels

Apamine-sensitive small conductance potassium (SK) channels belong to the group of calcium-dependent/calcium-activated potassium channels. Mostly expressed in SN DA neurons is SK3 (Wolfart et al., 2001) in the soma, and to a lesser extent in the dendritic arbour. SK2 is expressed in distal dendrites in SN DA neurons from juvenile mice (Deignan et al., 2012). SK channel activity in SN DA neurons is preferentially coupled to the trigger Ca²⁺ influx through T-type calcium channels (see chapter 1.2.4; (Wolfart et al., 2001; Wolfart and Roeper, 2002)). Through controlling the medium (speed) afterhyperpolarisation ([m]AHP) of the action potential, these channels also play an important role in regulating the precision of the pacemaker. Inhibition of SK channels can cause SN DA neurons to switch from pacemaker to burst firing in *in vitro* brain slice preparations (Wolfart et al., 2001). It has been demonstrated that block of SK2 influences only the precision of pacemaking (timing of action potentials), while block of SK3 additionally decreases action potential frequency (Deignan et al., 2012).

ATP-dependent potassium channels (K_{ATP}) contain Kir6.2 as poreforming and SUR1 as regulating subunit. These channels are metabolic sensors that integrate a variety of metabolic signals into their open-probability (Ashcroft and Rorsman, 2013; Liss and Roeper, 2010). *In vitro*, activation of K_{ATP} channels in response to metabolic stress (like PD-trigger factors) can lead to complete silencing of murine SN DA neurons (Liss et al., 2005). *In vivo* K_{ATP} channel activity in medial SN DA neurons is essential for triggering their burst activity, and for the related behaviour, like exploration of novel environments (Schiemann et al., 2012).

A prominent role of K_{ATP}-channels, as well as LTCCs, has already been described for the particularly high vulnerability of SN DA neurons to degeneration in PD and its chronic rodent models, as detailed for LTCCs in chapter 1.3.1 (Chan et al., 2007; Guzman et al., 2010; Ilijic et al., 2011; Liss et al., 2005; Sulzer and Surmeier, 2013; Surmeier et al., 2011b).

1.2.4 Voltage-gated T-type calcium channels

T-type calcium channels belong to the group of low voltage activated (LVA) ion channels – in contrast to LTCCs which are high voltage activated (HVA) ion channels (see 1.3) – and are expressed in many tissues of the body (Perez-Reyes, 2003). The T in their name stands for “transient”, since after their activation they generate a transient Ca²⁺ inward current that is fully inactivated after a few tens of milliseconds (Cueni et al., 2009).

In neuronal cell types the highest density of T-type calcium channels is often found in dendrites and spines, for instance in thalamocortical and nucleus reticularis thalami neurons or medium spiny neurons of the striatum (Lambert et al., 2013). The first role that had been determined for these channels was the creation of the so-called “low threshold spike”. The “low threshold spike” is created when a low depolarisation of the membrane potential activates the T-type channels which, if their density is high enough, will eventually lead to a positive shift in the membrane potential to approximately -40 mV, which in turn will activate sodium channels so that high frequency action potentials will occur on the crest of this depolarisation (Cain and Snutch, 2010). Their localisation in dendrites and their low threshold of activation also make them suitable to boost excitatory signals.

But T-type channels also play a role in tonic firing, as it has been shown that they co-localise with Na⁺ channels in the axon initial segment of for example cochlear nucleus interneurons or cerebellar Purkinje cells. Interestingly only T-type channels in the axon initial segments are sensitive to dopamine, since they are under control of D1 receptors that, via protein kinase C, downregulate T-type currents, whereas somatodendritic T-type channels are not affected (Cueni et al., 2009).

Three genes code for the pore-forming α_1 -subunits of T-type calcium channels (in human and mouse genome): CACNA1G (on human chromosome 17q22), CACNA1H (on human chromosome 16p13) and CACNA1I (on human chromosome 22q13), coding for Cav3.1, Cav3.2 and Cav3.3 respectively. These three genes are comparatively large, ranging from 70–130 kb and contain 35–38 exons, which can be alternatively spliced; alternative splicing for instance has been described of exons 14, 25/26, 34, 35 and 38 for CACNA1G (Perez-Reyes, 2006). 12 missense SNPs of CACNA1H have also been implicated in epilepsy, as T-type channels play important roles in neurological rhythmogenesis (Cueni et al., 2009; Perez-Reyes, 2006).

The α_1 -subunit is comprised of four homologous domains I–IV which are connected via linkers of different length, with each domain consisting of six transmembrane regions S1–S6, S4 being the voltage sensor necessary for gating. It is not yet clear whether these channels use the same auxiliary subunits as HVA channels or have specific subunits of their own or any additional subunits at all (Zhang et al., 2013) – experiments indicate that, if they have specific subunits, they might not have a big impact on channel function (Perez-Reyes, 2006). γ_6 has been suggested to inhibit T-type channels (Buraei and Yang, 2010).

Pharmacologically it was difficult to suitably study T-type currents for a long time, since the often used Ni^{2+} ion concentrations that block T-type currents also have effects on the other calcium channels, while the other often used drug, mibefradil, not only additionally inhibited HVA calcium channels, but also sodium currents and K_V and K_{ATP} channels (Cueni et al., 2009; Eller et al., 2000; Nilius et al., 2006). Many neuroleptics are potent T-type channel blockers preferentially binding to the inactivated channel, but their primary targets are D2-receptors which makes them rather unsuited to studying T-type currents when D2-receptors are expressed. The diphenylbutylpiperidines pimozide and penfluridol are high affinity T-type calcium channel blockers, the butyrophenone haloperidol also blocks T-type channels but with less affinity than pimozide and penfluridol, and the diphenylpiperazine derivative flunarizine preferentially blocks α_{1G} and α_{1I} compared to α_{1H} (Santi et al., 2002).

Only recently highly selective T-type channel blockers have been developed, piperidine derivatives like TTA-P2 (Shipe et al., 2008) and piperazine-based derivatives like Z941 and Z944, with Z944 even progressing into a phase 1 human study against absence epilepsy seizures (Tringham et al., 2012).

Electrophysiologically, T-type channels activate in the subthreshold range, on average around -60 mV in isolated neurons (with $\text{Cav}3.3$ opening and closing at about 10 mV more depolarized potentials compared to $\text{Cav}3.2$ and $\text{Cav}3.1$ (Cain and Snutch, 2010), the average threshold in slices is around -70 mV) and their current peaks at -45 mV (in slices around -30 mV). The different values obtained in slices might be due to troubles with voltage clamping neurons in slices, where additionally T-type currents are generally much larger compared to cell culture due to the localisation of T-type channels in dendrites (Lambert et al., 2013; Ng et al., 1996). $\text{Cav}3.1$ and $\text{Cav}3.2$ have faster activation and inactivation kinetics than $\text{Cav}3.3$, whereas $\text{Cav}3.3$ displays the fastest deactivation kinetics (Cain and Snutch, 2010).

In contrast to LTCCs, increases in temperature did not have effects on the voltage dependence of T-type channels, but instead on the current amplitudes and activation/inactivation speed (bigger and more accelerated the higher the temperature, even though the effect is non-linear; (Ng et al., 1996)). Small changes in external pH however were shown to affect voltage dependence, with a change in pH from 7.3 to 6.9 adding 3 mV to the activation and inactivation threshold, and similarly changes from pH 7.3 to 7.7 having the opposite effect (Ng et al., 1996).

The exact molecular composition of T-type channels in SN DA neurons is not known. In adult rat brains in the SN only Cav3.1 and Cav3.2 were expressed at low levels, Cav3.3 expression was below the detection threshold (Talley et al., 1999). In the murine brain only Cav3.1 was found to be expressed moderately to low in the SN while the other channels could not be detected (CACNA1G expression: experiment 71587822; CACNA1H expression: experiment 72119638; CACNA1I expression: experiment 74512007; allen brain atlas: www.mouse.brain-map.org). However, our own preliminary experiments on single-cell SN DA neurons from juvenile mice indicate that mRNA of all α_1 -subunits is expressed.

Not much is known about T-type calcium channels in SN DA neurons of juvenile mice – except for their selective coupling to SK channels and thus their control of pacemaker precision and burst activity ((Wolfart and Roeper, 2002), see 1.2.3). In 6–12 day old rats, T-type calcium channels are coupled to calcium-activated ryanodine receptors (RyR) that in turn will activate SK channels (Cui et al., 2004).

It was found in neuronal cell cultures of DA neurons from rat embryos that the observed neuroprotective effect of nicotine in PD is indirectly mediated by T-type calcium channels ((Toulorge et al., 2011); note that the T-type blocker used in this study was flunarizine which affects D2-receptors (Brucke et al., 1995)).

1.3 Cav1.3 L-type calcium channels

L-type calcium channels are voltage-gated ion channels (Cav), belonging to the group of HVA channels, and are expressed ubiquitously in most tissues of the body (Catterall et al., 2005). The L in the name stands for “long lasting”.

Four genes code for the pore-forming α_1 -subunits of L-type calcium channels (in human and mouse genome): CACNA1S, CACNA1C, CACNA1D and CACNA1F, coding for Cav1.1, Cav1.2, Cav1.3 and Cav1.4 respectively. Deletion of CACNA1C leads to death at day 14.5 during embryonic development in mice, whereas the deletion of CACNA1D has no dramatic effects on embryonic development (Xu et al., 2003). In the brain, only Cav1.2 and Cav1.3 are expressed (Catterall et al., 2005). The α_1 -subunit of LTCCs, which holds most of the target sites for pharmacological substances, toxins and second messengers, is comprised of four homologous domains I–IV connected via linkers of different length. Each domain has six transmembrane regions S1–S6, of which S4 is the voltage sensor necessary for gating. Auxiliary regulatory β -, $\alpha_2\delta$ - and possibly γ -subunits complete the channel (Catterall et al., 2005; Chen et al., 2007; Dolphin, 2006) but are not necessary for functional

INTRODUCTION

channel formation (Catterall et al., 2005). Alternative splicing of the α_1 -subunit creates an even bigger variety in the biophysical properties of the expressed channels. For instance the human CACNA1C gene contains 50/55 exons of which 19/20 can be alternatively spliced (Abernethy and Soldatov, 2002; Cheng et al., 2007; Liao et al., 2005; Soldatov, 1994; Tang et al., 2004). Different publications describe different numbers; ensembl lists only five variants with maximal 45 exons for the murine CACNA1C (ENSMUSG00000051331 on 10.02.2014).

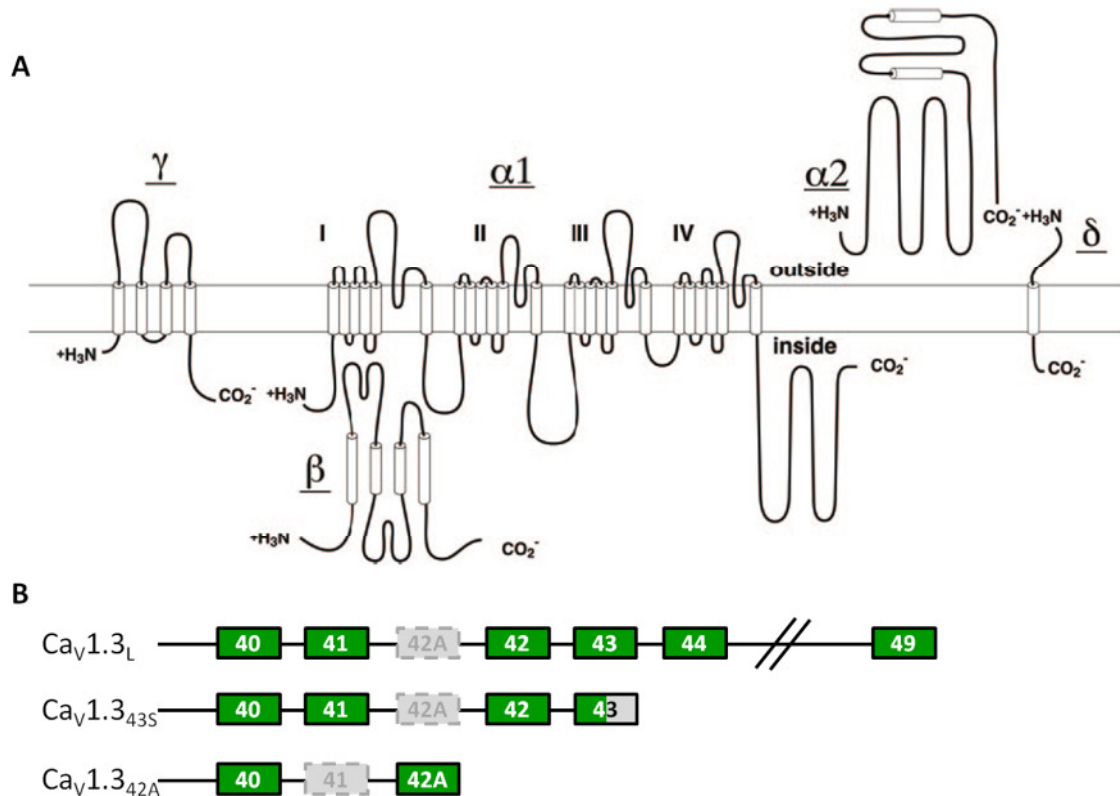


Figure 1-3: Schematic build of LTCCs and schematic of $\text{Cav}1.3$ splice variants

A: Schematic drawing of the general build of LTCCs. Shown are the α_1 -subunit with auxiliary β -, $\alpha_2\delta$ - and γ - subunits. Graphic from (Catterall et al., 2005). **B:** Scheme of the three best analysed C-terminal $\text{Cav}1.3$ splice variants, found both in humans and mice. $\text{Cav}1.3_L$ is the full length channel; $\text{Cav}1.3_{43S}$ stops with a shortened exon 43 and $\text{Cav}1.3_{42A}$ is the shortest splice variant, which stops in the alternate exon 42A. Graphic modified after (Bock et al., 2011). Expressed exons in green, spliced exons in grey.

Cav1.3 channels can be alternatively spliced in humans, with many of the splice variants also found in mice and other species (Baig et al., 2011; Koschak et al., 2001; Singh et al., 2008).

For mice two N-terminal splice variants of $\text{Cav}1.3$ have been described ($\text{Cav}1.3a$ and $\text{Cav}1.3b$ (Klugbauer et al., 2002; Xu et al., 2003)) as well as several C-terminal splice variants (Singh et al., 2008). Functional differences between the two N-terminal variants

include current density, inactivation and sensitivity to the calcium channel blocker nisoldipine (Xu et al., 2003).

C-terminal splicing occurs tissue specific and also affects gating properties (Lieb et al., 2012). For instance one C-terminal splice variant with alternative splicing in exon 41 (it might be caused by different labelling of exons, but this variant does not seem to correspond exactly with any of the splice-variants shown in see Figure 1-3; it might be Cav1.3_{43S}, since it has been described to have almost no CDI) seems to be only expressed in the inner ear and pancreatic islets (Ihara et al., 1995; Shen et al., 2006).

There are three well characterised splice variants that are expressed in the murine brain (also in humans). Alternatively spliced in these variants are exons 42 and 43. A long C-terminal splice variant of the channel is Cav1.3_L (also named Cav1.3₄₂ or Cav1.3_{8A}), whose mRNA is expressed at higher levels compared to the short variant Cav1.3_{42A} in the mouse brain (Singh et al., 2008). Cav1.3_{42A} seems to be more abundantly expressed in the SN and the VTA compared to other brain regions (Bock et al., 2011). An intermediate variant is Cav1.3_{43S} which is abundantly expressed in the brain but not in the heart (Bock et al., 2011).

These three splice variants show differences in voltage dependence and calcium-dependent inactivation (CDI), e.g. voltage dependence of Cav1.3_{42A} is shifted towards more hyperpolarising potentials (Singh et al., 2008) and the CDI is more pronounced. In contrast Cav1.3_{43S} has a less pronounced CDI (Bock et al., 2011). Striessnig et al. also reported two additional C-terminal splice variants that have not been further characterised yet (Bock et al., 2011). Additionally it was found that CDI can be influenced through RNA editing, independently of the splice variants (Huang et al., 2012).

Electrophysiologically Cav1.3 channels (rat neuronal clones) heterologously expressed in tsA201 cells have a half maximal activation in the subthreshold range at approximately -40 mV; in comparison Cav1.2, in the same expression system, had a half maximal activation at around -16 mV with 2 mM Ca²⁺ as charge carrier. The activation threshold for Cav1.3 and Cav1.2 under these conditions was between -60/-70 mV and -50/-40 mV respectively (Helton et al., 2005; Lipscombe et al., 2004). Relatively similar results for activation threshold and half maximal activation for Cav1.3 were obtained with 1.3 mM Ca²⁺ as charge carrier in isolated inner cochlear hair cells of 3 day old mice (Platzer et al., 2000). Human clones of Cav1.3 and Cav1.2 channels, heterologously expressed in

INTRODUCTION

tsA201 cells together with $\text{Cav}\beta_3$ and $\alpha_2\delta_1$ -subunits, recorded with 15 mM Ba^{2+} as charge carrier, had activation thresholds around -45 mV and -31 mV respectively (Koschak et al., 2001; Striessnig and Koschak, 2008).

The aforementioned different C-terminal splice variants also differ significantly in their biophysical properties (Bock et al., 2011), see Table 1-1.

channel	half maximal activation [mV]	Vmax [mV]	activation threshold [mV]
$\text{Cav}1.3_L$	-2.4 \pm 0.6	12.6 \pm 0.5	-32.6 \pm 0.3
$\text{Cav}1.3_{43S}$	-13.0 \pm 0.7	1.7 \pm 0.8	-35.5 \pm 0.6
$\text{Cav}1.3_{42A}$	-12.1 \pm 1.6	0.6 \pm 3.5	-32.0 \pm 1.0

Table 1-1: Biophysical properties of $\text{Cav}1.3$ α_1 splice variants

Shown are the different values for half maximal activation, peak voltage (Vmax) and activation threshold of three different $\text{Cav}1.3$ α_1 splice variants, heterologously expressed in tsA201 cells with 15 mM Ca^{2+} as charge carrier. Data taken from (Bock et al., 2011).

Additionally, Peloquin et al. showed that the gating of $\text{Cav}1.4$ and $\text{Cav}1.2$ is strongly temperature dependent, with lower activation threshold the higher the temperature (Peloquin et al., 2008). It is therefore not unlikely, due to the similarities in structure and sequence (Catterall et al., 2005), that this might also be the case for $\text{Cav}1.3$. This idea is being supported by recordings in gerbil inner cochlear hair cells that showed a significantly reduced Ca^{2+} current at room temperature (21–23°C), compared to near-body temperature (34–37°C) (Johnson and Marcotti, 2008), considering that about 90 % of Ca^{2+} current in inner cochlear hair cells is mediated by $\text{Cav}1.3$ (Platzer et al., 2000).

Pharmacologically it is not possible to discriminate between different LTCCs, since they all are blocked by typical LTCC blockers like dihydropyridines (DHP), phenylalkylamines or benzothiazepines (Striessnig et al., 2006). However, their sensitivity to those blockers differs depending on regulatory subunit composition. $\text{Cav}1.3$ and $\text{Cav}1.4$ are significantly less sensitive to DHP agonists and antagonists, like nimodipine and isradipine, compared to $\text{Cav}1.2$ channels (Lipscombe et al., 2004). Human $\text{Cav}1.3$ α_1 -subunits were about 20 fold less sensitive to inhibition by nimodipine in comparison to $\text{Cav}1.2$ when expressed in xenopus oocytes (Xu and Lipscombe, 2001) and are only partially inhibited (Helton et al., 2005). Comparable results (10 fold less sensitivity) were obtained with isradipine by Koschak et al., even though they also demonstrated that binding affinity from isradipine is similar for both $\text{Cav}1.2$ and $\text{Cav}1.3$ and highlighting that block of $\text{Cav}1.3$ by DHPs is voltage dependent (better block at more positive voltages; (Koschak et al., 2001)).

General Cav1.3 knockout mice (Cav1.3 KO; see 2.1.1 for details on the construct), show a very complex phenotype, including deafness and sinoatrial node dysfunction with pronounced resting bradycardia and resting arrhythmia (Platzner et al., 2000). Very similar symptoms were found in humans with the recently discovered disease sinoatrial node dysfunction and deafness (SANDD) who have non-functional Cav1.3 channels (Baig et al., 2011). Cav1.3 KO mice were also reported to have significantly lower body weight in comparison to the wildtype, which might be due to existing hypoinsulinemia and glucose intolerance (Clark et al., 2003; Striessnig et al., 2006). Furthermore they show antidepressant-like behaviour and have a long-term fear memory impairment with no dysfunction in fear acquisition and extinction (Busquet et al., 2010; Striessnig et al., 2006). However, no disturbance of motor functions (balance, coordination and spontaneous motor activity), or mechanical and thermal nociceptive thresholds was observed (Clark et al., 2003). Busquet et al. showed that Cav1.3 KO mice exhibit a “temperature phenotype” with a significantly reduced basal body temperature at 12:00 and 15:00 hours (Busquet et al., 2010). Evoked burst firing in SN DA neurons from adult Cav1.3 KO mice was shown to be similar to wildtype (WT) mice (Blythe et al., 2009). It was also suggested that pacemaker activity of SN DA neurons of Cav1.3 KO mice depends on HCN channels, in contrast to WT mice where in the adult animal it is thought to depend on LTCCs and only in juvenile mice on HCN channels (Chan et al., 2007).

1.3.1 Role of Cav1.3 channels in SN DA neurons and PD

SN DA neurons express Cav1.2 and Cav1.3 poreforming α_1 -subunits (Chan et al., 2007; Olson et al., 2005). The expression of β -, $\alpha_2\delta$ - and γ -subunits is unclear, as is the exact molecular identity of the α_1 -subunit splice variants of these LTCCs in SN DA neurons (Buraei and Yang, 2010; Chen et al., 2007; Dolphin, 2003; Hobom et al., 2000). In cultured SN DA neurons from one to three day old mice it has been shown that most Cav1.3 protein is located in the cell soma with a modestly decreasing channel density the further away (Dryanovski et al., 2013).

The function of Cav1.3 LTCCs in SN DA neurons is less clear. Their electrophysiological properties (see paragraph 1.3) allow Cav1.3 channels, in combination with hyperpolarising conductances, to create the SOPs which were thought to be driving pacemaking in dopaminergic midbrain neurons (Bean, 2007; Chan et al., 2007; Guzman et al., 2009; Liss and Roeper, 2008, 2010; Puopolo et al., 2007; Putzier et al., 2009). However this is a

controversial topic. It was reported that pacemaking in SN DA neurons of adult mice was completely dependent on Cav1.3-created SOPs, but pacemaker activity remained unperturbed even upon blockage of SOPs (Chan et al., 2007; Guzman et al., 2009; Liss and Roeper, 2008).

Puopolo et al. provided evidence that already in juvenile mice (PN 14–18) the SOPs are produced by LTCCs (Puopolo et al., 2007). Dynamic clamp recordings of SN DA neurons (juvenile Sprague Dawley rats PN 14–21) indicated that it was not the Ca^{2+} provided by Cav1.3 activity that was necessary for pacemaker-generation but the positive charge and unique voltage dependence of activation of these channels (Putzier et al., 2009). The Surmeier group however showed that pacemaking in SN DA neurons of mice (ages PN 21–32) was not inhibited by LTCC blockers in concentrations that sufficiently blocked distal dendritic Ca^{2+} oscillations, as well as all SOPs, without affecting pacemaker activity (5 μM and 200 nM isradipine, respectively; (Guzman et al., 2009)). This ongoing controversial debate has been addressed by Drion et al. and with their modelling approach they could show that those drastically different experimental results can already arise from neurons whose biophysical properties and conductances differ by only 1 % (Drion et al., 2011).

Our own group gained strong evidence for a crucial role of Cav1.3 LTCCs for a cocaine-induced non-desensitisation of the D2-autoreceptor response in SN DA neurons from juvenile mice (Dragicevic et al., 2014).

It has been shown that LTCC function in murine SN DA neurons *in vitro* generates dendritic Ca^{2+} oscillations, which are on one hand associated with SN DA pacemaker activity and, on the other hand, with mitochondrial membrane potential flickering and oxidative stress causing their vulnerability to degeneration in PD (Guzman et al., 2010; Mosharov et al., 2009). It was also suggested that adult SN DA neurons are more prone to degeneration due to the hypothesised age-dependent switch in pacemaker drive from HCN (juvenile) to Cav1.3 (adult) and thus to a more stressful pacemaker mechanism due to the calcium load (Chan et al., 2007; Sulzer and Surmeier, 2013; Surmeier, 2007a; Surmeier et al., 2011b; Surmeier and Schumacker, 2013). However, the physiological functions and the (possibly pathophysiological) consequences of Cav1.3 activity in SN DA neurons are still unclear and controversial.

Nevertheless blood brain barrier permissive LTCC blockers of the DHP-type (prescribed to treat high blood pressure) were indeed shown to reduce the risk to develop PD in humans by about 30 % (Ritz et al., 2010; Surmeier et al., 2011a), and they protect SN DA neurons in PD mouse models in a dose-dependent manner (Ilijic et al., 2011). Although the underlying mechanism is still unknown, clinical trials with established LTCC blockers have already been conducted (ClinicalTrials.gov Identifier: NCT00909545, (Parkinson Study, 2013; Simuni et al., 2010)), and the development of more specific and selective Cav1.3 blockers is also underway (Kang et al., 2013).

1.4 The aim of this work

Roles for Cav1.3 channels and particularly their blockers as novel therapeutic, neuroprotective options/strategies in the treatment of PD are emerging, but their mode of action is mechanistically still unclear. Therefore the understanding of the physiological functions of defined LTCCs in SN DA neurons is necessary to minimise side effects when developing new blood brain barrier permissive specific blockers.

Accordingly, the aim of this PhD project was to address the functional role of Cav1.3 LTCCs in SN DA neurons by electrophysiologically characterising SN DA neurons of juvenile (PN 11–14) and adult (~PN 90) Cav1.3 KO mice in comparison to wildtype (C57BL/6 and/or Cav1.3^{+/+}) in *in vitro* brain slice preparations via patch-clamp techniques (whole-cell, on-cell and perforated-patch recordings). In particular, basal biophysical properties of action potentials during pacemaker activity as well as the dopamine D2-autoreceptor response (including temperature dependence) were analysed, as our previous findings suggested a role for Cav1.3 LTCCs for plasticity of the D2-AR response.

In addition, as the results gained within this PhD-project indicated a T-type channel compensation in SN DA neurons from the Cav1.3 KO mouse – which added further complexity to the analysis of Cav1.3 channel function – another aim was to test the effect of the selective T-type channel blocker Z941 on SN DA neurons to elucidate this novel possible LTCC-T-type channel interaction.

2 MATERIALS AND METHODS

2.1 Materials

2.1.1 Animals

All mice were bred in the animal facility of Ulm University. Juvenile (PN 11-14) or adult (PN ~90) C57BL/6, Cav1.3 knockout (Cav1.3 KO) or Cav1.3 wildtype (Cav1.3^{+/+}) mice were analysed. General Cav1.3 KO mice were kindly provided by Prof. Dr. Jörg Striessnig (University of Innsbruck), and obtained from Tübingen (in 2008, Jutta Engel).

The targeting construct for the Cav1.3 KO mice consisted of the thymidine kinase gene (TK), a 1.4 kb fragment 5' to exon 2, the neomycine resistance (neo) gene driven by the *pgk* promoter inserted in reverse direction into the *Clal* site on exon 2, a 5 kb genomic fragment 3' to exon 2, and the plasmid pKO V90 (Platzer et al., 2000).

The Cav1.3 KO mice that were used had a mixed C57BL/6 × sv129 background; they were backcrossed twice to C57BL/6 (maybe three times; unfortunately it is not completely clear if the mice were backcrossed only once or already twice before we obtained them). As additional control Cav1.3^{+/+} mice were generated in a third backcross to C57BL/6. Cav1.3^{+/+} mice showed no significant differences when electrophysiological parameters of their SN DA neurons were compared to C57BL/6.

All animal procedures (sacrificing of animals for organ harvesting) were approved by Regierungspräsidium Tübingen (Aktenzeichen: 35/9185.81-3, Reg. Nr. 0.147).

2.1.2 Chemicals, gases and stock solutions

chemical / gas	information	storage
CaCl ₂	Calcium chloride, SigmaUltra, purity minimum 99.0 %	room temperature
Carbogen (MTI Industriegase AG, Germany)	Carbogen 5, 95 % O ₂ R, 5 % CO ₂	room temperature
DNIP/srDNIP (Genscript, USA)	small cell-permeant D2-R/NCS-1 interfering peptide designed to compete with NCS-1 binding to the D2-R; for details see (Saab et al., 2009)	-20°C
DNQX d.s. (Tocris)	6,7-Dinitroquinoxalin-2,3-dion disodium salt	room temperature

MATERIALS AND METHODS

DOMITOR (Orion Pharma, Finland)	injection solution (active compound: Medetomidin-hydrochloride 1.0mg/ml)	4°C
DPBS (Gibco®, Life Technologies, EU)	10× Dulbecco's phosphate buffered saline, no calcium, no magnesium	room temperature
Forene (Abbott, Switzerland)	2-chloro-2-(difluoromethoxy)-1,1,1-trifluoroethane (Isoflurane), 100 % (V/V)	room temperature
Gabazine (Tocris)	SR-95531 hydrobromide; >98 %	room temperature
Glucose	D-(+)-Glucose, SigmaUltra, purity 99.5 % GC	room temperature
Gramicidin	linear polypeptide antibiotic complex, from <i>Bacillus aneurinolyticus</i> , mixture of gramicidins A, B, C and D	4°C
γ-cyclodextrin	γ-cyclodextrin, purity minimum 99 %	room temperature
Heparin (ratiopharm, Germany)	Heparin-Natrium25000-ratiopharm, injection solution, 25000 I.E.	4°C
HEPES	4-(2-hydroxyethyl)-1-piperazine-ethanesulfonic acid, purity minimum 99.5 % (titration)	room temperature
Isradipine (Tocris)	L-type Ca ²⁺ channel blocker; dihydropyridine; purity >99 %	room temperature
KCl	potassium chloride, purity minimum 99.0%	room temperature
Ketamin (Inresa Arzneimittel GmbH, Germany)	50 mg/ml injection solution	4°C
K-gluconate	Potassium D-gluconate, purity minimum 99 %	room temperature
Kynurenic acid	Kynurenic acid, purity minimum 98 %	4°C
Magnesium-ATP	Adenosine-5'-triphosphate sodium salt, from bacterial source, purity 96 % (HPLC)	-20°C
NaCl	Sodium chloride, Biotech performance certified, cell culture tested	room temperature
NaH ₂ PO ₄	Monosodium phosphate, monobasic, water free, SigmaUltra, purity minimum 99.0 %	room temperature
NaHCO ₃	Sodium bicarbonate, ACS reagent, purity 99.7-100.3 %	room temperature
NEUROBIOTIN™ (Vector Laboratories, USA)	NEUROBIOTIN™ Tracer	4°C
PFA (Alfa Aesar, USA)	Paraformaldehyde, purity 97 %	room temperature

MATERIALS AND METHODS

Sodium-GTP	Guanosine-5'-triphosphate sodium salt, purity minimum 95 %	-20°C
Z941	T-type calcium channel blocker; obtained from T. P. Snutch (University of British Columbia, Canada); for details see (Tringham et al., 2012)	4°C
ZD7288 (Tocris)	HCN channel blocker, purity >99 %	4°C

Table 2-1: Overview over used chemicals and gases

Given are information about compounds and storage of all chemicals and gasses used. If not stated otherwise chemicals were obtained from Sigma Aldrich (Germany). Tocris stands for Tocris Cookson Ltd. (UK).

stock solution	contains	storage
10× ACSF	1250 mM NaCl, 250 mM NaHCO ₃ , 25 mM KCl, 12.5 mM NaH ₂ PO ₄ in H ₂ O	4°C
CaCl ₂	1 M calcium chloride in H ₂ O	4°C
DNQX disodium salt	10 mM 6,7-dinitroquinoxaline-2,3-dion disodium salt in H ₂ O	-20°C
Dopamine	100 mM 3-hydroxytyramine hydrochloride (dopamine hydrochloride) in 1× ACSF	no storage, direct use
EGTA	10 mM ethylene glycol-bis(β-aminoethyl ether)-N,N,N',N'-tetraacetic acid, minimum 97 % (titration) in H ₂ O; pH ~10	4°C
external HEPES buffered ACSF	145 mM NaCl, 2.5 mM KCl, 10 mM HEPES, 2 mM CaCl ₂ , 2 mM MgCl ₂ in H ₂ O; pH adjusted to 7.4 with 1 M NaOH	4°C
Gabazine	10 mM SR-95531 in H ₂ O	-20°C
Gramicidin	5 mM mg/ml gramicidin in 100 mg/ml γ-cyclodextrin (in internal solution “standard”) à 55 µl; for details see 2.2.1.2.1	-20°C
internal solution “high EGTA”	135 mM K-gluconate, 5 mM KCl, 10 mM HEPES, 10 mM EGTA, 0.1 mM NaGTP, 5 mM MgATP in H ₂ O; pH adjusted to 7.33 with 1 M KOH	4°C
internal solution “standard”	135 mM K-gluconate, 5 mM KCl, 10 mM HEPES, 0.1 mM EGTA, 0.1 mM NaGTP, 5 mM MgATP in H ₂ O; pH adjusted to 7.33 with 1 M KOH	4°C
internal solution “standard”/histo	135 mM K-gluconate, 5 mM KCl, 10 mM HEPES, 0.1 mM EGTA, 0.1 mM NaGTP, 5 mM MgATP, 1 % NEUROBIOTIN™ in H ₂ O; pH adjusted to 7.33 with 1 M KOH	-20°C

MATERIALS AND METHODS

Isradipine	20 mM isradipine (Tocris) in DMSO	-20°C
KOH	1 M potassium hydroxide in H ₂ O	4°C
MgCl ₂	1 M magnesium chloride in H ₂ O	4°C
NaGTP	0.1 M sodium GTP in H ₂ O	-20°C
PFA	4 % PFA (Alfa Aesar) in 1× DPBS (Life Technologies)	4°C
Z941	10 mM Z941 in DMSO	-20°C
ZD7288	25 mM ZD7288 (Tocris) in H ₂ O	-20°C

Table 2-2: Overview over used stock solutions

Given are detailed information about composition, concentration and storage of used stock solutions. If not stated otherwise chemicals were obtained from Sigma Aldrich (Germany). Tocris stands for Tocris Cookson Ltd. (UK).

For additional details on solutions and their preparation see 2.2.1.

2.1.3 Electrophysiology hardware, instruments, accessories and software

Electrophysiological *in vitro* brain slice measurements were carried out on two comparable setups with the specifications as shown in Table 2-3 and Figure 2-2. Additional hardware, instruments and accessories not directly associated with the recording setups are listed with details where they appear in the text in 2.2.

	Setup 1	Setup 2
patch-clamp amplifier:	EPC10 (HEKA Elektronik, Germany)	EPC10 plus (HEKA Elektronik, Germany)
Data acquisition software:	Pulse8.8 (HEKA Elektronik, Germany)	PatchMaster 2.73.1 (HEKA Elektronik, Germany)
Computer operating system:	Windows 2000 (Microsoft Corporation)	Windows XP SP3 (Microsoft Corporation)
Vibration isolated workstation:	Newport Corporation, USA	Newport Corporation, USA
Microscope:	Axioskop 2 FS plus (Zeiss, Germany)	Axio Examiner.D1 (Zeiss, Germany)

MATERIALS AND METHODS

Objectives:	Zeiss Achroplan 4x/0.10, ∞/-; Zeiss Achroplan 40x/0.80, ∞/0 water immersion	Zeiss Achroplan 4x/0.10, ∞/-; Zeiss Achroplan 40x/0.75, ∞/0 water immersion
Camera:	CF 8/4 (Kappa opto-electronics GmbH, Germany)	Clara (Andor Technology plc., Northern Ireland)
Micromanipulator:	SM-5 (Luigs & Neumann, Germany)	SM-5 9 (Luigs & Neumann, Germany)
Automatic brightness and contrast adjustment:	Remote Control RC (Kappa opto-electronics GmbH, Germany)	Imaging Control Unit & Live Acquisition Software (TILL Photonics/FEI Munich GmbH, Germany)
Temperature controller:	Badcontroler V (Luigs & Neumann, Germany)	Badcontroler V (Luigs & Neumann, Germany)
Peristaltic pump:	REGLO (Ismatec, Germany)	REGLO (Ismatec, Germany)
Silicone tubing:	Ø 0.8 mm, Ø 1.6 mm (Rio-Rad Laboratories INC., USA)	Ø 0.8 mm, Ø 1.6 mm (Rio-Rad Laboratories INC., USA)
Tygon tubing (gas tight):	Ø 1.6 mm (Kobe, Germany); Ø 2.79 mm (Ismatec, Germany)	Ø 1.6 mm (Kobe, Germany); Ø 2.79 mm (Ismatec, Germany)
Data analysis software:	FitMaster 2.71 (HEKA Elektronik, Germany); Igro Pro 6.34A (WaveMetrics Inc. USA); Microsoft Excel 2007/2012 (Microsoft Corporation); Neuroexplorer 4 (Nex Technologies, USA); the R project for statistical computing (R-Development-Core-Team, 2009); RExcel (http://rcom.univie.ac.at/download.html); (Baier and Neuwirth, 2007)); GraphPad Prism 6.04 for Windows (GraphPad Software, USA, www.graphpad.com)	

Table 2-3: Comparison of the used electrophysiological recording setups and used software

Overview of the technical equipment, software and accessories of the recordings setups, including analysis software installed on personal computers. Recording setup 1 was upgraded to Windows 7 and PatchMaster in January 2014; see also Figure 2-2. In addition to the objectives both setups are equipped with an additional 2× lens (from Luigs & Neumann) for up to 80× magnification.

A DMZ Universal Puller (Zeitz-Instrumente GmbH, Germany) was used to pull pipettes from thin filament borosilicate glass capillaries (GC15OTF-15 1.5 mm O.D. × 1.17 mM I.D., Harvard Apparatus, UK). Program 10 with the default settings, but without tip-polishing, was used; P(B) H was changed to adjust pipette tip size (see Table 2-4). The pulled pipettes had a resistance of 1.8-3 MΩ (filled with internal solution, without air pressure) for standard whole-cell recordings and perforated-patch, and 4.5–6.0 MΩ for on-cell recordings. Pipettes were filled with a syringe (Becton Dickinson S.A., Spain), using a non-metallic syringe filling needle (gauge 28, World Precision Instruments Inc., USA), mounted on a syringe filter (4 mm syringe filter, 0.2 μm nylon membrane, Nalgene, USA).

P(A)

H	400	Heat for glass softening.
F(TH)	20	Preliminary pull, force for glass elongation.
s(TH)	20	Distance threshold for elongation (H and F(TH) terminate when reached).
t(H)	50	Position of right-hand electrode for polishing.
s(H)	50	Position of left-hand electrode for polishing.
AD	121	Low heat range for main pull, two preliminary pulls i.e. a three-stage pull, low heat range at polishing.

P(B)

H	560	Heat strength for main pull (see AD above).
F(TH)	25	Sensing pull, force for sensing glass stiffness.
s(TH)	10	Distance threshold for elongation (F(TH) terminates).
t(H)	30	Delay before heat is terminated; starts at s(TH).
s(H)	0	Distance threshold for termination of heat. Mutually exclusive with t(H).
t(F1)	120	Delay before starting main pull F1; starts at s(TH).
F1	170	Force, first phase of main pull.
s(F2)	2	Distance threshold for start of second force phase, main pull F2. Distance measured from s(TH)
F2	185	Force for second phase of main pull.
AD	245	Polishing program activated with AD = 245, 2 = 2 s duration, heat strength 45 = 450. To deactivate polishing set AD = 045.

Table 2-4: Detailed description of Puller Program P10

Detailed description of default parameters of program P10 of the DMZ-Zeitz-Universal Puller by Zeitz-Instrumente GmbH. P(B) H was changed to adjust tip size of the pipette; polishing was deactivated with AD = 045. Information taken from the DMZ-Zeitz-Puller User Manual (available online with additional information at www.zeitz-inst.hompage.t-online.de/Support/Manual/6-Tables/kapitel66-tables.html).

2.2 Methods

2.2.1 Preparation of solutions

2.2.1.1 ACSF solutions

Juvenile mice: For the experiments the 10× ACSF Stock (Table 2-2) was diluted to 1× and glucose was added, as well as CaCl₂ and MgCl. Final concentrations in the solution, which was used for both, recording and preparation (in mM): 125 NaCl, 25 NaH₃CO₃, 2.5 KCl, 1.25 NaH₂PO₄, 2 CaCl₂, 2 MgCl₂ and 25 glucose.

Adult mice: As for juvenile mice the 10× ACSF Stock was diluted to 1× and glucose and sucrose were added, as well as the respective amounts of CaCl₂ and MgCl (preparation solution: 0.1 mM CaCl₂, 6 mM MgCl₂; recording solution: 2 mM each) and for preparation additionally kynurenic acid. The final concentrations were as follows: adult mice preparation solution (in mM): 125 NaCl, 25 NaH₃CO₃, 2.5 KCl, 1.25 NaH₂PO₄, 2.5 glucose, 50 sucrose, 0.1 CaCl₂, 6 MgCl₂, 3 kynurenic acid; adult mice recording solution: 125 NaCl, 25 NaH₃CO₃, 2.5 KCl, 1.25 NaH₂PO₄, 2.5 glucose, 22.5 sucrose, 2 CaCl₂ and 2 MgCl₂.

All 1× ACSF solutions were gassed with carbogen to adjust pH.

To block fast synaptic transmission (AMPA, Kainate and GABA_A receptors respectively), 10 μM DNQX disodium salt (Tocris) and 10 μM gabazine (Tocris) were added to the recording ACSF.

For recordings with isradipine, ZD7288 or Z941, the appropriate amounts of stock solutions (see Table 2-2) were added to the recording ACSF to obtain concentrations of 300 nM, 25 μM and 10 μM respectively. The peptides DNIP or srDNIP (D2-R/NCS-1 Interfering Peptide, Genscript, (Saab et al., 2009)) were added to the recording solution to a final concentration of 10 μM respectively. Slices were incubated for at least 40 minutes in isradipine and 30 minutes in ZD7288/Z941/DNIP/srDNIP before the start of recording. One control cell was patched and recorded on each slice prior to incubation with pharmacological agents to check for general vitality of the brain slice.

The dopamine stock solution was always made right before the experiment. Approximately 5 mg of dopamine hydrochloride were weighed into an eppendorf tube and 1× ACSF recording solution was added to an end concentration of 100 mM dopamine. For the experiment this stock was added to the 1× ACSF recording solution to a final concentration of 100 μM dopamine in ACSF; the solution needs to be kept lightsafe throughout the recording and the rest of the dopamine stock should be discarded.

2.2.1.2 Internal solutions

For standard whole-cell recordings, an aliquot of the internal solution “standard” or “standard”/histo stock (see Table 2-2) was thawed and then kept light-safe on ice for the duration of the experiment.

For on-cell recordings the appropriate amount of glucose (25 mM for juvenile mice) was added to HEPES buffered ACSF.

2.2.1.2.1 Gramicidin solution for perforated-patch recordings

A 100 mg/ml solution of γ -cyclodextrin was made by weighing approximately 100 mg into an eppendorf tube and adding the appropriate amount of internal solution (“standard”, see Table 2-2), before it was heated and dissolved on a Thermomixer® compact (Eppendorf AG, Germany) at 38°C for about ten minutes. Gramicidin was added to the solution to an end concentration of 5 mg/ml. This solution was sonicated for 30 minutes and then kept on the Thermomixer® at 38°C for two hours. The resulting stock solution was aliquotted (55 μ l) in lightsafe eppendorf tubes and kept at -20°C.

For experiments an aliquot was thawed on the Thermomixer® (38°C, 15 minutes). Then 50 μ l of the thawed stock were added to 1250 μ l of (“standard”) internal solution. This solution was sonicated for five minutes and afterwards 500 μ l were mixed again with 500 μ l of the (“standard”) internal solution. Then the syringe was loaded with the mixture and kept light safe throughout the experiment.

2.2.2 Preparation of coronal vital brain slices

2.2.2.1 Juvenile animals (PN 11-13)

Preparation was essentially done as described in (Liss et al., 1999; Pötschke, 2008, 2010). Animals were terminally narcotised with Isoflurane (Forene) and decapitated. The skull was carefully opened, the brain dissected and 250 μ m thick coronal brain slices covering the whole caudo-rostral midbrain axis were cut in ice-cold 1 \times ACSF perfusion solution using a vibratome (Vibroslice™ type: HA752, Campden Instruments, UK, see also Figure 2-1). Prior to recordings, 30 minutes of recovery time at room temperature were allowed. The brain slices were kept free floating on cell culture inserts (25 mm Tissue Culture Inserts, 8.1 μ m

Polycarbonate Membrane, Nalge Nunc International) in gassed (Carbogen) 1× ACSF perfusion solution at room temperature (~20°C) until recordings.

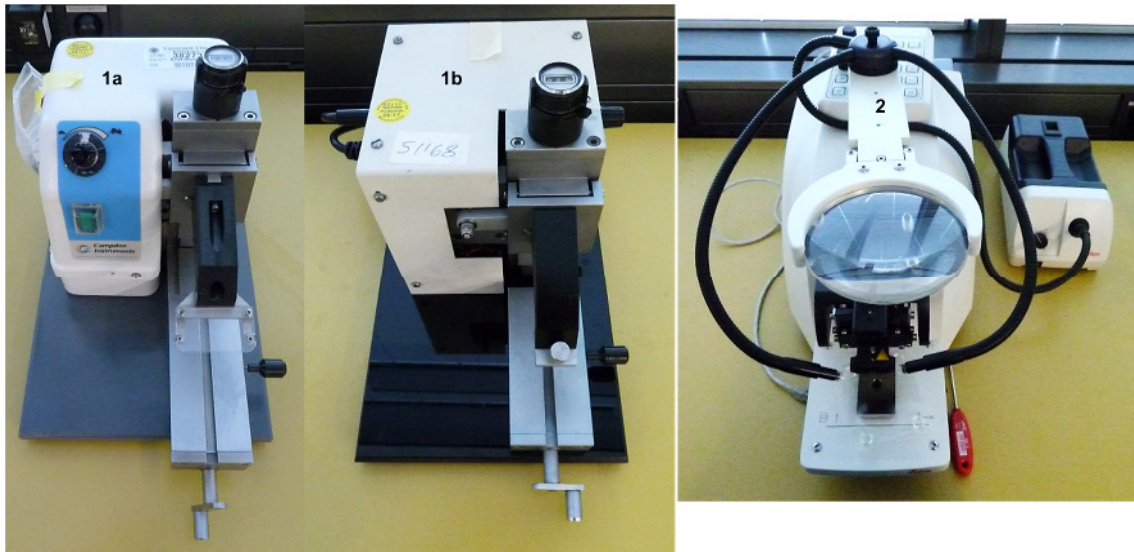


Figure 2-1: Vibratomes for preparing acute brain slices

1a and **1b** are vibratomes (Vibroslice™) from Campden Instruments, UK. **1a** is the newer model, both models are no longer manufactured. **2** is the VT1200S from Leica, which is fully motorised, and includes a cold light source. Not shown for all vibratomes are cutting chambers and blades.

2.2.2.2 Adult animals (PN ~90)

Preparation was essentially done as described in (Lammel et al., 2008; Liss et al., 2005). Animals were terminally narcotised with 300 µl of an anaesthetic mixture containing 400 µl of 50 mg/ml Ketamin and 200 µl of 1 mg/ml DOMITOR (see Table 2-1). The ribcage was opened and 50 µl of Heparin (see Table 2-1) injected into the left ventricle of the heart. Afterwards, an intracardial perfusion was done using iced 1× ACSF preparation solution for approximately five minutes. The skull was then carefully opened, the brain dissected and 200 µm thick coronal midbrain slices were cut using a vibratome (VT1200S, Leica, Germany, see Figure 2-1). Brain slices were kept free floating on cell culture inserts (25 mm Tissue Culture Inserts, 8.1 µm Polycarbonate Membrane, Nalge Nunc International) in gassed (Carbogen) recording ACSF solution for adult mice (see Table 2-2) for 90 minutes at 36°C (recovery time) and then at room temperature (~20°C) until recordings.

2.2.3 Patch-clamp recordings

Electrophysiological recordings were either carried out in the whole-cell configuration (either with 0.1 mM or 10 mM EGTA) or the perforated-patch and on-cell configuration on one of the two recording setups (see Figure 2-2 and Table 2-3). For recordings, brain slices were

transferred to the recording chamber (see insert in Figure 2-2), which was continuously perfused with the respective oxygenated 1× ACSF recording solution, and held in place with a small grid made of platinum wire and nylon strings.

Unless specifically stated otherwise, all electrophysiological recordings on SN DA neurons from juvenile mice were performed at $33^{\circ}\text{C} \pm 1$, the temperature was controlled by Badcontroller V (Luigs & Neumann, Germany) and additionally checked with a hand thermometer after recordings. In general, data were digitalised at 10 kHz; for the 40 minute recordings digitalisation was 5 kHz to keep file size smaller. Data were filtered with Bessel Filter 1: 10 kHz; Bessel Filter 2: 5 kHz.

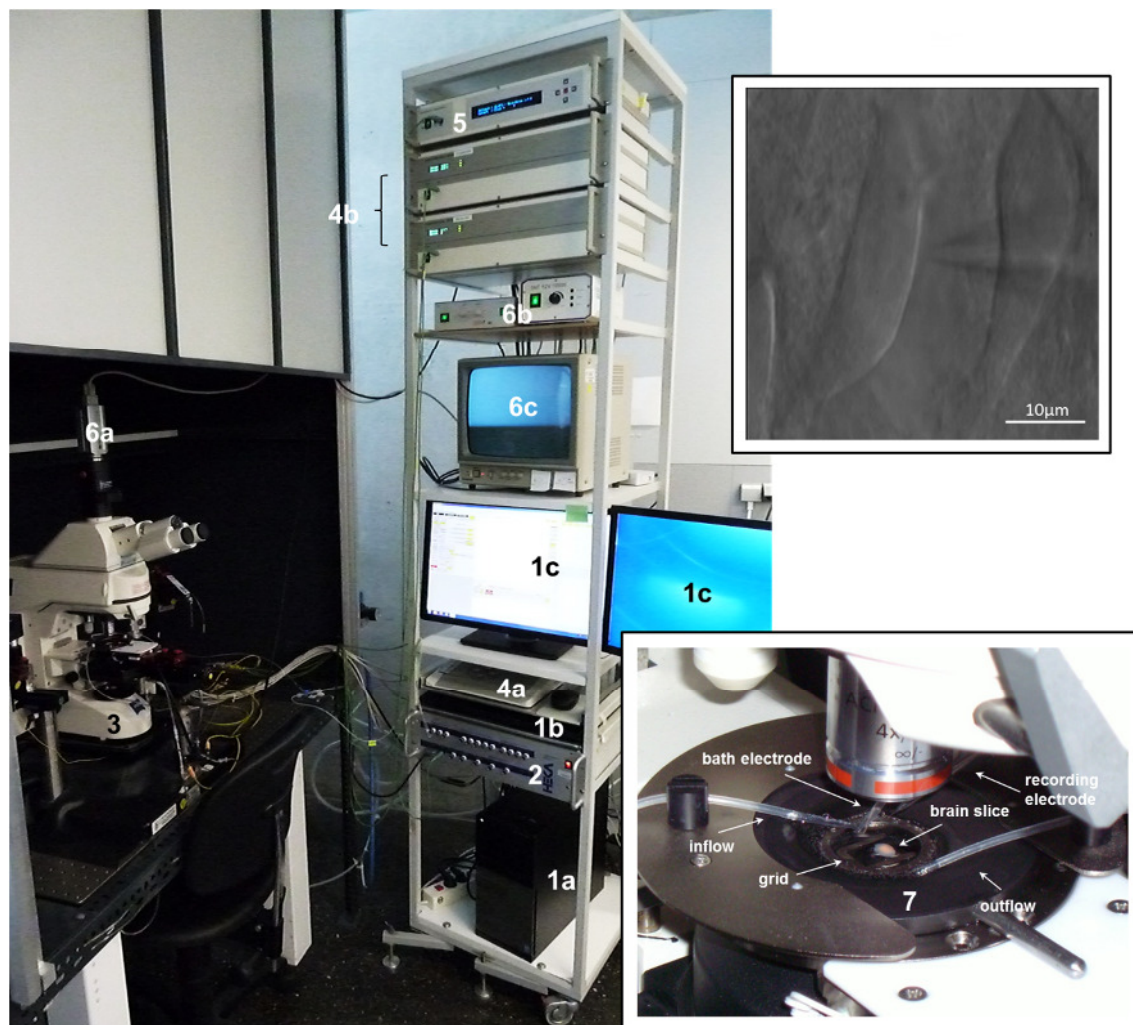


Figure 2-2: Electrophysiological recording setup

Shown is number one of the electrophysiological recording setups (see Table 2-3), with an insert depicting a dopaminergic neuron as seen on 6c with the patch-pipette nearing it (and another neuron nearby) and a second insert with a detailed picture of the recording chamber (7 as part of 3). 1 Computer workstation: a computer, b keyboard, c monitors. 2 HEKA EPC10 patch-clamp amplifier. 3 Zeiss Axioskop 2 FS plus microscope. 4 Luigs & Neumann micromanipulator: a controls, b SM-5 Master & Slave. 5 Luigs & Neumann Badcontroller V for temperature control. 6 Camera setup: a camera CF 8/4, b automatic brightness and contrast control, c monitor (example

picture shown in insert, taken with 80× resolution). **7** (as insert) recording chamber as part of **3**, detailed picture with brain slice, grid, recording and bath electrode, as well as inflow and outflow of solution marked – heated through **5**.

For whole-cell recordings, patch-pipettes were filled with the internal solution “standard”, “standard”/histo or “high EGTA” and the solution was kept light safe and on ice. For perforated-patch recordings an internal solution that contained gramicidin was used (for details see 2.2.1.2.1).

Since the functional DNIP peptide seemed to interfere with the gramicidin perforation, on-cell recordings were also used for DNIP experiments. Usage of the scrambled control peptide (srDNIP, Genscript, (Saab et al., 2009)) interestingly did not necessitate on-cell recordings and were done in perforated-patch. For on-cell recordings, patch-pipettes were filled with an external HEPES buffered ACSF solution (see Table 2-2 and 2.2.1.2).

To study dopamine D2-AR responses, in the presence or absence of pharmacological agents, activity of neurons was recorded over 40 minutes using either the perforated-patch configuration, the whole-cell configuration (for EGTA effects) or, for recordings with the DNIP peptide, on-cell configuration. For the 40 minute whole-cell recordings, patch-pipettes with higher resistance (4.0–5.0 MΩ) were used. After recording a stable baseline frequency for at least five minutes, 100 μM dopamine was applied via bath perfusion for 15 minutes, followed by 20 minutes of dopamine washout.

Neurons were selected based on location – and size (also measured as capacitance) – on the brain slice for recording. Recorded neurons were then further selected for statistical analysis based on their sag-component (for details see 2.2.4).

2.2.4 Data analysis and statistics

2.2.4.1 Parameters

Recorded neurons from basal characterisation experiments (whole-cell recordings) were included in the statistic when the sag-component at -150 mV was bigger than 40 mV, only neurons that fit this criterion were analysed. The exception to this are recordings in ZD7288 since this blocker abolishes HCN activity and therefore the sag-component. (These neurons were filled with NEUROBIOTIN™ during the recording through usage of the internal solution “standard”/histo. After the recording the slices were fixed with a 4 % PFA solution [see Table 2-2]. Then the slices were immuno-histochemically fluorescence double stained for tyrosine hydroxylase and, streptavidin-based, for NEUROBIOTIN™ by Stefanie Schulz, Desiree

Spaich or Sonja Müller [AG Liss].) Neurons from perforated-patch recordings were included in the statistic when they showed autoinhibition of their pacemaker activity in response to dopamine and/or a sag-component either while still in perforated-patch or during whole-cell repatch (this is also the case for on-cell recordings).

All recorded whole-cell data was analysed and assessed as previously described (Kemmler, 2009; Pötschke, 2008). Input resistances were calculated according to Ohm's law by using the initial membrane potential in response to injection of -50 pA hyperpolarising current. The electrical capacitance of the neuron was obtained, after reaching the whole-cell configuration, from the inbuilt Cslow capacitance correction algorithm of the EPC10 and software (HEKAManuals).

For whole-cell recordings (maximal) AHP, overshoot, threshold and action potential width at threshold were analysed of spontaneous action potentials (see Figure 2-3); the values were averaged from five 5 second traces for AHP and overshoot and from five single action potentials for threshold and action potential width at threshold. With injection of either positive or negative current, sag-component (see Figure 2-3), input resistance, and maximal inducible frequency were examined.

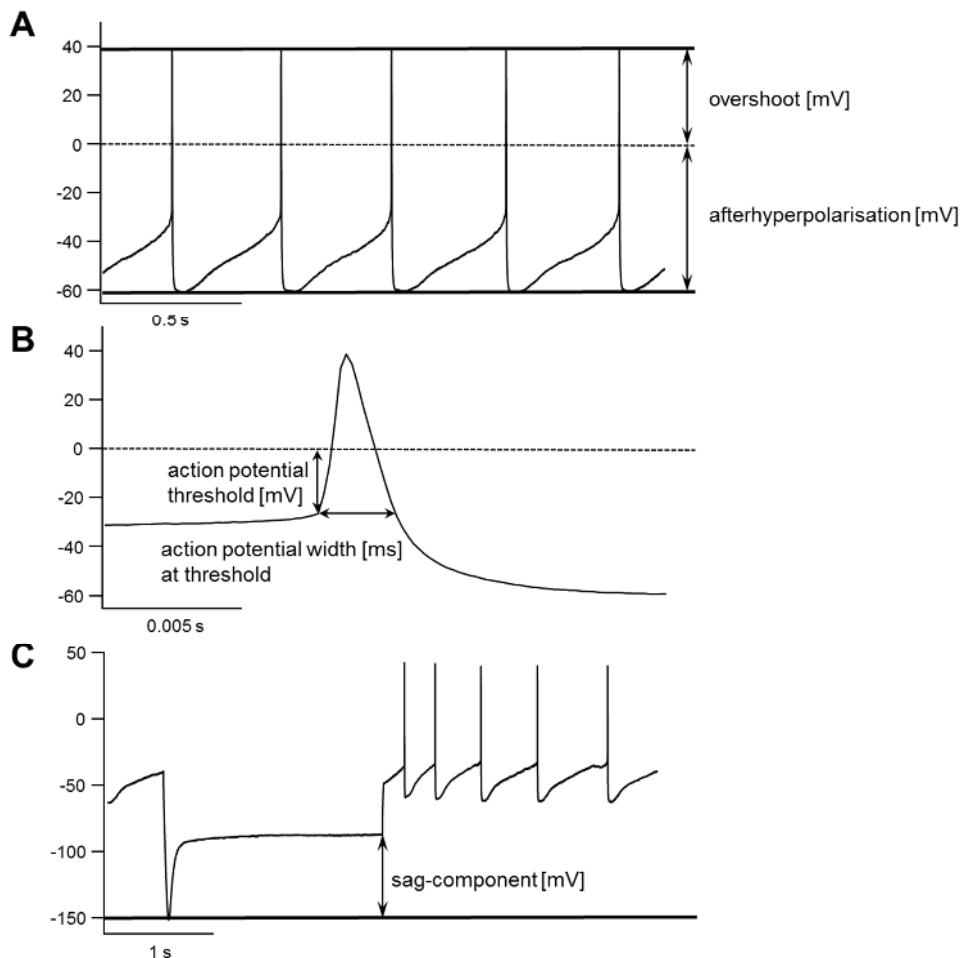


Figure 2-3: Analysis of action potential parameters and sag-component of SN DA neurons

Schematic drawings illustrating analysis of parameters. **A:** Overshoot and (maximal) afterhyperpolarisation of spontaneous action potentials. **B:** Action potential threshold and action potential width at threshold of spontaneous action potentials. **C:** The sag-component in response to injection of hyperpolarising current to a membrane potential of -150 mV.

For assessment of changes in pacemaker activity patterns during the short whole-cell recordings, neurons were categorised into four groups based on their spontaneous activity during 25 s: pacemaker activity, irregular activity, sporadic spikes (which means there were < 10 action potentials in 25 s without a regular pattern) and inactive when no action potentials occurred.

For a more detailed analysis of the pacemaker activity the following parameters were assessed from five minute recordings of spontaneous activity (either perforated-patch, on-cell or, for recordings with 10 mM EGTA in the pipette solution, whole-cell): mean basal frequency and pacemaker precision through the coefficient of variation of the interspike interval (CV ISI). CV ISI was calculated in Neuroexplorer 4 (analysis: interspike interval histograms; result: Coeff.Var.ISI).

For analysis of the kinetic of D2-AR responses (for details of the experiment see 2.2.3) the frequency of each minute was normalised against the mean basal frequency (see paragraph above) of the neuron and then plotted against time in so-called frequency plots. Minute 23 of a frequency plot marks the last minute when dopamine is still present during the recording.

2.2.4.2 Statistics

Analysis of rawdata was performed using FitMaster. For CV ISI analysis time stamps from the action potentials were exported from FitMaster into Neuroexplorer 4 for further analysis.

Statistical analysis and graphical presentation was then done with the help of Igor Pro 6, GraphPad Prism 6 or the R project for statistical computing (R-Development-Core-Team, 2009) with help of RExcel (Baier and Neuwirth, 2007); see also Table 2-3. All data presented in this work is given as mean \pm SEM (where applicable).

Data was tested for outliers via the ROUT function of GraphPad Prism 6. Unless more than one parameter of a neuron deviated from the norm, the outlier was only removed for the particular analysis and not completely from the statistic. Statistical significant differences were identified via exact Wilcoxon-Mann-Whitney-U-two-sample-rank-test with a defined level of significance of 0.05 either in GraphPad Prism 6 or R (function: `wilcox.exact` from the `exactRankTests` package). P-values < 0.05 will be noted with (*), < 0.005 with (**) and < 0.0005 with (***), respectively.

2.2.5 Genotyping

All Cav1.3 KO (and Cav1.3^{+/+}) mice analysed in this work were genotyped for -/- (or +/-) genotype verification. Genotyping was carried out with standard PCR-protocols by Desiree Spaich, Stefanie Schulz or Sonja Müller (from the same work group).

The RedTaqReadyMix from Sigma was used. PCR-cycles as follows: hot start: 94°C, 3 min; denaturation: 94°C, 30 s; annealing: 54°C, 1 min; elongation: 72°C, 1 min; final elongation: 72°C, 7 min; final hold: 4°C, indefinitely until stopped. The PCR ran for 40 cycles (denaturation, annealing and elongation). Cav1.3^{+/+}: 300 bp PCR-fragment; Cav1.3 KO: 450 bp PCR-fragment

Genotyping Primers:

Cav 1.3 antisense: TACTTCCATTCCACTATACTAATGCAGGCT

Cav1.3^{+/+} sense: GCAAACCTATGCAAGAGGCACCAGA

MATERIALS AND METHODS

Cav1.3 KO sense: TTCCATTTGTCACGTCCTGCACCA

3 RESULTS

3.1 Whole-cell characterisation – basal electrophysiological parameters

To test if general loss of Cav1.3 had any effect on basal electrophysiological parameters, SN DA neurons of juvenile and adult, C57BL/6, Cav1.3^{+/+} and Cav1.3 KO mice were analysed. The AHP, the overshoot, the threshold, and the action potential width at threshold (see also 4.1.6 for additional notes on threshold and width) were analysed from spontaneous action potentials. Additionally, the frequency of spontaneous activity, as well as the size of the sag-component at -150 mV, the maximal inducible frequency and the input resistance at a current injection of -50 pA were compared.

This data was obtained in whole-cell recordings under control conditions (0.1 mM EGTA), with high EGTA (10 mM EGTA) in the pipette solution, and under pharmacological challenge with 300 nM isradipine (LTCC blocker) and/or 25 μ M ZD7288 (HCN channel blocker; since most neurons were inactive in ZD7288, action potential parameters were not analysed for this group) or 10 μ M Z941 (T-type channel blocker). Since no significant statistical differences could be found between the analysed whole-cell parameters of SN DA neurons from Cav1.3^{+/+} and C57BL/6 (see also 2.1.1), this data was pooled and is here referred to as WT (data and statistics for C57BL/6 and Cav1.3^{+/+} separately can be found in Supplemental Table 2 and Supplemental Table 3). Accordingly, pharmacological experiments for the WT were carried out with SN DA neurons from C57BL/6 mice (with the exception of data for Z941, which used Cav1.3^{+/+}).

3.1.1 Whole-cell comparison of SN DA neurons from juvenile WT and Cav1.3 KO mice

Significant differences between SN DA neurons of juvenile Cav1.3 KO and WT mice were found when comparing the various parameters gained from whole-cell recordings. The sag-component, the AHP and the action potential threshold showed significant differences under control conditions. In isradipine the maximal inducible frequency and the action potential width were significantly different, while with high EGTA only the input resistance showed a significant difference. Pacemaker frequencies – when neurons were spontaneously active – showed no significant differences (see Supplemental Table 3).

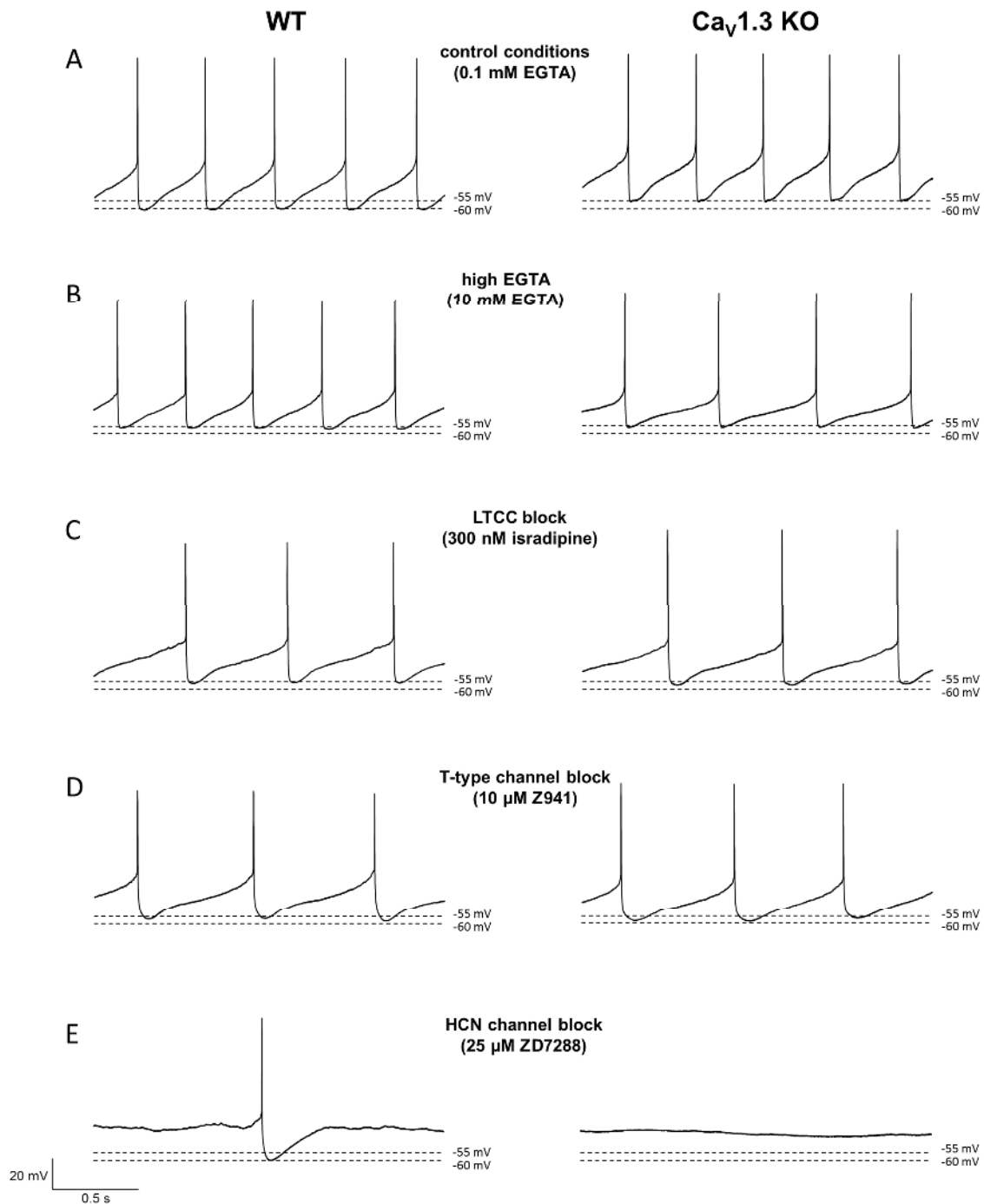


Figure 3-1: Sample traces of spontaneous activity from whole-cell recordings of SN DA neurons from juvenile mice

Shown are two minute sample traces from whole-cell recordings of SN DA neurons from juvenile WT (left) and $Ca_v1.3$ KO (right) mice. Black dashed lines were added at -55 mV (average AHP of SN DA neurons from juvenile $Ca_v1.3$ KO mice under control conditions, for details see 3.1.1.1) and -60 mV (average AHP of SN DA neurons from juvenile WT mice under control conditions, for details see 3.1.1.1). **A:** Control conditions (0.1 mM EGTA). **B:** Recorded with 10 mM EGTA in the pipette solution. **C:** Recorded in 300 nM isradipine. **D:** Recorded in 10 μ M Z941. **E:** Recorded in 25 μ M ZD7288.

3.1.1.1 SN DA neurons from juvenile Cav1.3 KO mice depend more on HCN channels for pacemaking and display significantly smaller AHPs

While under control conditions, when recorded with high EGTA, in Z941 and in isradipine, almost all SN DA neurons from juvenile WT and Cav1.3 KO mice displayed spontaneous activity (in most cases regular pacemaker activity). This was not the case after incubation with ZD7288. In ZD7288 33.3 % of SN DA neurons from juvenile WT mice were inactive and 20 % showed regular pacemaker activity, while in Cav1.3 KO mice the effect of HCN block was more dramatic, with 72 % of neurons inactive and only 4 % still showing regular pacemaker activity. To test if block of both LTCCs and HCN channels would have the same effects on the WT as were observed with Cav1.3 KO in ZD7288, brain slices from WT mice were incubated in both, isradipine and ZD7288. However, this did not particularly increase the percentage of inactive neurons in WT mice (42.9 %) compared to only incubation in ZD7288 (33.3 %; see Figure 3-2 and for detailed listing of neurons Supplemental Table 1).

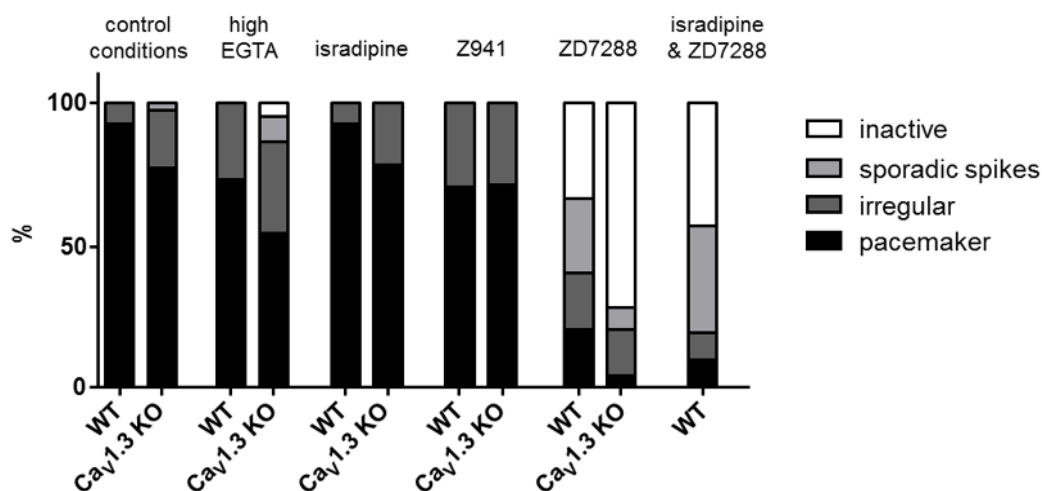


Figure 3-2: The HCN channel blocker ZD7288 dramatically changes the proportion of active/inactive SN DA neurons of juvenile WT and Cav1.3 KO mice

For assessment of changes in pacemaker activity patterns, neurons were categorised into four groups based on their spontaneous activity (recorded for 25 s): pacemaker activity, irregular activity, sporadic spikes (which means there were < 10 action potentials in 25 s without a regular pattern) and inactive, when no action potentials occurred. Under control conditions 92.8 % of SN DA neurons from WT mice ($n = 64$ of 69, for details see Supplemental Table 1) and 77.5 % of Cav1.3 KO mice ($n = 31$ of 40) showed regular pacemaker activity, 7.2 % and 20 % respectively showed irregular activity and only 2.5 % of SN DA neurons from Cav1.3 KO showed only sporadic action potentials. When recorded with high (10 mM) EGTA 73.3 % of SN DA neurons showed spontaneous pacemaker activity in the WT ($n = 11$ of 15) and 54.6 % in the Cav1.3 KO ($n = 12$ of 20), with 26.7 % and 31.8 % irregular, respectively, and 9.1 % sporadic spikes and 4.5 % inactive in the Cav1.3 KO. LTCC block by isradipine had only a minor effect on the activity of SN DA neurons from juvenile mice, with 92.9 % in the WT ($n = 13$ of 14) and 78.6 % in the KO ($n = 11$ of 14) being regularly active and 7.1 % and 21.4 % irregular, respectively. After block of T-type channels by Z941 70.6 % of SN DA neurons from WT mice ($n = 12$ of 17) and 71.4 % from Cav1.3 KO ($n = 10$ of 14) mice showed pacemaker activity, with 29.4 % and 28.6 % showing

RESULTS

irregular activity, respectively. Under HCN block by ZD7288 only 20 % of SN DA neurons from juvenile WT mice ($n = 3$ of 15) displayed pacemaker activity, 20 % irregular activity, 26.7 % showed sporadic spikes and 33.3 % were inactive, while only 4 % of SN DA neurons from juvenile Cav1.3 KO mice ($n = 1$ of 25) displayed pacemaker activity in ZD7288, 16 % were irregularly active and 8 % had sporadic spikes while the majority of SN DA neurons (72 %) were inactive. Incubation in both ZD7288 and isradipine, had similar effects on SN DA neurons of WT mice (total $n = 21$) as incubation in ZD7288 alone, with 9.5 % pacemaker activity, 9.5 % irregular activity, 38.1 % sporadic spikes and 42.9 % inactivity. Note that still not all neurons were inactive, even though both ion channels that were thought to be essential for pacemaking were blocked.

The spontaneous action potentials of SN DA neurons from juvenile Cav1.3 KO showed a significantly smaller AHP in comparison to WT mice under control conditions (WT: $-59.24 \text{ mV} \pm 0.6$, $n = 59$; Cav1.3 KO: $-55.26 \text{ mV} \pm 0.9$, $n = 40$; $p = 0.0008$; see also Figure 3-1). The more prominent AHPs in SN DA neurons from juvenile WT mice seemed to depend on internal Ca^{2+} levels, as they were absent in high EGTA recordings (and after incubation in isradipine), when AHP-sizes of SN DA neurons from both Cav1.3 KO and WT mice, resembled those of the KO under control conditions (see Figure 3-3, Figure 3-1 and Supplemental Table 2). Accordingly, in high EGTA the AHP of SN DA neurons from WT mice was significantly smaller compared to control conditions (WT high EGTA: $-56.25 \text{ mV} \pm 0.7$, $n = 15$; $p = 0.004$).

The action potential threshold of SN DA neurons from juvenile Cav1.3 KO mice was significantly lower than in WT mice under control conditions (WT: $-28.7 \text{ mV} \pm 0.4$, $n = 59$; Cav1.3 KO: $-25.81 \text{ mV} \pm 0.5$, $n = 39$; $p = 0.00004$), but significantly higher compared to Cav1.3 KO in high EGTA (Cav1.3 KO high EGTA: $-28.41 \text{ mV} \pm 0.7$, $n = 19$; $p = 0.006$; see Figure 3-3, Supplemental Table 2 and Supplemental Table 3). The threshold of SN DA neurons from juvenile WT mice was also significantly higher after incubation in isradipine compared to control conditions (WT isradipine: $-25.99 \text{ mV} \pm 0.5$, $n = 12$; $p = 0.0006$).

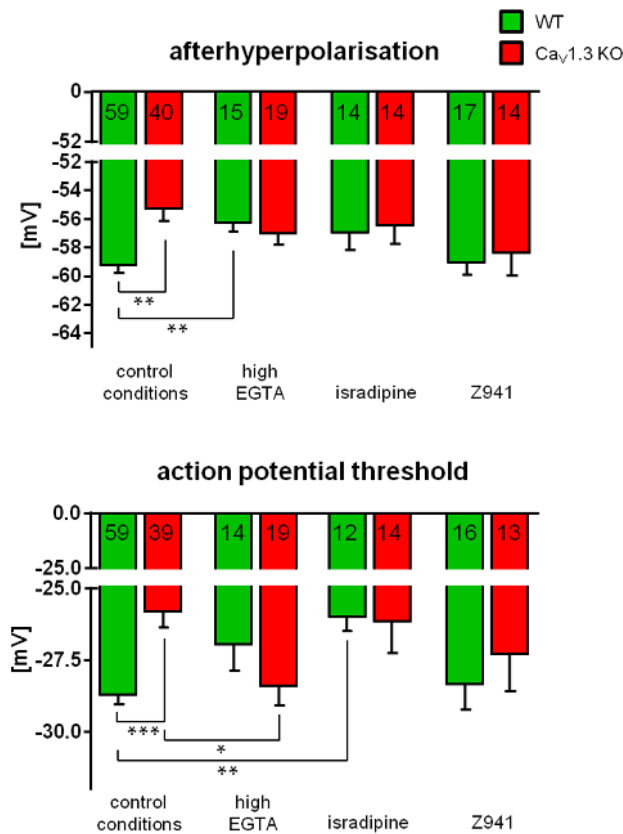


Figure 3-3: Afterhyperpolarisation and threshold of action potentials from SN DA neurons of juvenile WT and Cav1.3 KO mice

Data from whole-cell recordings; bargraphs show mean \pm SEM. WT in green. Cav1.3 KO in red. Significant differences are indicated by *. **Upper:** The (AHP) of action potentials from SN DA neurons of juvenile mice under control conditions (0.1 mM EGTA), in high EGTA (10 mM), in 300 nM isradipine and in 10 μ M Z941. Note that larger AHPs in WT seem to depend on internal Ca^{2+} and Cav1.3 KO activity. **Lower:** The action potential threshold of action potentials from SN DA neurons of juvenile mice under control conditions (0.1 mM EGTA), in high EGTA (10 mM), in 300 nM isradipine and in 10 μ M Z941.

The input resistance of SN DA neurons from juvenile WT and Cav1.3 KO mice did not show any differences under control conditions (WT: $1.4 \text{ G}\Omega \pm 0.02$, $n = 66$; Cav1.3 KO: $1.4 \text{ G}\Omega \pm 0.03$, $n = 36$). However, when recorded with high EGTA the input resistance from SN DA neurons from WT mice was significantly increased in comparison to control conditions (WT high EGTA: $1.62 \text{ G}\Omega \pm 0.5$, $n = 11$; $p = 0.0003$), also in comparison to Cav1.3 KO in high EGTA, which remained unchanged (Cav1.3 KO high EGTA: $1.43 \text{ G}\Omega \pm 0.4$, $n = 20$; $p = 0.003$). In isradipine, the input resistance of SN DA neurons from juvenile Cav1.3 KO mice was significantly decreased in comparison to control conditions (Cav1.3 KO isradipine: $1.27 \text{ G}\Omega \pm 0.05$, $n = 11$; $p = 0.0498$). For additional details see Supplemental Table 2 and Supplemental Table 3.

RESULTS

After incubation in isradipine, the maximal inducible frequency of SN DA neurons from juvenile Cav1.3 KO mice was significantly lower than that of WT (WT isradipine: 17 Hz \pm 1.8, n = 14; Cav1.3 KO isradipine: 11.5 Hz \pm 0.5; n = 14; p = 0.0036). The maximal inducible frequencies in SN DA neurons are relatively low (adult mesostriatal ~10 Hz (Lammel et al., 2008)) due to the limits imposed through a supposed depolarisation block (Tucker et al., 2012). This limit seems to depend on internal Ca²⁺, as in high EGTA recordings frequencies of about 50 Hz could be induced in SN DA neurons of WT as well as Cav1.3 KO mice. The maximal inducible frequency in SN DA neurons of WT mice was about five times (WT high EGTA: 47.1 Hz \pm 4, n = 14; p = 5.6e⁻¹⁵) and in Cav1.3 KO mice almost six times higher (Cav1.3 KO high EGTA: 61 Hz \pm 5.7, n = 16; p = 2e⁻¹³) when recorded with high EGTA compared to control conditions (WT: 14.1 Hz \pm 0.5, n = 66; Cav1.3 KO: 12.8 Hz \pm 0.6, n = 36; see Figure 3-4, Supplemental Table 2 and Supplemental Table 3).

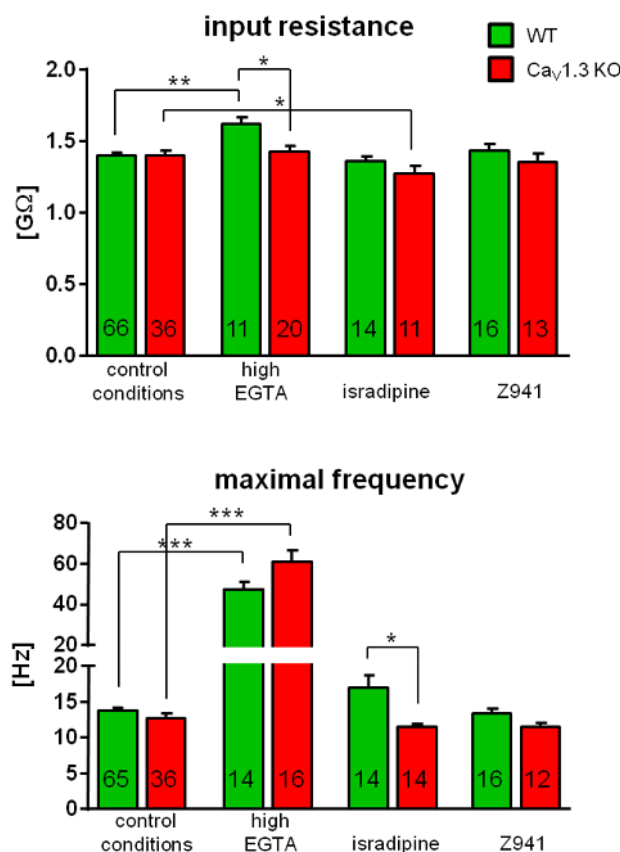


Figure 3-4: Input resistance and maximal inducible frequency of SN DA neurons from juvenile WT and Cav1.3 KO mice

Data from whole-cell recordings; bargraphs show mean \pm SEM. WT in green. Cav1.3 KO in red. Significant differences are marked by *. **Upper:** The input resistance at a current injection of -50 pA from SN DA neurons from juvenile WT and Cav1.3 KO mice under control conditions (0.1 mM EGTA), in high EGTA (10 mM), in 300 nM isradipine and in 10 μ M Z941. **Lower:** The maximal

RESULTS

inducible frequency of SN DA neurons from juvenile WT and $\text{Ca}_v1.3$ KO mice under control conditions (0.1 mM EGTA), in high EGTA (10 mM), in 300 nM isradipine and in 10 μM Z941.

3.1.2 Whole-cell comparison of SN DA neurons from adult WT and $\text{Ca}_v1.3$ KO mice

Under control conditions, significant differences could be found between SN DA neurons from adult $\text{Ca}_v1.3$ KO and WT mice for the AHP and action potential width, as well as the input resistance. In isradipine, only the action potential threshold showed a significant difference (recordings with 10 mM EGTA were not possible for adult mice due to a rapid washout of the neurons and activation of K_{ATP} channels when tested under these conditions). The frequency of pacemaker activity showed no difference between the analysed groups (WT and $\text{Ca}_v1.3$ KO under control conditions, and WT and $\text{Ca}_v1.3$ KO in isradipine; see also Supplemental Table 2 and Supplemental Table 3).

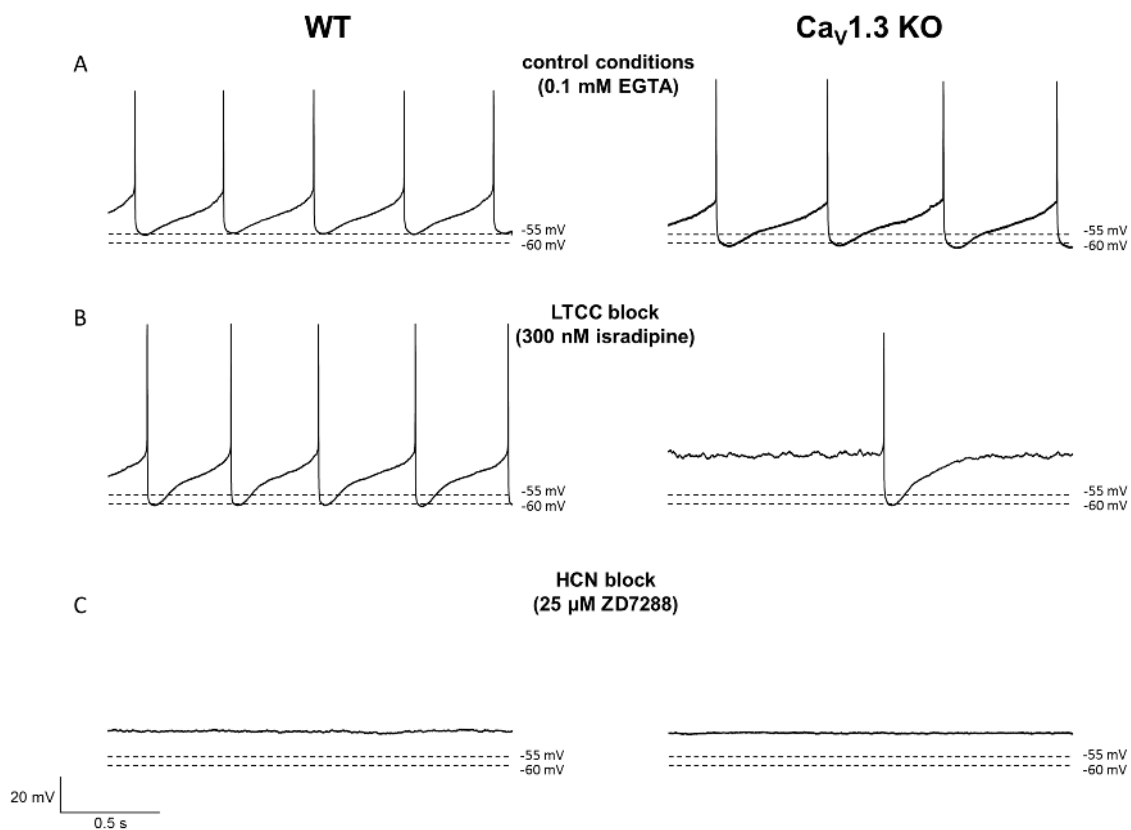


Figure 3-5: Sample traces of spontaneous activity from whole-cell recordings of SN DA neurons from adult mice

Shown are two second sample traces from whole-cell recordings of SN DA neurons from adult WT (left) and $\text{Ca}_v1.3$ KO (right) mice. Black dashed lines were added at -55 mV (average AHP of SN DA neurons from adult WT mice under control conditions, for details see 3.1.2.1) and -60 mV (average AHP of SN DA neurons from adult $\text{Ca}_v1.3$ KO mice under control conditions, for details see 3.1.2.1). **A:** Control conditions (0.1 mM EGTA). **B:** Recorded in 300 nM isradipine. Note that the majority (13 of 16) of neurons of adult $\text{Ca}_v1.3$ KO mice did not show regular pacemaker activity under these conditions (for details see 3.1.2.1). **C:** Recorded in 25 μM ZD7288.

3.1.2.1 SN DA neurons from adult Cav1.3 KO mice strongly depend on HCN channels for pacemaking and they display larger Ca²⁺ dependent AHPs compared to WT

Under control conditions or after incubation in isradipine almost all SN DA neurons of adult WT mice displayed spontaneous, regular pacemaker activity. In contrast to juvenile Cav1.3 KO, the pacemaker of SN DA neurons from adult Cav1.3 KO mice was surprisingly dramatically disturbed in the LTCC blocker isradipine and completely absent in the HCN channel blocker ZD7288 (for details see Figure 3-6). Furthermore, the majority of SN DA neurons from adult WT mice was inactive in ZD7288 – a trend that was already present in the juveniles (see 3.1.1.1). Therefore it seems that particularly in SN DA neurons from adult mice, the pacemaker activity depended on HCN channels. In adult Cav1.3 KO mice, in addition to HCN, it might also depend on other LTCCs, which would explain the effect of isradipine and hint at a compensatory role of Cav1.2 LTCCs for SN DA pacemaking in adult Cav1.3 KO mice.

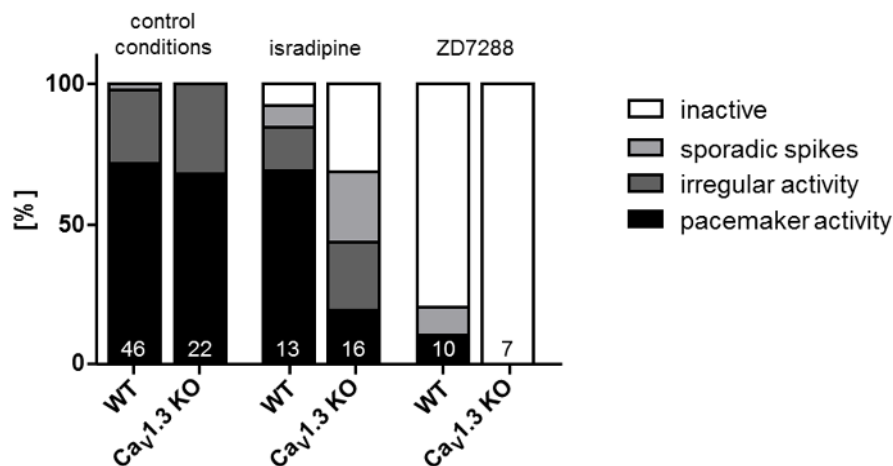


Figure 3-6: Block of HCN channels dramatically affects pacemaker activity of SN DA neurons from both adult WT and Cav1.3 KO mice; LTCC block affects Cav1.3 KO

For assessment of changes in pacemaker activity patterns, neurons were categorised into four groups based on their spontaneous activity during 25 s: pacemaker activity, irregular activity, sporadic spikes (which means there were < 10 action potentials in 25 s without a regular pattern) and inactive, when no action potentials occurred. Under control conditions 71.7 % of SN DA neurons from adult WT mice (n = 33 of 46, for details see Supplemental Table 1) and 68.2 % of Cav1.3 KO mice (n = 15 of 22) showed regular pacemaker activity, 21.1 % and 31.8 %, respectively, showed irregular activity and only 2.2 % of SN DA neurons from WT mice showed only sporadic spikes. Isradipine had only a slight effect on the pacemaker activity of SN DA neurons from WT mice (n = 13), with 69.2 % displaying pacemaker activity, 15.5 % being irregularly active, and only 7.7% showing sporadic spikes or being completely inactive. In Cav1.3 KO mice (n = 16) however, it had a surprisingly dramatic effect: only 18.75 % of neurons were active, 25 % were irregular in their activity, while the majority, 25 % and 31.25 %, showed either only sporadic spikes or were completely inactive. In ZD7288 only SN DA neurons from WT mice (n = 10) showed any activity at all, with one neuron displaying pacemaker activity and one sporadic spikes,

RESULTS

while the rest was inactive. For Cav1.3 KO ($n = 7$) all SN DA neurons recorded under HCN channel block were completely inactive.

The AHP of SN DA neurons from adult Cav1.3 KO mice was significantly bigger compared to WT under control conditions (WT: $-56.28 \text{ mV} \pm 0.8$, $n = 43$; Cav1.3 KO: $-59.28 \text{ mV} \pm 1.5$, $n = 21$; $p = 0.02$). This is in contrast to the finding for juvenile mice where the SN DA neurons from Cav1.3 KO mice displayed significant smaller AHP compared to WT (see 3.1.1.1). The AHP of SN DA neurons from adult Cav1.3 KO mice under control conditions was similar to those of both WT and Cav1.3 KO in isradipine, indicating that the AHP in adult WT SN DA neurons seemed to inversely depend on Cav1.3 LTCCs (WT isradipine: $-59.81 \text{ mV} \pm 1.3$, $n = 12$; Cav1.3 KO isradipine: $-59.3 \text{ mV} \pm 1.5$, $n = 11$; WT control conditions versus WT isradipine $p = 0.04$; see Figure 3-5, Figure 3-7 and Supplemental Table 2). This finding, in addition to the finding that blocking LTCCs with isradipine had a much bigger effect on SN DA neurons from adult Cav1.3 KO mice compared to WT (see Figure 3-6), suggests a compensatory mechanism that might involve Cav1.2 channels as calcium source in adult Cav1.3 KO mice.

No significant differences were detected for the overshoot or the sag-component at -150 mV of SN DA neurons from adult mice (see Supplemental Table 2 and Supplemental Table 3).

The action potential threshold of SN DA neurons from adult Cav1.3 KO mice was significantly lower compared to WT – but only after incubation in isradipine (WT isradipine: $-24.75 \text{ mV} \pm 0.7$, $n = 10$; Cav1.3 KO isradipine: $-28.65 \text{ mV} \pm 0.09$, $n = 8$; see Figure 3-7 and Supplemental Table 2).

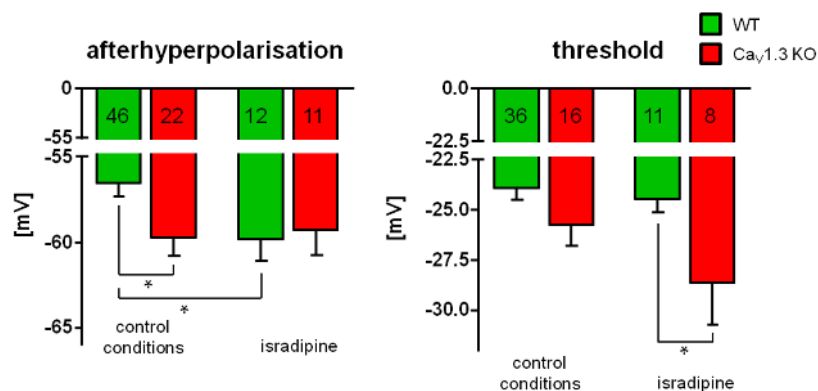


Figure 3-7: AHP and threshold of action potentials of SN DA neurons from adult WT and Cav1.3 KO mice

Data from whole-cell recordings; bargraphs show mean \pm SEM. WT in green. Cav1.3 KO in red. Significant differences are marked by *. **Right:** The afterhyperpolarisation of action potentials from SN DA neurons of adult mice under control conditions (0.1 mM EGTA), and in 300 nM isradipine. **Left:** The threshold of action potentials from SN DA neurons of adult mice under control conditions (0.1 mM EGTA), and in 300 nM isradipine.

RESULTS

The input resistance of SN DA neurons from adult Cav1.3 KO mice was significantly higher compared to WT under control conditions (WT: $1.27 \text{ G}\Omega \pm 0.04$, $n = 38$; Cav1.3 KO: $1.49 \text{ G}\Omega \pm 0.05$, $n = 19$; $p = 0.004$; see Figure 3-8), resembling the input resistance seen in SN DA neurons from juvenile mice (see Figure 3-4, Supplemental Table 2).

The maximal inducible frequency of SN DA neurons from adult Cav1.3 KO mice was significantly higher compared to Cav1.3 KO after incubation in isradipine (Cav1.3 KO control conditions: $13.55 \text{ Hz} \pm 0.9$, $n = 20$; Cav1.3 KO isradipine: $12.69 \text{ Hz} \pm 2.3$, $n = 14$; $p = 0.03$; see Figure 3-8 and Supplemental Table 2).

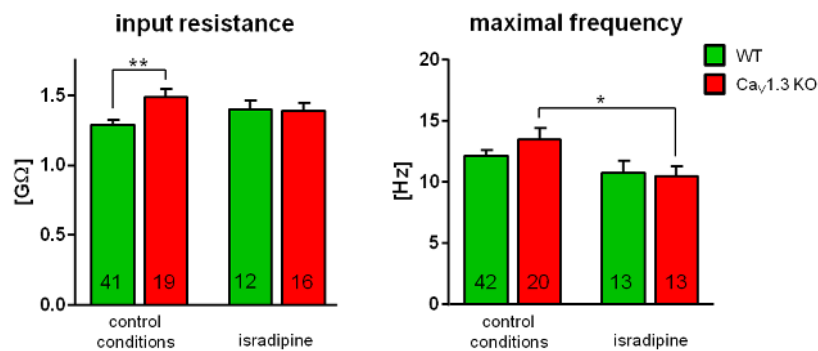


Figure 3-8: Input resistance and maximal frequency of SN DA neurons from adult WT and Cav1.3 KO mice

Data from whole-cell recordings; bargraphs show mean \pm SEM. WT in green. Cav1.3 KO in red. Significant differences are marked by *. **Right:** The input resistance of SN DA neurons from adult mice under control conditions (0.1 mM EGTA), and in 300 nM isradipine. **Left:** The maximal inducible frequency of SN DA neurons from adult mice under control conditions (0.1 mM EGTA), and in 300 nM isradipine.

3.1.3 Age-dependent differences between SN DA neurons from juvenile and adult mice

The activity of SN DA neurons from adult mice seemed to be more affected by pharmacological block of ion channels compared to that of juvenile mice. This was true for WT, and pronounced in adult Cav1.3 KO mice, whose activity was surprisingly strongly affected by LTCC blockers, which barely influenced the adult WT (see Figure 3-9).

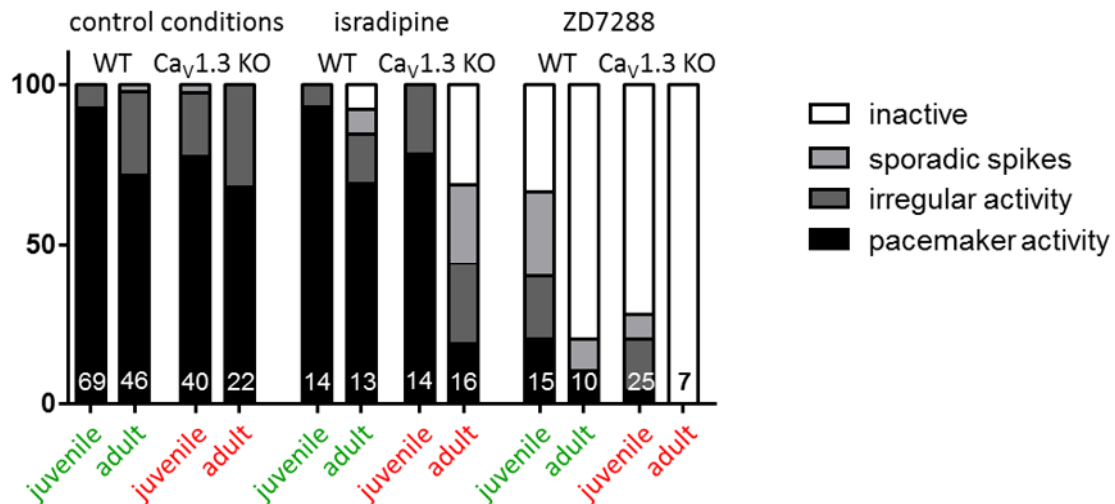


Figure 3-9: The pacemaker of SN DA neurons from adult mice is less stable compared to juvenile mice and depends particularly on HCN channel activity

For assessment of changes in pacemaker activity patterns, neurons were categorised into four groups based on their spontaneous activity during 25 s: pacemaker activity, irregular activity, sporadic spikes (which means there were < 10 action potentials in 25 s without a regular pattern) and inactive, when no action potentials occurred. Data from Figure 3-2 and Figure 3-6.

In WT mice under control conditions the threshold of action potentials from SN DA neurons of juvenile mice was significantly lower compared to adult (juvenile WT: $-28.71 \text{ mV} \pm 0.4$, $n = 36$; adult WT: $-23.9 \text{ mV} \pm 0.6$, $n = 36$, $p = 9e^{-10}$). The sag-component as well was significantly smaller in SN DA neurons from juvenile WT mice compared to adult mice (juvenile WT: $58.72 \text{ mV} \pm 0.7$, $n = 69$; adult WT: $61.45 \text{ mV} \pm 1$, $n = 46$; $p = 0.03$). The input resistance from SN DA neurons of adult WT mice on the other hand was significantly smaller compared to juvenile WT mice ($p = 0.003$, for values see chapters above or Supplemental Table 2).

The maximal frequency of SN DA neurons from juvenile WT mice was significantly higher compared to adult WT, both under control conditions (juvenile WT: $13.81 \text{ Hz} \pm 0.4$, $n = 65$; adult WT: $12.15 \text{ Hz} \pm 0.5$, $n = 42$, $p = 0.003$) and after incubation in isradipine (juvenile WT isradipine: $16.98 \text{ Hz} \pm 1.8$, $n = 14$, adult WT isradipine: $10.78 \text{ Hz} \pm 1$, $n = 13$; $p = 0.002$).

Looking at action potential width there was no significant difference when comparing SN DA neurons from juvenile Cav1.3 KO mice to WT under control conditions (WT: $3.2 \text{ ms} \pm 0.07$, $n = 59$; Cav1.3 KO: $3.39 \text{ ms} \pm 0.1$, $n = 39$). In isradipine, the action potential width of SN DA neurons from WT mice was significantly smaller compared to Cav1.3 KO (WT isradipine: $2.77 \text{ ms} \pm 0.1$, $n = 12$; Cav1.3 KO isradipine: $3.35 \text{ ms} \pm 0.2$, $n = 14$; $p = 0.01$) and to WT under

RESULTS

control conditions ($p = 0.002$; see also Figure 3-10, Supplemental Table 2 and Supplemental Table 3). In adult mice on the other hand the action potential width at threshold of SN DA neurons from adult Cav1.3 KO mice was significantly bigger compared to WT under control conditions (WT: $2.1 \text{ ms} \pm 0.07$, $n = 33$; Cav1.3 KO: $2.3 \text{ ms} \pm 0.09$; $n = 14$; see Figure 3-10 and Supplemental Table 2). Additionally, most prominent looking at this parameter was that the action potential width of SN DA neurons from juvenile mice was always significantly broader compared to that of adult mice (e.g. juvenile WT: $3.2 \text{ ms} \pm 0.07$, $n = 59$; adult WT: $2.1 \text{ ms} \pm 0.07$, $n = 34$; $p = 2.2 \times 10^{-16}$; see Figure 3-10 and for more parameters see Supplemental Table 2 and Supplemental Table 3).

When comparing the AHPs from SN DA neurons of juvenile mice with adult under control conditions, both WT and Cav1.3 KO showed significant differences. Figure 3-10 quite nicely illustrates that the AHP was a value, where acute block of LTCCs via isradipine in WT SN DA neurons “turned” them into Cav1.3 KO mice. The AHP of WT SN DA neurons from juvenile mice was significantly bigger compared to adult (juvenile WT: $-59.2 \text{ mV} \pm 0.6$, $n = 59$, adult WT: $-55.26 \text{ mV} \pm 0.9$, $n = 46$; $p = 0.01$). However, in Cav1.3 KO mice it was significantly smaller (juvenile Cav1.3 KO: $-55.25 \text{ mV} \pm 0.9$, $n = 40$; adult Cav1.3 KO: $-59.75 \text{ mV} \pm 1.1$, $n = 22$; $p = 0.003$).

Incubation in isradipine reversed the values from WT mice (juvenile WT isradipine [now like juvenile KO without isradipine]: $-56.94 \text{ mV} \pm 1.2$, $n = 14$; adult WT isradipine [now like adult KO without isradipine]: $-59.81 \text{ mV} \pm 1.3$, $n = 12$; $p = 0.053$), but had no effect on the AHPs of Cav1.3 KO mice (juvenile Cav1.3 KO isradipine: $-56.44 \text{ mV} \pm 1.3$, $n = 14$; adult Cav1.3 KO isradipine: $-59.3 \text{ mV} \pm 1.5$, $n = 11$; $p = 0.2$; see Supplemental Table 2 and Supplemental Table 3). This indicates an intricate change in modulation of the calcium-dependent AHP during post-natal maturation in SN DA neurons, and that Cav1.3 (and not another LTCC like Cav1.2 in the KO) is involved in this complex mechanism.

Combined, the age-dependent differences in action potential width at threshold and the age-dependent differences in AHPs hinted at a change in action potential shape with post-natal maturation, suggesting that different ion channels and conductances have different impact on the age-dependent action potential generation of murine SN DA neurons (Dufour et al., 2014).

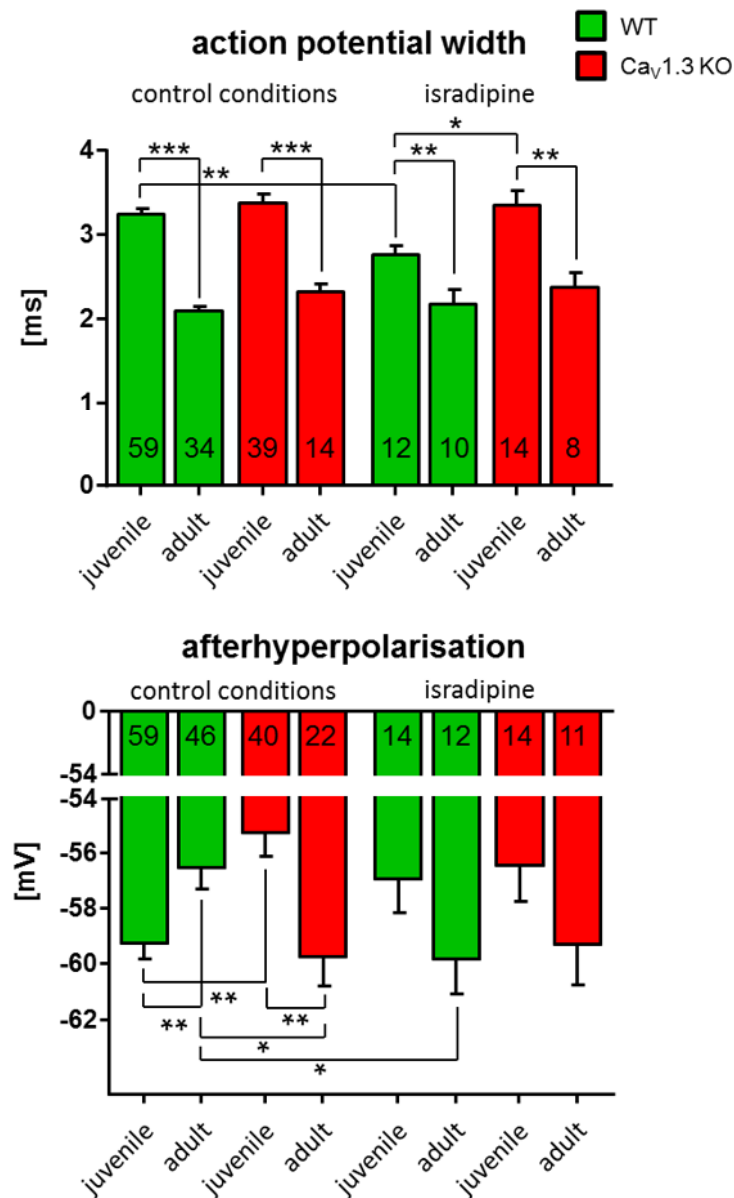


Figure 3-10: The afterhyperpolarisation and action potential width of SN DA neurons from juvenile and adult mice under control conditions and in isradipine

Data from whole-cell recordings (see also Figure 3-3 and Figure 3-7); bargraphs show mean \pm SEM. WT in green. Ca_V1.3 KO in red. Significant differences are marked by *. **Upper:** The action potential width of SN DA neurons from juvenile and adult mice under control conditions (0.1 mM EGTA) and in 300 nM isradipine. **Lower:** The AHP of SN DA neurons from juvenile and adult mice under control conditions (0.1 mM EGTA), and in 300 nM isradipine.

3.2 Pacemaker characterisation in perforated-patch recordings: Basal pacemaker frequency and its precision

Since the recordings from the whole-cell characterisation with only 25 seconds in duration, and dialysis of the cytoplasm with the internal pipette solution, were not suitable for a thorough physiological examination of the pacemaker activity of SN DA neurons, an in-depth analysis on five minute traces recorded in the perforated-patch patch-clamp configuration, which allows for more physiologic recording conditions, was performed (exception: high EGTA recordings were whole-cell recordings).

The only difference detected when comparing the mean basal frequency of spontaneous activity of SN DA neurons from juvenile and adult WT and Cav1.3 KO mice, was that the frequency from SN DA neurons of juvenile Cav1.3 KO mice was significantly lower compared to adult Cav1.3 KO mice under control conditions (juvenile Cav1.3 KO: $2.1 \text{ Hz} \pm 0.3$, $n = 9$; adult Cav1.3 KO: $3.3 \text{ Hz} \pm 0.3$, $n = 13$; $p = 0.01$). Neither pharmacological agents, nor recordings using high EGTA whole-cell had any significant effect on the mean basal frequency (see Figure 3-11 and Supplemental Table 2).

Comparing the pacemaker precision, as described by the coefficient of variation of the interspike interval (CV ISI) of basal frequency under control conditions, the CV ISI from SN DA neurons of juvenile Cav1.3 KO (juvenile Cav1.3 KO: $16.8 \% \pm 4$, $n = 9$) mice was significantly bigger compared to WT (juvenile Cav1.3^{+/+}: $8.4 \% \pm 1$, $n = 11$; $p = 0.02$) indicating a less precise pacemaker activity in the KO mouse (see Figure 3-11 and Supplemental Table 2, Supplemental Table 4 and Figure 4-1). For SN DA neurons from adult mice no significant differences were detected, indicating that Cav1.3 channels seemed to be only critical for pacemaker precision before post-natal maturation of SN DA neurons.

The only pharmacological challenge affecting the CV ISI was incubation in the T-type channel blocker Z941 which, as expected (see introduction 1.2.4), significantly increased the CV ISI of WT mice indicating, higher irregularity of the pacemaker under T-type channel block (juvenile Cav1.3^{+/+} control conditions: $8.4 \% \pm 1$, $n = 11$; juvenile Cav1.3^{+/+} Z941: $12.4 \% \pm 1$, $n = 7$; $p = 0.04$; juvenile Cav1.3 KO control conditions: $16.8 \% \pm 4$, $n = 9$; juvenile Cav1.3 KO Z941: $12.25 \% \pm 1.4$, $n = 7$; see Figure 3-11, Figure 4-1, Supplemental Table 2 and Supplemental Table 4 for more details). SN DA neurons from adult mice were not yet analysed in the T-type channel blocker.

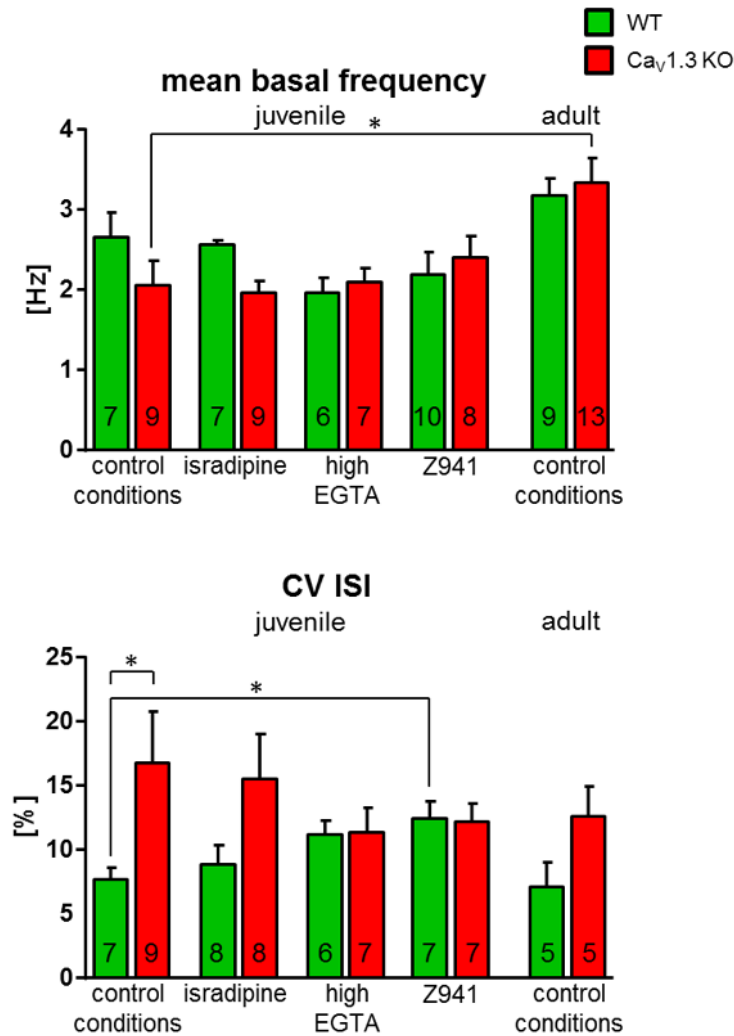


Figure 3-11: pacemaker frequency and its precision (CV ISI) of SN DA neurons from SN DA neurons of WT and Ca_v1.3 KO mice

Data from perforated-patch recordings (high EGTA in whole-cell); bargraphs show mean \pm SEM. WT (for Z941 Ca_v1.3^{+/+}, everything else C57BL/6) in green. Ca_v1.3 KO in red. Significant differences are marked by *. **Upper:** The mean membrane potential of SN DA neurons from juvenile and adult mice under control conditions (0.1 mM EGTA) and in 300 nM isradipine, recorded with high EGTA and in Z941. **Lower:** The CV ISI of SN DA neurons from juvenile and adult mice under control conditions (0.1 mM EGTA), and in 300 nM isradipine, recorded with high EGTA and in Z941. Under control conditions the CV ISI of Ca_v1.3 KO mice is significantly bigger only compared to Ca_v1.3^{+/+} not C57BL/6 – note that the graph does show the C57BL/6 value with the *; for statistical details see Figure 4-1, Supplemental Table 2 and Supplemental Table 4.

3.3 Analysis of the Ca^{2+} dependent dopamine D2-autoreceptor response in SN DA neurons

3.3.1 Kinetics of D2-AR responses in SN DA neurons from WT and Cav1.3 KO mice

A link between Cav1.3 LTCC function, free internal Ca^{2+} and the degree of desensitisation of dopamine D2-AR responses in SN DA neurons has recently been discovered in our group (Dragicevic et al., 2014).

The whole-cell data of this work, as described, pointed to altered internal Ca^{2+} signalling due to compensation of loss of Cav1.3 with other calcium channels in SN DA neurons from Cav1.3 KO mice (see 4.2.3). Therefore, it was examined whether the general loss of Cav1.3 had effects on the D2-autoreceptor response of the SN DA neurons. To test this, SN DA neurons from juvenile or adult WT (C57BL/6 or Cav1.3^{+/+}, which did not show any significant differences in their D2-AR response or their pacemaking parameters, for details see Supplemental Table 2, Supplemental Table 4 and Figure 4-1) or Cav1.3 KO mice were analysed in 40 minute recordings in perforated-patch recordings (control conditions, to contain intracellular integrity and signalling). During the 40 minute recording, dopamine was applied for 15 minutes on spontaneously active SN DA neurons and then washed out.

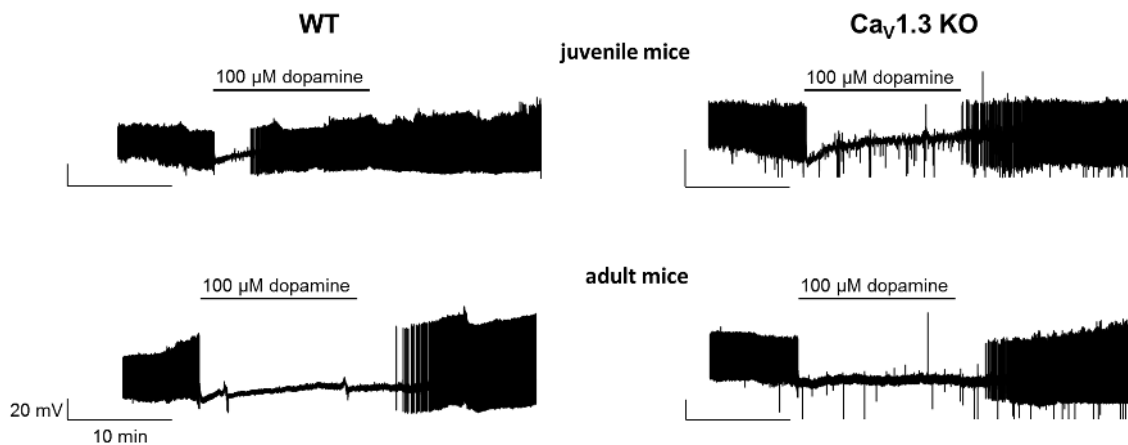


Figure 3-12: Sample traces of SN DA neurons from juvenile and adult WT and Cav1.3 KO mice show prominent desensitisation of D2-AR in juvenile WT mice, that is absent in adult mice, as well as juvenile Cav1.3 KO

Shown are 40 minute sample traces from perforated-patch recordings of SN DA neurons from juvenile (upper) WT (left) and Cav1.3 KO (right) and adult (lower) mice recorded under control conditions. Scalebars always show 20 mV/10 min and were adjusted for each graph. The duration of dopamine application is marked in the graph by black bars. Note the maturation of the dopamine D2-AR response in WT (loss of desensitisation in adult SN DA) that is absent in SN DA neurons from Cav1.3 KO mice (loss of desensitisation in juvenile and adult SN DA neurons from Cav1.3 KO mice).

RESULTS

Next, to address the Ca^{2+} sensitivity of D2-AR response in SN DA neurons, similar experiments were performed for juvenile mice with high EGTA in the pipette solution (10 mM EGTA, whole-cell for general Ca^{2+} buffering) and under pharmacological challenge with 300 nM isradipine (perforated-patch, to address LTCC contribution), or 10 μM Z941 (perforated-patch, to address T-type channel contribution). Sample 40 minute traces from SN DA neurons of each group are shown in Figure 3-12 and Figure 3-13 and data is presented in the following chapters.

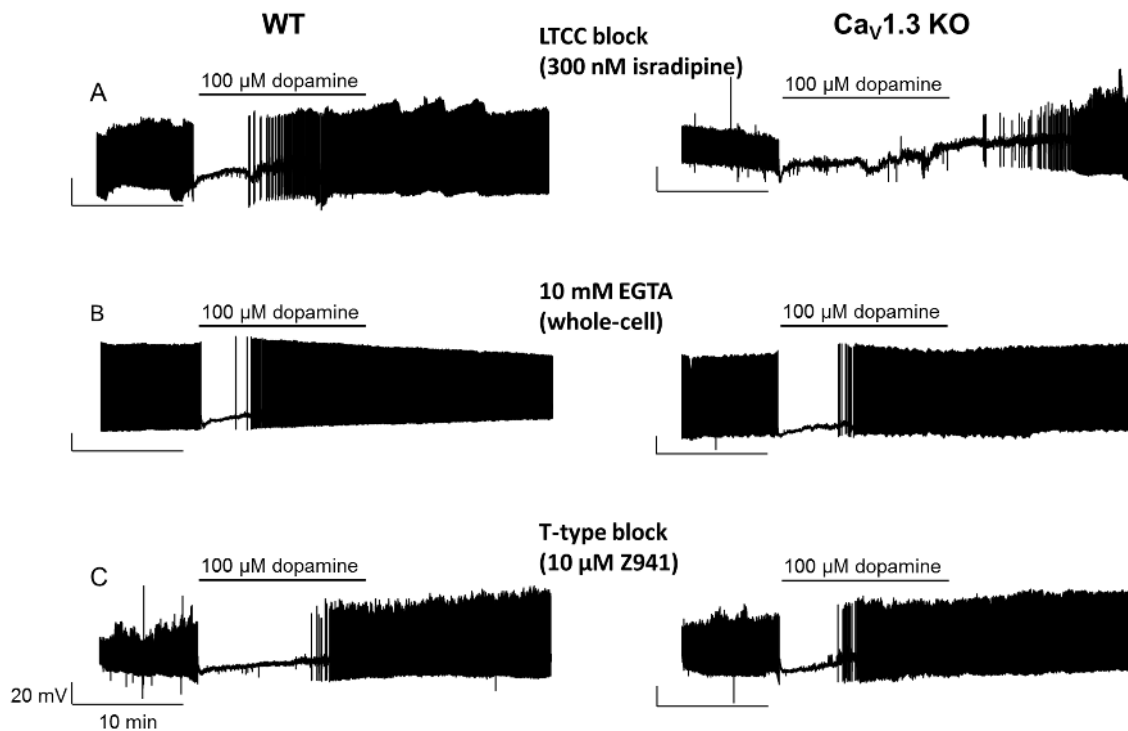


Figure 3-13: Non-desensitising D2-AR responses in SN DA neurons from juvenile Cav1.3 KO mice depend on T-type calcium channel function

Shown are 40 minute sample traces from perforated-patch (and for 10 mM EGTA whole-cell) recordings of SN DA neurons from juvenile WT (left, C57BL/6, except for Z941 which shows Cav1.3^{+/+}) and Cav1.3 KO (right) mice. Scalebars always show 20 mV/10 min and were adjusted for each graph. The duration of dopamine application is marked in the graph by black bars. **A:** Recorded in 300 nM isradipine. **B:** Recorded with 10 mM EGTA in the pipette solution (whole-cell). **C:** Recorded in 10 μM Z941. Not that recordings with high EGTA as well as with the T-type blocker induced WT-like D2-AR in juvenile Cav1.3 KO.

3.3.2 The D2-AR response from juvenile WT mice displays prominent dopamine-dependent desensitisation, whereas juvenile Cav1.3 KO mice display adult-like, non-desensitising D2-AR responses

Figure 3-14 shows the frequency plots (normalised pacemaker activity plotted over time for each minute, see also 2.2.4.1) of SN DA from juvenile and adult C57BL/6 and Cav1.3 KO mice recorded under control conditions (perforated-patch). Whereas in SN DA neurons from juvenile WT mice activity was already restored while dopamine was still present, demonstrating a

RESULTS

desensitisation of the D2-AR, this was not the case for adult WT mice (significant differences in activity in minutes 16–32, 38–40). In contrast, in $\text{Cav}1.3$ KO mice, non-desensitising D2-AR responses were already observed in SN DA neurons from juvenile mice (and not only adult mice; see Figure 3-14). Significant differences between SN DA neurons from juvenile C57BL/6 and $\text{Cav}1.3$ KO mice can be found in minutes 18–33, 39–40.

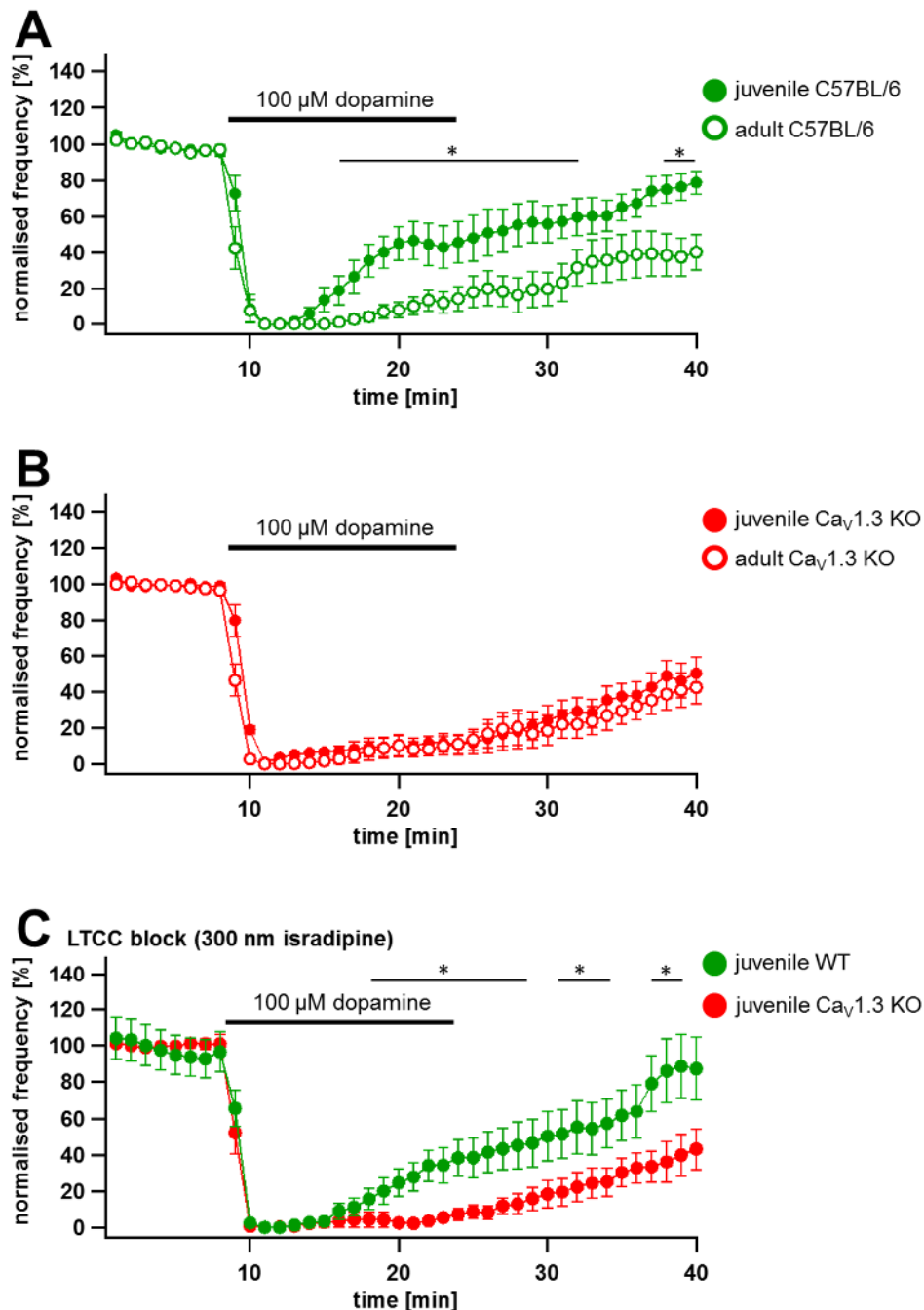


Figure 3-14: The D2-autoreceptor response from juvenile WT mice shows prominent receptor desensitisation, whereas juvenile $\text{Cav}1.3$ KO mimics those from adult mice

Shown are frequency plots (see 2.2.4.1 for details) with the normalised frequency of each minute plotted against time, mean \pm SEM; the duration of dopamine application is marked in the graph. Dark green juvenile WT, red juvenile $\text{Cav}1.3$ KO, hollow dark green adult WT, hollow red adult

Cav1.3 KO. Significant differences are indicated by *. **A:** Frequency plot of SN DA neurons from juvenile (n = 5–7) and adult WT (n = 7–9) mice. Significant differences in minutes 16–32, 38–40. **B:** Frequency plot of SN DA neurons from juvenile (n = 7–9) and adult (n = 8–13) Cav1.3 KO mice; there are no significant differences. Significant differences between juvenile WT and Cav1.3 KO in minutes 18–33, 39–40. **C:** Frequency plot of SN DA neurons from juvenile WT (n = 5–8) and Cav1.3 KO (n = 8–9) mice recorded in 300 nM isradipine. Significant differences in minutes 18–29, 31–34, 37–39.

3.3.3 Isradipine has no effect on the D2-AR response of juvenile WT or Cav1.3 KO mice

To test if acute block of LTCCs could induce similar changes in the D2-AR response as seen in SN DA neurons with general constitutive loss of Cav1.3 in juvenile KO mice, juvenile brain slices were incubated in 300 nM isradipine, which affected neither mean basal frequency nor CV ISI of SN DA neurons (see 3.2 and Figure 3-11). Surprisingly, incubation in isradipine had no effect on the kinetic of the D2-AR response of SN DA neurons from juvenile WT or Cav1.3 KO mice compared to control conditions either (significant differences between Cav1.3 KO and WT in minutes 18–29, 31–34, 37–39, see Figure 3-15). Most importantly, acute LTCC block by isradipine did not induce a non-desensitising D2-AR response in SN DA neurons from juvenile WT mice, like the chronic loss of Cav1.3 did in general Cav1.3 KO mice. These findings indicate that the loss of Cav1.3 alone does not explain the changes seen in D2-AR response in SN DA neurons from juvenile Cav1.3 KO mice, and instead point to a compensatory phenotype in juvenile KO mice, which seems not to be mediated by Cav1.2 channels (as whole-cell data might suggest).

3.3.4 Buffering internal Ca²⁺ with 10 mM EGTA induces WT-like, desensitising D2-AR responses in SN DA neurons from juvenile Cav1.3 KO mice

Since LTCC block with isradipine did neither alter the non-desensitising phenotype of the D2-AR of SN DA neurons from juvenile Cav1.3 KO mice, nor induce it in SN DA neurons from WT mice, next it was examined whether internal Ca²⁺ was necessary at all for the D2-AR response of SN DA neurons from juvenile WT and Cav1.3 KO mice. 10 mM EGTA in the pipette solution were used in 40 minute whole-cell recordings to buffer internal Ca²⁺, which did not change mean basal frequency nor CV ISI of the recorded SN DA neurons in comparison to perforated-patch recordings (see 3.2).

Buffering internal Ca²⁺ indeed affected the D2-AR response: it induced WT-like desensitisation in SN DA neurons from juvenile Cav1.3 KO mice and left the WT unaffected (see Figure 3-15; significant differences between high EGTA compared to control conditions for Cav1.3 KO in minutes 15–27). This finding suggests that loss of Cav1.3 is not the cause for

the altered D2-AR response in SN DA neurons from juvenile Cav1.3 KO mice, but that it is rather due to altered internal Ca²⁺ signalling.

3.3.5 The T-type blocker Z941 induces WT-like, desensitising D2-AR responses in SN DA neurons of juvenile Cav1.3 KO mice

Subsequently to the EGTA-buffering experiments, next the possible compensatory calcium source that might be responsible for the adult-like non-desensitising D2-AR responses in juvenile Cav1.3 KO mice was addressed. As described in 1.2.3, T-type channels deliver the trigger Ca²⁺ for SK channel activity, which determines the AHP in SN DA neurons. In view of the described complex changes in calcium-dependent AHP in SN DA neurons from juvenile and adult Cav1.3 KO mice (see 3.1.1.1 and 3.1.2.1), it was therefore addressed whether T-type channel activity might be the compensatory calcium source in SN DA neurons of juvenile Cav1.3 KO mice affecting D2-AR responses.

Indeed, after incubation in 10 µM of the T-type channel blocker Z941, the D2-AR response of SN DA neurons from juvenile Cav1.3 KO mice now showed WT-like receptor desensitisation, while the WT D2-AR response was not altered (significant differences in activity between juvenile Cav1.3 KO control conditions and Cav1.3 KO Z941 in minutes 20--24, 26, 32-33, 35--40, see Figure 3-15). This indicates that T-type calcium channels compensate for the loss of Cav1.3 in SN DA neurons from Cav1.3 KO mice, and that this compensation alters the local internal free Ca²⁺ and thus changes the D2-AR response.

3.3.6 Adult-like, non-desensitising D2-AR responses of SN DA neurons from juvenile Cav1.3 KO mice depend on interaction of NCS-1 with D2-ARs

We have already shown that the interaction of the neuronal calcium sensor NCS-1 with the D2-AR prevents D2-AR desensitisation in juvenile WT SN DA neurons (Dragicevic et al., 2014). Thus next it was tested if the internal Ca²⁺ and T-type channel dependent, non-desensitising, adult-like D2-AR response in SN DA neurons from juvenile Cav1.3 KO mice also depended on NCS-1/D2-AR interaction. We used 10 µM of a peptide that prevents NCS-1/D2-AR interactions (DNIP) or its scrambled version srDNIP as control, which neither affected basal frequency nor CV ISI (Supplemental Table 2 G and Supplemental Table 4) of the neurons.

RESULTS

Similar to the T-type channel blocker, DNIP indeed induced WT-like D2-AR desensitisation in SN DA neurons from juvenile $\text{Ca}_v1.3$ KO mice, while srDNIP had no effect on the D2-AR response (see Figure 3-15; significant differences between DNIP and srDNIP in minutes 15–18, 21–25; significant differences between $\text{Ca}_v1.3$ KO control conditions and $\text{Ca}_v1.3$ KO DNIP in minutes 16–18).

This demonstrated that the non-desensitising D2-AR response seen in SN DA neurons from juvenile $\text{Ca}_v1.3$ KO mice depends on calcium-dependent NCS-1/D2 interaction, which seemed to be more pronounced in $\text{Ca}_v1.3$ KO mice due to their compensatory T-type channel activity.

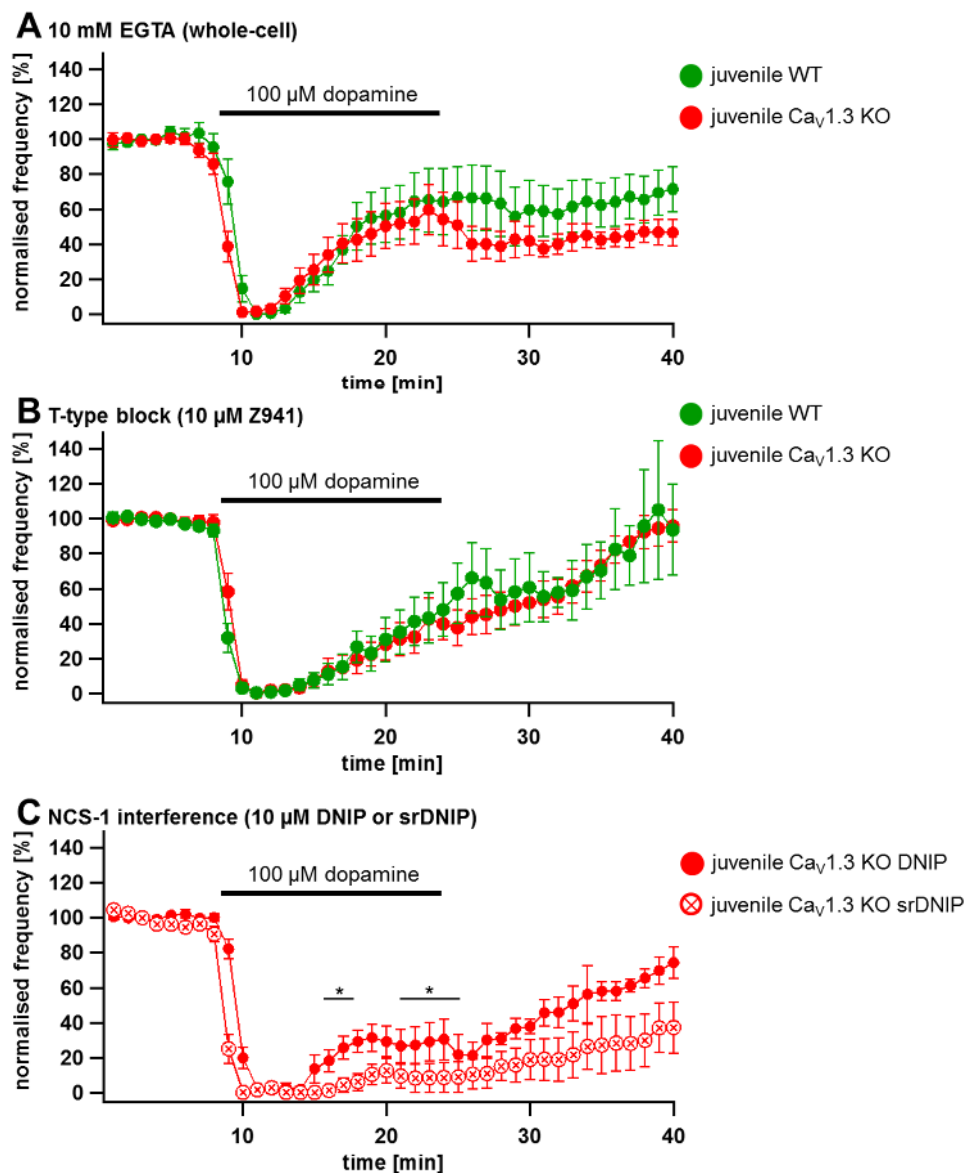


Figure 3-15: Non-desensitising D2-AR responses in SN DA neurons from juvenile $\text{Ca}_v1.3$ KO mice depend on internal Ca^{2+} , T-type calcium channels, and calcium-dependent NCS-1/D2-AR interaction

RESULTS

Shown are frequency plots (see 2.2.4.1 for details) with the normalised frequency of each minute plotted against time, mean \pm SEM; the duration of dopamine application is marked in the graph. Green WT (C57BL/6 with the exception that graph C shows $\text{Ca}_v1.3^{+/+}$), red $\text{Ca}_v1.3$ KO. Significant differences are indicated by *. **A:** Frequency plot of SN DA neurons from juvenile WT ($n = 8$) and $\text{Ca}_v1.3$ KO ($n = 6-8$) recorded with 10 mM EGTA in the pipette solution (whole-cell). **B:** Frequency plot of SN DA neurons from juvenile WT ($n = 5-10$) and $\text{Ca}_v1.3$ KO ($n = 7-8$) mice recorded with 10 μM Z941. **C:** Frequency plot of SN DA neurons from juvenile $\text{Ca}_v1.3$ KO mice recorded in DNIP ($n = 1-11$) and srDNIP ($n = 5-10$). Significant differences in minutes 15–18, 21–25. Note that DNIP also seemed to destabilise the recordings during (and after) dopamine application in perforated-patch and in on-cell recordings, as evidenced by the high deviation between data points.

4 DISCUSSION

4.1 Methodical aspects and minor findings

4.1.1 Patch-clamp configurations: whole-cell vs. perforated-patch/on-cell recordings

The patch-clamp recordings described in this thesis have been conducted in the whole-cell (for basal electrical/biophysiological characterisation) and the perforated-patch or on-cell configuration (for analysis of neurons under metabolic intact physiological signalling conditions). The advantage of the whole-cell configuration, besides being much easier and quicker to establish, is that it provides the possibility to control the inner cell milieu through the internal pipette solution. Thus biophysical properties of neurons can be analysed under controlled signalling conditions. Whole-cell recordings offer a high resolution of action potentials and due to lower R_s (series resistance) also offer the possibility to conduct and properly resolve voltage-clamp recordings of currents with faster kinetics.

The perforated-patch configuration on the other hand allows long-term recordings under physiological conditions without perturbing internal signalling cascades, leaving thereby the physiological profile of the cell intact. In contrast to the whole-cell configuration it is time consuming (approx. 10–15 minutes) to achieve a stable perforation of the membrane without breaking into whole-cell, and input resistances are generally too high to perform voltage-clamp measurements. The on-cell configuration offers the same advantage as the perforated-patch configuration but is less time consuming; however, perforated-patch recordings have an added advantage over on-cell recordings because it is possible to inject current. This allows – depending on the quality of the perforation – for direct examination of for instance the sag-component of a neuron after the recording for confirmation of the SN DA phenotype of the neuron, whereas neurons recorded with the on-cell configuration needed to be repatched for whole-cell characterisation, which equalised time costs between the recording methods. Perforated-patch was however the preferred method because directly observing action potentials (in contrast to the action potential derived changes in currents in on-cell recordings) made it easier to see irregularities during the recording and interfere if necessary.

4.1.2 Use of 100 μ M dopamine

In this work 100 μ M dopamine was used via bath application to study the dopamine D2-AR response of SN DA neurons in brain slices. This concentration is relatively high and does

probably not mimic the physiological kinetics and variable concentrations of somatodendritically released dopamine (Chen et al., 2011; Rice et al., 2011). The half maximal effective concentration (EC_{50}) of dopamine for D2-AR mediated activity inhibition of SN DA neurons from juvenile mice under the here described recording conditions is $\sim 6.5 \mu M$ (Dragicevic et al., 2014). We used $100 \mu M$ as a saturating concentration to ensure full activation of dopamine receptors (i) because once solved dopamine oxidises – especially in a gassed solution where oxygen is permanently added – as can be seen by a slight rose-brown tinge of the solution after some time has passed, which reduces the amount of actively working compound, and (ii) to reduce diffusion times and ensure a rapid wash-in on the brain slice. Alternative approaches would be rapid direct application of dopamine (Ford et al., 2009), or instead to evoke physiological dopamine release by electrical stimulation – an approach that has been utilised particularly for analysis of SN DA neurons in horizontal brain slices (Beckstead et al., 2007; Beckstead et al., 2004). Coronal slices as used in this work however offer the possibility of direct and easy comparison of SN DA and VTA DA neurons.

4.1.3 Comparing of SN DA neurons from C57BL/6 vs. Cav1.3^{+/+} and Cav1.3 KO mice: strain differences?

The Cav1.3 KO mice used for this work were crossed back twice (see for details 2.1.1) into C57BL/6 and therefore definitely of mixed background, since it is assumed that only after ten backcrosses a 99.9 % C57BL/6 background is obtained and even then most likely the so-called “flanking region” of the ablated gene often still contains unknown percentages of sv129 genetic material (Eisener-Dorman et al., 2009). For this reason parameters from C57BL/6 were compared to Cav1.3^{+/+}, to exclude any electrophysiological differences due to background or gene flanking issues. No significant differences in basal electrophysiologic parameters were detected when comparing Cav1.3^{+/+} to C57BL/6. Thus data was pooled and for pharmacological tests only C57BL/6 were used (with the exception of Z941) for comparison against the Cav1.3 KO values, for practical reasons, i.e. breeding capacities in our animal facility.

The D2-AR response kinetic of SN DA neurons from Cav1.3^{+/+} mice compared to C57BL/6 (Figure 4-1) were not completely identical. However, there were no statistically significant differences detected. This could be a background effect, but it is as likely that the variations are caused by fluctuations in the complex 40 minutes long perforated-patch recordings. Many neurons of the D2-AR desensitisation phenotype could not be recorded until the end of the 40 minute period because they destabilised and were lost earlier on (for instance looking at

DISCUSSION

$\text{Ca}_v1.3^{+/+}$ all of the 10 neurons that were not recorded until minute 40 had a desensitising D2-AR response; six were even only silenced by the dopamine application for five minutes or less). Numbers were increased in an attempt to outbalance this issue. This higher rate of loss of the recording for desensitising neurons is a trend that was observed in all recorded groups, but only seemed to have a strong influence on the frequency plot for $\text{Ca}_v1.3^{+/+}$ mice.

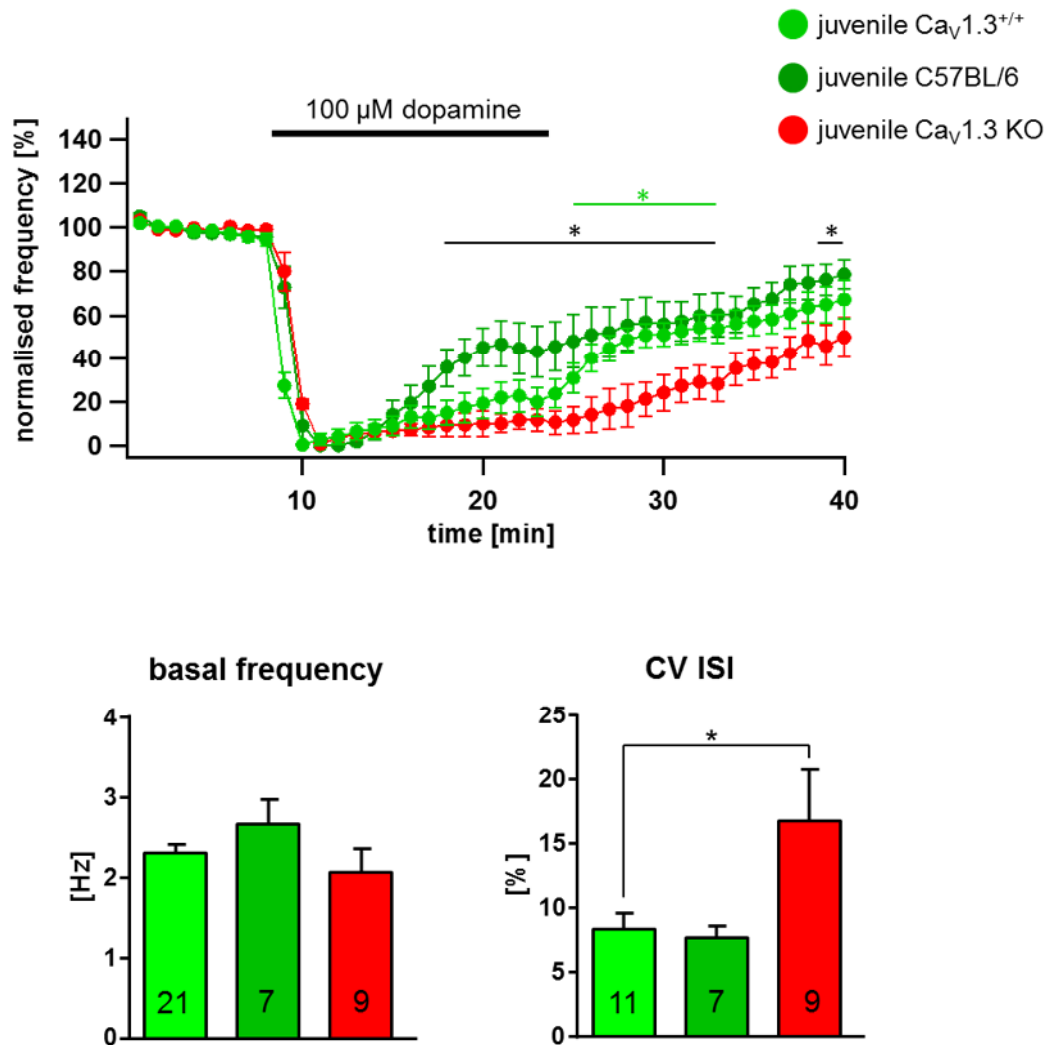


Figure 4-1: Comparison of D2-AR, basal frequency and CV ISI of SN DA neurons from juvenile $\text{Ca}_v1.3^{+/+}$ and C57BL/6 mice

Upper: Shown is a frequency plot (see 2.2.4.1 for details) of SN DA neurons from juvenile mice, recorded under control conditions (perforated-patch), mean \pm SEM; the duration of dopamine application is marked in the graph. Bright green juvenile $\text{Ca}_v1.3^{+/+}$, dark green juvenile C57BL/6, red juvenile $\text{Ca}_v1.3$ KO. Significant differences between C57BL/6 and $\text{Ca}_v1.3$ KO are marked with * in black (minutes 18–33, 39–40); significant differences between $\text{Ca}_v1.3^{+/+}$ and $\text{Ca}_v1.3$ KO are marked with * in bright green (26–33). There are no significant differences between $\text{Ca}_v1.3^{+/+}$ and C57BL/6. **Lower:** Bargraphs show mean \pm SEM, significant differences marked with *; n's given in each bar. **Left:** Basal frequency of SN DA neurons from juvenile $\text{Ca}_v1.3^{+/+}$, C57BL/6 and $\text{Ca}_v1.3$ KO. There are no significant differences between C57BL/6 and $\text{Ca}_v1.3^{+/+}$. **Right:** CV ISI of SN DA neurons from juvenile $\text{Ca}_v1.3^{+/+}$, C57BL/6 and $\text{Ca}_v1.3$ KO. There are no significant

differences between C57BL/6 and Cav1.3^{+/-}; for information on the CV ISI see 3.2 and Supplemental Table 2).

4.1.4 Comparison of SN DA neurons from juvenile WT and Cav1.3 KO mice at different temperatures: full compensation at 36°C?

All data for this work was recorded at 33°C ± 1 temperature in the bath (not at room temperature) for a more physiological setting. As a compensatory phenotype in Cav1.3 KO SN DA neurons was detected, it was also tested if this compensation might be “perfect”, i.e. not visible at the even more physiological bath temperature of 36°C (at which slices unfortunately remain less long vital). Indeed, when recorded at 36°C, no significant differences were detected between WT and Cav1.3 KO mice (neither for basal electrophysiologic parameters nor the D2-AR response, see Figure 4-2). This also underlines that the compensatory mechanism in the general Cav1.3 KO mouse by T-type calcium channels fully compensates for the loss of Cav1.3 LTCCs in SN DA neurons. Functional compensation is a known drawback of general KO mice (Picciotto and Wickman, 1998). At 36°C the AHP of juvenile Cav1.3 KO mice was significantly bigger compared to 33°C, thus this difference between SN DA neurons of WT and Cav1.3 KO mice was absent at 36°C (see Supplemental Table 2 and Supplemental Table 3). This apparently at physiological temperatures optimised compensatory mechanism likely also explains why neither Cav1.3 KO mice nor the patients suffering from SANDD have so far been noticed to show obvious irregularities and impairments in processes that would need the D2-AR response of SN DA neurons.

At 36°C also the mean basal frequency of SN DA neurons from juvenile mice was significantly increased in comparison to 33°C in Cav1.3 KO mice; for WT it is not a significant difference ($p = 0.055$, see Supplemental Table 2, Supplemental Table 4 and Figure 4-2). The increased frequency could be caused by the vanilloid transient receptor potential channels TRPV3 and TRPV4. These temperature sensitive cation channels have been shown not only to be expressed in SN DA neurons, but also to be responsible for an increase in frequency upon temperature increase and vice versa in these neurons (Guatteo et al., 2005). However, it is also likely that the frequency is simply increased according to thermodynamics and faster reaction kinetics at higher temperatures, which accordingly affect gating properties of the voltage-gated ion channels that define pacemaker generation and its frequency in SN DA neurons (Hille, 2001).

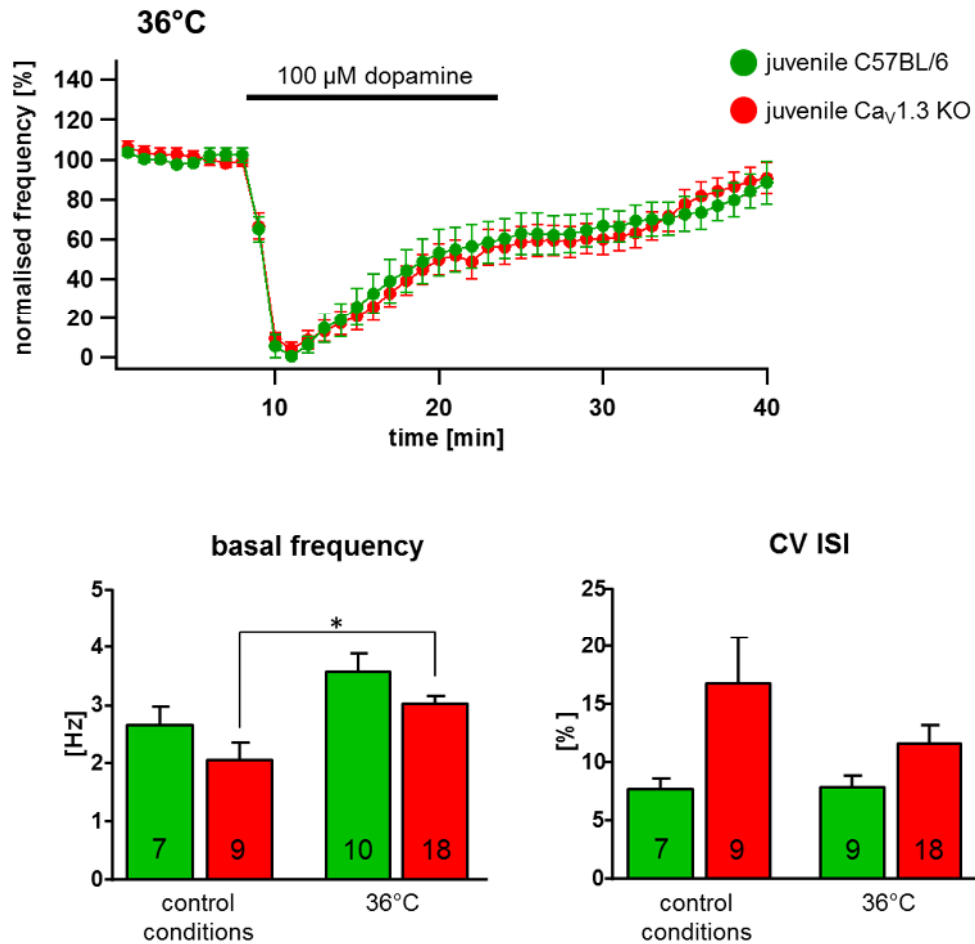


Figure 4-2: Comparison of D2-AR, basal frequency and CV ISI of SN DA neurons from WT and Cav1.3 KO mice under control conditions and at 36°C

Upper: Shown is a frequency plot (see 2.2.4.1 for details) of SN DA neurons from juvenile mice, recorded with 36°C (perforated-patch), mean \pm SEM; the duration of dopamine application is marked in the graph. Green juvenile C57BL/6, red juvenile Cav1.3 KO. There are no significant differences between WT and Cav1.3 KO when recorded at 36°C. **Lower:** Bargraphs show mean \pm SEM, significant differences marked with *. **Left:** Basal frequency of SN DA neurons from juvenile C57BL/6 and Cav1.3 KO, recorded under control conditions or at 36°C. The frequency of SN DA neurons from juvenile Cav1.3 KO mice recorded at 36°C is significantly ($p = 0.003$) bigger compared to control conditions; for WT the difference is not significant ($p = 0.055$). **Right:** CV ISI of SN DA neurons from juvenile C57BL/6 and Cav1.3 KO recorded under control conditions and at 36°C. There are no significant differences.

4.1.5 Capacitance difference between SN DA neurons from juvenile versus adult mice

A difference that could be found in all groups when comparing SN DA neurons from juvenile mice with those from adult mice is the significantly smaller capacitance of adult SN DA neurons (e.g. juvenile WT: $56.48 \text{ pF} \pm 1.8$, $n = 69$; adult WT: $34.26 \text{ pF} \pm 1.4$, $n = 46$; $p = 2.9 \times 10^{-16}$, see Supplemental Table 2 and Supplemental Table 3). The capacitance was examined to have an approximation of size of the neuron. However, since neurons are no ideal model spheres – but instead have complex dendrites – this approach has its limitations. Neurons from adult brains

have a bigger dendritic tree, which can't be fully clamped, compared to juvenile, thus the values from juvenile mice cannot be directly compared to those from adult mice.

4.1.6 Action potential threshold and width at threshold

As shown in chapters 3.1.1.1 and 3.1.2.1 there are several significant differences in action potential threshold and action potential width at threshold to be found when comparing all the different groups from either juvenile or adult WT and Cav1.3 KO mice. However, this analysis of the action potential shape was carried out in a subjective manner that relied on visual identification of the threshold when zoomed in on the action potential (a more objective test that involved the second derivative of the action potential to determine the threshold (Lammel et al., 2008) was also tested but didn't always result in meaningful values and was then rejected).

With this methodological caveat in mind, there is still one consistent difference: the action potential width at threshold is always significantly broader in SN DA neurons of juvenile mice in comparison to adult mice. This indicates that action potentials from SN DA neurons of juvenile mice have a different shape and follow a different kinetic, which is probably due to a qualitative or quantitative difference in the set of involved ion channels in course of post-natal maturation (see also 4.2.3).

4.1.7 Differences in sag-component and overshoot

The sag-component at a current injection to -150 mV was significantly bigger in SN DA neurons of juvenile Cav1.3 KO mice in comparison to the WT under control conditions (see Supplemental Table 2 and Supplemental Table 3). It is only a very small difference in the values that was nonetheless statistically significant. However, for evaluating a possible biological significance, one has to keep in mind that the sag-component was one of the selection criteria for typical SN DA neurons for statistical analysis (see 2.2.4), as VTA DA neurons for instance display a less prominent HCN channel mediated sag-component (Lammel et al., 2008). In addition, this parameter is subject to some variations since not all neurons always did exactly reach -150 mV through the current injections, some went below it, and others stayed slightly above it. Thus, the sag-component is only a qualitative, not a quantitative assessment of HCN-currents. HCN-currents were addressed more direct in preliminary voltage-clamp recordings, but so far there are no obvious hints for altered HCN channel activity (amplitude of the I_h current or area under the curve) in SN DA neurons of Cav1.3 KO mice (see Supplemental Table 2 and

Supplemental Table 3). This question however is of particular importance, as a switch from a Cav1.3 driven pacemaker to an HCN driven pacemaker in SN DA neurons from Cav1.3 KO mice has been reported previously (Chan et al., 2007). The amount of current that had to be injected to reach -150 mV is only significantly smaller in SN DA neurons from juvenile WT mice when recorded with high EGTA, which is with high likelihood due to the significantly increased input resistance under those conditions (see 3.1.1.1 and Figure 3-4).

Other significant differences that are of questionable physiological relevance were found for the overshoot, which was significantly smaller in SN DA neurons from juvenile WT mice when recorded with high EGTA compared to control conditions. It is possible that this also was influenced by the above mentioned significantly different input resistance when recorded with high EGTA. The overshoot of SN DA neurons from juvenile Cav1.3 KO mice when recorded with Z941 was also significantly smaller compared to control conditions.

4.1.8 Side effects of the functional DNIP peptide

A noticeable phenomenon in experiments with the DNIP peptide was the destabilisation of the recordings during (and after) dopamine application, when the functional DNIP peptide – not the scrambled DNIP peptide – was used on SN DA neurons from juvenile Cav1.3 KO mice, leading to a lot of prematurely stopped recordings (see the big error bars in Figure 3-15). A colleague did similar DNIP-recordings on SN DA neurons from juvenile C57BL/6 mice and did not observe this instability. Thus it might be due to an unclear interaction of the DNIP peptide with something specific for the Cav1.3 KO mouse. Additionally, during experiments with DNIP, from time to time random frequency increases in neurons for short periods of time were observed (usually too short to affect the average frequency or pacemaker precision significantly, but definitely noticeable). These points both indicate that there might be side effects of the DNIP peptide that manifest particularly in SN DA neurons from Cav1.3 KO mice.

4.2 Main findings: differences between SN DA neurons from juvenile and adult WT and Cav1.3 KO mice

4.2.1 Buffering internal Ca^{2+} with 10 mM high EGTA disables the depolarisation block in SN DA neurons of juvenile mice

It has been well established that murine SN DA neurons have a relatively low pacemaker frequency (between 0.5 to 5 Hz *in vitro*, *in vivo* slightly higher, reviewed in (Liss and Roeper, 2010)) and that their frequency *in vitro* will not increase greatly above ~10 Hz (Grace and Bunney, 1984; Lammel et al., 2008) even when stimulated via current injections. Instead, when depolarised further, neurons will cease all activity due to a so-called depolarisation block that is thought to be caused by the increased number of inactivated ttx-sensitive Na_v channels at higher depolarisations (Kuznetsova et al., 2010; Tucker et al., 2012). It had been demonstrated that density of somatic Na_v channels defines the depolarisation block; the higher the density, the less susceptible were neurons to undergo depolarisation block (Tucker et al., 2012).

One unexpected novel finding of the here performed experiments was that the depolarisation block at about 10 Hz was more or less absent when 10 mM EGTA was used in the pipette solution to buffer internal Ca^{2+} of the neurons, enabling SN DA neurons from both juvenile WT and Cav1.3 KO mice to reach maximal frequencies five to six times faster than under control conditions. This indicates that the depolarisation block, in a still molecularly unclear way, also depends on internal Ca^{2+} levels of the neurons.

4.2.2 Pacemaking of SN DA neurons is extremely robust

Figure 3-2, Figure 3-6 and Figure 3-9 underline that SN DA neurons seem to possess a back-up mechanism to maintain their spontaneous pacemaker activity, in the presence of – pharmacological or genetic – perturbation. Especially in juvenile mice, blocking one ion channel species or changing recording conditions (10 mM EGTA or temperature) will barely impact the pacemaker activity in WT and, to a certain extent, even in Cav1.3 KO mice. Pacemaking in SN DA neurons, it seems, is very resilient, with inbuilt fail-safe mechanisms to weather even through difficult circumstances, underlining its physiologic importance (dopamine release and the related functions of the basal ganglia network). This is particularly striking in SN DA neurons from juvenile WT mice, where some neurons still maintained their ability to produce spontaneous pacemaker activity even after both ion channels (HCN channels and LTCCs), that had been suggested to be crucial for creating this activity (Chan et al., 2007),

were blocked: incubation in isradipine did not affect their pacemaker activity at all, block of HCN channels did affect their pacemaker activity, but was still not completely blocking it, and neither was blocking both LTCCs and HCN channels.

SN DA neurons from adult mice seem less well adjusted to cope with perturbation of their in pacemaking involved ion channels, even though the pacemaker of SN DA neurons from adult WT mice still shows resilience. Here we can see an effect of the KO as particularly SN DA neurons from adult Cav1.3 KO mice seem less able to compensate acute block of ion channel conductances. Particularly striking is that incubation in isradipine, which barely affected the adult WT, (and can obviously not block Cav1.3 LTCCs in the Cav1.3 KO mice) had a surprisingly strong effect on their pacemaker activity, indicating that LTCC channels other than Cav1.3 – Cav1.2 – might play an increased role in the adult KO mouse; however, we had no other evidence for Cav1.2 compensation as e.g. the molecular level of Cav1.2 was not upregulated in SN DA neurons from Cav1.3 KO mice (Duda et al., 2014). Additionally, the rather big impact that HCN channel block had on activity of particularly of adult SN DA neurons points toward the interpretation that HCN channels activity might increase with post-natal maturation.

4.2.3 Whole-cell data indicate that loss of Cav1.3 is differently compensated in SN DA neurons from juvenile and adult mice

The in 4.2.3 already described impact – or rather lack of impact – of pharmacological perturbations on the very resilient pacemaker activity of SN DA neurons aside, there is another interesting result from the whole-cell experiments that needs to be considered. The sizes of the AHPs indicated that loss of Cav1.3 had different effects in juvenile and adult mice – or at least that the compensatory mechanisms seem to be age-dependent. While in SN DA neurons from juvenile Cav1.3 KO mice the (Ca^{2+} and SK3 dependent) AHP was smaller than in the WT, explainable by reduced internal Ca^{2+} and thus activation of SK3 channels, it was significantly bigger in the adult KO compared to WT, pointing to a compensatory change in calcium signalling with post-natal maturation. The significant differences in action potential width between SN DA neurons from juvenile and adult mice also point towards an age-dependent change of the set of ion channels that contribute to shape the action potential (Dufour et al., 2014).

4.2.4 The non-desensitising adult-like D2-AR response of SN DA neurons from juvenile Cav1.3 KO mice cannot be induced in the WT by acute block of LTCCs

The major finding of this work is, that in SN DA neurons from juvenile Cav1.3 KO mice a shift in the D2-AR response happened: from desensitising to non-desensitising adult-like compared to the juvenile WT (see 3.3.1). If this shift in response would have been caused by loss of Cav1.3 function, the acute block of LTCCs in SN DA neurons from juvenile WT mice by incubation in isradipine (even though it would have blocked both, Cav1.2 and Cav1.3 and not just Cav1.3) should have induced a similar response in the WT.

The used concentration of 300 nM isradipine should have been high enough to completely block Cav1.3 (as well as Cav1.2) channels despite their lower sensitivity to DHPs compared to Cav1.2 (Koschak et al., 2001; Lipscombe et al., 2004), but not so high as to have unspecific effects on other channels. Calculation data indicated that 100 nM isradipine should block about 90 % of Cav1.3 channels at a mean membrane potential of -50 and -60 mV (the here recorded SN DA neurons had a mean membrane potential between -40 and -50 mV, see Supplemental Table 2), whereas at -90 mV the same concentration would only block about 30 % (Surmeier et al., 2011b).

However, 300 nM isradipine had no effect on the D2-AR response of SN DA neurons from juvenile WT mice. Neither did it affect the D2-AR of Cav1.3 KO mice, indicating that not loss of Cav1.3 but rather the compensation of the general loss of Cav1.3 caused the altered, adult-like D2-AR phenotype in SN DA neurons from juvenile Cav1.3 KO mice, and that Cav1.2 does not play a role in the changed – compensatory – response (similarly to what has been shown, albeit in a slightly different context in (Dragicevic et al., 2014)).

These findings strongly support the interpretation of the whole-cell data that loss of Cav1.3 is compensated in the KO mouse.

4.2.5 The non-desensitising D2-AR response in SN DA neurons of juvenile Cav1.3 KO mice depends on free internal Ca²⁺ levels

We had already identified that desensitisation of D2-AR in SN DA neurons from juvenile mice is inversely correlated with the calcium-dependent interaction of D2-AR with the calcium sensor NCS-1 (Dragicevic et al., 2014). Therefore it was surprising, that the lack of a calcium source in juvenile Cav1.3 KO mice resulted in a non-desensitising D2-AR response, instead of a more rapidly desensitising one. To probe whether the inverse calcium-dependency of D2-AR desensitisation was altered in the KO mice, 10 mM EGTA was used in the pipette solution in

whole-cell recordings to buffer free global internal Ca^{2+} in both SN DA neurons from Cav1.3 KO and WT mice.

Indeed buffering internal Ca^{2+} re-introduced desensitisation to the D2-AR response of SN DA neurons from juvenile Cav1.3 KO mice (while not affecting the WT). This shows that calcium-sensitivity of the D2-AR desensitisation is similar in WT and Cav1.3 KO, and hints at a compensatory change in internal calcium signalling in SN DA neurons from juvenile Cav1.3 KO mice.

4.2.6 Loss of Cav1.3 is compensated by T-type calcium channels in SN DA neurons of juvenile Cav1.3 KO mice

The D2-AR experiments with high EGTA suggested compensatory calcium signalling in SN DA neurons from juvenile Cav1.3 KO mice. In view of the observed differences in AHP in Cav1.3 KO mice, it was tested if another class of voltage-gated calcium channels, T-type calcium channels, might be mediating the compensatory calcium source in SN DA neurons from juvenile Cav1.3 KO mice by utilising the highly selective T-type channel blocker Z941.

Block of T-type channels did increase the irregularity of the pacemaker, similar as described in (Wolfart and Roeper, 2002). However, the T-type channel blocker used for this work did not induce burst firing (occasionally, whole-cell recordings with 10 mM EGTA actually induced burst firing; not shown) or affect the AHP of SN DA neurons from juvenile WT mice as it was previously reported (Wolfart and Roeper, 2002). It is likely that this difference can be attributed to the use of Ni^{2+} -ions to block T-type channel activity in the previous study which, as already mentioned in 1.2.4, can also affect the HVA calcium channels, and for instance also cyclic nucleotide gated channels (Matulef and Zagotta, 2003) or acid-sensing ion channels (Staruschenko et al., 2007), whereas the here used Z941 is a highly selective T-type channel blocker (Tringham et al., 2012). Additionally, the experiments from (Wolfart and Roeper, 2002) were performed at 22–24°C whereas recordings here were carried out at ~33°C, so temperature dependent changes in ion channel gating could play an additional role and explain some of these differences.

Indeed, as hypothesised blocking T-type channels did (re)induce WT-like desensitisation to the D2-AR response of SN DA neurons from juvenile Cav1.3 KO mice (leaving the WT unaffected). This strongly suggests that the non-desensitising D2-AR response is mediated by compensatory activity of T-type calcium channels.

Another interesting observation concerning these experiments was that after incubation in Z941, SN DA neurons regardless of their genotype reached almost 100 % of their initial activity within the dopamine washout phase (see Figure 3-15). Surprisingly, in WT mice a part of the neurons was able to reach frequencies that were drastically higher than their baseline activity (the highest normalised frequency was ~190 %) during their dopamine washout phase, whereas the other part of the neurons recovered from dopamine D2-autoinhibition comparable to control conditions (70–80 %; so the average was ~100 %), which explains the rather large error bars in Figure 3-15. In Cav1.3 KO mice on the other hand overall more neurons reached frequencies closer to their baseline during dopamine washout. This indicates that T-type channels are involved in mediating the deactivation of the D2-AR response and the recovery from dopamine D2/GIRK2 mediated autoinhibition of SN DA neurons from juvenile mice, particularly in frequency control. Up until now this has not been described (Beaulieu and Gainetdinov, 2011).

4.2.7 Interaction of NCS-1 with D2-AR is necessary for the non-desensitising, adult-like D2-AR response of SN DA neurons from juvenile Cav1.3 KO mice

Our previous data already established that the degree of calcium-dependent interaction of NCS-1 with the D2-AR is responsible for the non-desensitising D2-AR response to dopamine in SN DA neurons of juvenile mice, after *in vivo* cocaine treatment (Dragicevic et al., 2014). Thus it was tested if NCS-1/D2-AR interaction was also involved in mediating the non-desensitising D2-AR response of SN DA neurons from juvenile Cav1.3 KO mice. And indeed, similar to T-type channel block and buffering of internal free Ca^{2+} , the DNIP peptide (a short sequence of the third intracellular loop of the D2-receptor) which blocks NCS-1/D2-AR interaction (Kabbani et al., 2002) induced a WT-like desensitising D2-AR response in SN DA neurons from juvenile Cav1.3 KO mice, while the scrambled control peptide had no effect (see Figure 3-15).

4.3 Outlook

We recently identified the first physiological role for Cav1.3 channels in SN DA neurons of juvenile mice for the D2-AR response after *in vivo* high dopamine states (Dragicevic et al., 2014). However, its complex physiological roles for SN DA neurons and its role for determining the vulnerability of SN DA neurons for degeneration in PD and its mouse models remains unclear. Nevertheless, blood brain barrier permissive LTCC blockers are already in

clinical trials for PD therapy (Parkinson Study, 2013) and it was recently shown that expression of Cav1.2 and Cav1.3 are changed in PD patients in comparison to healthy controls, (Hurley et al., 2013). However, nothing is known concerning their physiological or pathophysiological functions. Thus the understanding of Cav1.3 channel function and the protective mechanism of LTCC blockers in SN DA neurons is of particular importance for developing tailored pharmacological therapies with hopefully low levels of side effects. Unfortunately, the Cav1.3 KO mouse, which has already been used as a model before (Chan et al., 2007), is not a suitable model to address these questions, since the work in this thesis shows that the chronic loss of Cav1.3 has been compensated in these mice by another calcium source: voltage-gated T-type channels. Instead, the analysis of a DA neuron specific inducible Cav1.3 KO is desirable, where a compensatory mechanism is not likely to develop (from a cooperation partner we will soon receive a DA neuron specific Cav1.3 KO mouse). However, a lower vulnerability of the general Cav1.3 KO mouse to degeneration had been suggested (Chan et al., 2007) and it would now be interesting to check whether that really is the case, considering the T-type calcium channel compensation that was unveiled in this thesis, since the protection of LTCC blockers in PD and its mouse models is assumed to be caused by a reduction of fluctuation of internal Ca^{2+} levels and associated levels of mitochondrial stress (Dryanovski et al., 2013; Guzman et al., 2010).

Additionally, this unexpected finding of a T-type compensatory phenotype in general KO mice raises a lot of new questions, particularly concerning the LTCC-T-type-channel plasticity and interplay. To address this, currently the expression levels of the pore-forming α_1 -subunits of T-type channels (Cav3.1-3.3) in SN DA neurons from WT and Cav1.3 KO mice is being analysed in another project. Similarly, the apparently complex, but mechanistically not understood role of HCN channels – and also potentially of A-type K_v channels, as it has been shown that these channels (particularly with the KChIP3 isoform) are able to form a direct molecular association with T-type channels to modulate cell excitability (Turner and Zamponi, 2014) – is of great interest.

The next step now would be to analyse if the T-type channel blocker Z941 shows the same effects on SN DA neurons from adult mice as it did on the juveniles. Recently performed preliminary experiments by Elena Dragicevic (from the same work group) suggest at this point that this might not be the case, indicating that the compensatory mechanism in Cav1.3 KO mice might change with age. There is also the question whether the T-type blocker would

“rejuvenate” the D2-AR response of SN DA neurons from adult WT mice, similarly as – wrongly – suggested for Cav1.3 block before. Of particular interest in this context are also the other voltage-gated calcium channels, N-, P-, Q- or R-type channels, as it has for instance been shown that in rodent medullar chromaffin cells loss of Cav1.3 is mainly compensated by R-type channels (Marcantoni et al., 2010), and N-type channels (besides T-type channels) provide ~25 % of the calcium for the SK-mediated AHPs in SN DA neurons (Wolfart and Roeper, 2002). It will also be very valuable to investigate Cav1.3 KO mice or Cav1.3 function in SN DA neurons in *in vivo* recordings. Particularly it is interesting to test *in vivo* within the basal ganglia network if activity is changed in Cav1.3 KO mice in comparison to WT and what effects isradipine and T-type blockers (which are also used in PD therapy, albeit their target is not the substantia nigra or the striatum but the subthalamic nucleus (Yang et al., 2014)) have on the *in vivo* activity of SN DA neurons.

Calcium imaging does provide an additional tool for finding out how and – depending on the technical specifications of the used microscope – in which cell compartment intracellular changes in Ca²⁺ levels might be crucial for the observed differences and further elucidate the mechanisms behind it.

Furthermore, it would be interesting to investigate if long-term administration of isradipine (for instance through implantation of pharmacological pellets) would have effects on the activity of SN DA neurons of mice. This would help answering the main question that arises concerning LTCCs block as neuroprotective PD therapy: does long-term therapy with dihydropyridines, not only as it is used at the moment to cure hypertension, but in the future possibly also in context of PD, induce similar compensatory mechanisms as I have found in the general Cav1.3 KO mouse? And if it does, what the long-term effects of this compensation would be. In this context would also be of interest to see whether the SANDD patients have a higher or maybe lower risk to develop PD, but the mutation has only been found recently and in only a few patients, so that the long-term studies that would be needed to assess the PD risk cannot be done in the near future.

5 SUMMARY: GENERAL KO OF $\text{Ca}_v1.3$ CAUSES COMPENSATORY T-TYPE CHANNEL ACTIVITY, WHICH ENHANCES Ca^{2+} MEDIATED NCS-1/D2-AR INTERACTION, AND THUS PREVENTION OF D2-AR DESENSITISATION IN SN DA NEURONS FROM JUVENILE $\text{Ca}_v1.3$ KO MICE

In this work, the electrophysiological properties of SN DA neurons of juvenile (~PN 13) and adult (~PN 90) WT and $\text{Ca}_v1.3$ KO mice were studied to elucidate the still unclear functional roles of $\text{Ca}_v1.3$ LTCCs for SN DA function, in particular pacemaker activity. SN DA neurons in *in vitro* brain slices were analysed, utilising whole-cell, perforated-patch or on-cell recording techniques, under control conditions or pharmacological challenges (LTCC block, T-type channel block and HCN channel block), as well as internal Ca^{2+} buffering and block of NCS-1/D2-AR interaction through a peptide. The data indicates that $\text{Ca}_v1.3$ LTCCs, and even more so the related calcium signalling, are important for the AHP of murine SN DA neurons, as well as for determining their maximal firing frequency (as buffering internal Ca^{2+} seemed to abolish the normally present depolarisation block) and their D2-AR response to dopamine. The data also revealed a still unclear interplay with T-type calcium channels, hinting at a contribution of T-type calcium channels to the deactivation of D2-AR and/or recovery from its mediated autoinhibition in SN DA neurons of juvenile mice.

More precisely, the experiments analysing the D2-AR response of juvenile mice revealed – and the results from whole-cell experiments hinted at – that the general loss of the LTCC $\text{Ca}_v1.3$ was compensated in SN DA neurons via T-type calcium channel activity in SN DA neurons from juvenile $\text{Ca}_v1.3$ KO mice. The DNIP experiments demonstrated that for this compensatory D2-AR signalling, similar as in WT, calcium-dependent interaction of the calcium sensor NCS-1 with the D2-AR in SN DA neurons from juvenile mice is necessary. The compensatory mechanism in SN DA neurons from adult mice seems to be different from that found in juveniles.

The results from this thesis also add more to our knowledge about the highly disputed, age-dependent role of $\text{Ca}_v1.3$ LTCCs for the pacemaker activity of SN DA neurons (Chan et al., 2007; Drion et al., 2011; Guzman et al., 2009): $\text{Ca}_v1.3$ is not essential for SN DA pacemaker activity or its precision. The data also illustrates that pacemaker activity is a highly flexible mechanism which is age-dependently utilising and relying on a still unclear interplay of distinct ion channels that indeed include, but are not limited to or single-handedly dependent on, $\text{Ca}_v1.3$ and HCN channels. And the data highlights that the general $\text{Ca}_v1.3$ KO mouse – due to a

SUMMARY

compensatory phenotype involving T-type calcium channels in juvenile mice and a still undefined compensatory mechanism in adult mice – is not well-suited for addressing the proposed neuroprotective role of Cav1.3 channels (and its blockers) in SN DA neurons in PD or its mouse models.

LITERATURE

- Abernethy, D.R., and Soldatov, N.M. (2002). Structure-functional diversity of human L-type Ca²⁺ channel: perspectives for new pharmacological targets. *J Pharmacol Exp Ther* 300, 724-728.
- Abi-Dargham, A., Slifstein, M., Kegeles, L., and Laruelle, M. (2010). Dopamine Dysfunction in Schizophrenia. In *Dopamine Handbook*, S.D.I. Leslie L. Iversen, Stephen B. Dunnett, Anders Björklund, ed. (OXFORD, University press), pp. 511-519.
- Arnsten, A.F., and Pliszka, S.R. (2011). Catecholamine influences on prefrontal cortical function: relevance to treatment of attention deficit/hyperactivity disorder and related disorders. *Pharmacol Biochem Behav* 99, 211-216.
- Ashcroft, F.M., and Rorsman, P. (2013). K(ATP) channels and islet hormone secretion: new insights and controversies. *Nat Rev Endocrinol* 9, 660-669.
- Baier, T., and Neuwirth, E. (2007). Excel :: COM :: R. *Computational Statistics*, 22, pp. 91-108.
- Baig, S.M., Koschak, A., Lieb, A., Gebhart, M., Dafinger, C., Nurnberg, G., Ali, A., Ahmad, I., Sinnegger-Brauns, M.J., Brandt, N., *et al.* (2011). Loss of Ca(v)1.3 (CACNA1D) function in a human channelopathy with bradycardia and congenital deafness. *Nat Neurosci* 14, 77-84.
- Bean, B.P. (2007). The action potential in mammalian central neurons. *Nat Rev Neurosci* 8, 451-465.
- Beaulieu, J.M., and Gainetdinov, R.R. (2011). The physiology, signaling, and pharmacology of dopamine receptors. *Pharmacol Rev* 63, 182-217.
- Beckstead, M.J., Ford, C.P., Phillips, P.E., and Williams, J.T. (2007). Presynaptic regulation of dendrodendritic dopamine transmission. *Eur J Neurosci* 26, 1479-1488.
- Beckstead, M.J., Grandy, D.K., Wickman, K., and Williams, J.T. (2004). Vesicular dopamine release elicits an inhibitory postsynaptic current in midbrain dopamine neurons. *Neuron* 42, 939-946.
- Bjorklund, A., and Dunnett, S.B. (2007). Dopamine neuron systems in the brain: an update. *Trends Neurosci* 30, 194-202.
- Blythe, S.N., Wokosin, D., Atherton, J.F., and Bevan, M.D. (2009). Cellular mechanisms underlying burst firing in substantia nigra dopamine neurons. *J Neurosci* 29, 15531-15541.
- Bock, G., Gebhart, M., Scharinger, A., Jangsangthong, W., Busquet, P., Poggiani, C., Sartori, S., Mangoni, M.E., Sinnegger-Brauns, M.J., Herzig, S., *et al.* (2011). Functional properties of a newly identified C-terminal splice variant of Cav1.3 L-type Ca²⁺ channels. *J Biol Chem* 286, 42736-42748.
- Brucke, T., Wober, C., Podreka, I., Wober-Bingol, C., Asenbaum, S., Aull, S., Wenger, S., Ilieva, D., Harasko-van der Meer, C., Wessely, P., and *et al.* (1995). D2 receptor blockade by flunarizine and cinnarizine explains extrapyramidal side effects. A SPECT study. *J Cereb Blood Flow Metab* 15, 513-518.
- Buraei, Z., and Yang, J. (2010). The beta subunit of voltage-gated Ca²⁺ channels. *Physiol Rev* 90, 1461-1506.
- Busquet, P., Nguyen, N.K., Schmid, E., Tanimoto, N., Seeliger, M.W., Ben-Yosef, T., Mizuno, F., Akopian, A., Striessnig, J., and Singewald, N. (2010). Cav1.3 L-type Ca²⁺ channels modulate depression-like behaviour in mice independent of deaf phenotype. *Int J Neuropsychopharmacol* 13, 499-513.
- Cain, S.M., and Snutch, T.P. (2010). Contributions of T-type calcium channel isoforms to neuronal firing. *Channels (Austin)* 4, 475-482.
- Catterall, W.A., Perez-Reyes, E., Snutch, T.P., and Striessnig, J. (2005). International Union of Pharmacology. XLVIII. Nomenclature and structure-function relationships of voltage-gated calcium channels. *Pharmacol Rev* 57, 411-425.

- Chan, C.S., Guzman, J.N., Ilijic, E., Mercer, J.N., Rick, C., Tkatch, T., Meredith, G.E., and Surmeier, D.J. (2007). 'Rejuvenation' protects neurons in mouse models of Parkinson's disease. *Nature* 447, 1081-1086.
- Chen, B.T., Patel, J.C., Moran, K.A., and Rice, M.E. (2011). Differential calcium dependence of axonal versus somatodendritic dopamine release, with characteristics of both in the ventral tegmental area. *Frontiers in systems neuroscience* 5, 39.
- Chen, R.S., Deng, T.C., Garcia, T., Sellers, Z.M., and Best, P.M. (2007). Calcium channel gamma subunits: a functionally diverse protein family. *Cell Biochem Biophys* 47, 178-186.
- Cheng, X., Liu, J., Asuncion-Chin, M., Blaskova, E., Bannister, J.P., Dopico, A.M., and Jaggar, J.H. (2007). A novel Ca(V)1.2 N terminus expressed in smooth muscle cells of resistance size arteries modifies channel regulation by auxiliary subunits. *J Biol Chem* 282, 29211-29221.
- Chowdhury, R., Guitart-Masip, M., Lambert, C., Dayan, P., Huys, Q., Duzel, E., and Dolan, R.J. (2013). Dopamine restores reward prediction errors in old age. *Nat Neurosci* 16, 648-653.
- Clark, N.C., Nagano, N., Kuenzi, F.M., Jarolimek, W., Huber, I., Walter, D., Wietzorrek, G., Boyce, S., Kullmann, D.M., Striessnig, J., and Seabrook, G.R. (2003). Neurological phenotype and synaptic function in mice lacking the Cav1.3 alpha subunit of neuronal L-type voltage-dependent Ca²⁺ channels. *Neuroscience* 120, 435-442.
- Cueni, L., Canepari, M., Adelman, J.P., and Luthi, A. (2009). Ca(2+) signaling by T-type Ca(2+) channels in neurons. *Pflugers Arch* 457, 1161-1172.
- Cui, G., Okamoto, T., and Morikawa, H. (2004). Spontaneous opening of T-type Ca2+ channels contributes to the irregular firing of dopamine neurons in neonatal rats. *J Neurosci* 24, 11079-11087.
- D'Ardenne, K., Eshel, N., Luka, J., Lenartowicz, A., Nystrom, L.E., and Cohen, J.D. (2012). Role of prefrontal cortex and the midbrain dopamine system in working memory updating. *Proc Natl Acad Sci U S A* 109, 19900-19909.
- De Mei, C., Ramos, M., Iitaka, C., and Borrelli, E. (2009). Getting specialized: presynaptic and postsynaptic dopamine D2 receptors. *Curr Opin Pharmacol* 9, 53-58.
- Deignan, J., Lujan, R., Bond, C., Riegel, A., Watanabe, M., Williams, J.T., Maylie, J., and Adelman, J.P. (2012). SK2 and SK3 expression differentially affect firing frequency and precision in dopamine neurons. *Neuroscience* 217, 67-76.
- Dolphin, A.C. (2003). Beta subunits of voltage-gated calcium channels. *J Bioenerg Biomembr* 35, 599-620.
- Dolphin, A.C. (2006). A short history of voltage-gated calcium channels. *Br J Pharmacol* 147 Suppl 1, S56-62.
- Dragicevic, E., Poetschke, C., Duda, J., Schlaudraff, F., Lammel, S., Schiemann, J., Fauler, M., Hetzel, A., Watanabe, M., Ilijic, E., *et al.* (2014). Cav1.3 channels control D2-autoreceptor responses via NCS-1 in Substantia Nigra dopamine neurons (*in press*). *Brain*.
- Drion, G., Massotte, L., Sepulchre, R., and Seutin, V. (2011). How modeling can reconcile apparently discrepant experimental results: the case of pacemaking in dopaminergic neurons. *PLoS Comput Biol* 7, e1002050.
- Dryanovski, D.I., Guzman, J.N., Xie, Z., Galteri, D.J., Volpicelli-Daley, L.A., Lee, V.M., Miller, R.J., Schumacker, P.T., and Surmeier, D.J. (2013). Calcium entry and alpha-synuclein inclusions elevate dendritic mitochondrial oxidant stress in dopaminergic neurons. *J Neurosci* 33, 10154-10164.
- Duda, J., Pötschke, C., Dragicevic, E., Benkert, J., Striessnig, J., and Liss, B. (2014). Defining the role of L-type calcium channels in Substantia nigra dopaminergic midbrain neurons. In *Neuroscience Day 2014* (Innsbruck, Austria).

Dufour, M.A., Woodhouse, A., and Goillard, J.M. (2014). Somatodendritic ion channel expression in substantia nigra pars compacta dopaminergic neurons across postnatal development. *Journal of neuroscience research*.

Eisener-Dorman, A.F., Lawrence, D.A., and Bolivar, V.J. (2009). Cautionary insights on knockout mouse studies: the gene or not the gene? *Brain, behavior, and immunity* 23, 318-324.

Eller, P., Berjukov, S., Wanner, S., Huber, I., Hering, S., Knaus, H.G., Toth, G., Kimball, S.D., and Striessnig, J. (2000). High affinity interaction of mibefradil with voltage-gated calcium and sodium channels. *Br J Pharmacol* 130, 669-677.

Everitt, B.J., Belin, D., Dalley, J.W., and Robbins, T.W. (2010). Dopaminergic Mechanisms in Drug-Seeking Habits and the Vulnerability to Drug Addiction. In *Dopamine Handbook*, S.D.I. Leslie L. Iversen, Stephen B. Dunnett, Anders Björklund, ed. (OXFORD, University press), pp. 389-406.

Ford, C.P. (2014). The Role of D2-Autoreceptors in Regulating Dopamine Neuron Activity and Transmission. *Neuroscience*.

Ford, C.P., Gantz, S.C., Phillips, P.E., and Williams, J.T. (2010). Control of extracellular dopamine at dendrite and axon terminals. *J Neurosci* 30, 6975-6983.

Ford, C.P., Phillips, P.E., and Williams, J.T. (2009). The time course of dopamine transmission in the ventral tegmental area. *J Neurosci* 29, 13344-13352.

Ford, C.P., and Williams, J.T. (2008). Mesoprefrontal dopamine neurons distinguish themselves. *Neuron* 57, 631-632.

Franz, O., Liss, B., Neu, A., and Roeper, J. (2000). Single-cell mRNA expression of HCN1 correlates with a fast gating phenotype of hyperpolarization-activated cyclic nucleotide-gated ion channels (Ih) in central neurons. *Eur J Neurosci* 12, 2685-2693.

Gasser, T., Hardy, J., and Mizuno, Y. (2011). Milestones in PD genetics. *Mov Disord* 26, 1042-1048.

Gerfen, C.R., and Surmeier, D.J. (2011). Modulation of striatal projection systems by dopamine. *Annu Rev Neurosci* 34, 441-466.

Goldberg, M.S., Pisani, A., Haburcak, M., Vortherms, T.A., Kitada, T., Costa, C., Tong, Y., Martella, G., Tscherter, A., Martins, A., *et al.* (2005). Nigrostriatal dopaminergic deficits and hypokinesia caused by inactivation of the familial Parkinsonism-linked gene DJ-1. *Neuron* 45, 489-496.

Grace, A.A. (2012). Dopamine system dysregulation by the hippocampus: implications for the pathophysiology and treatment of schizophrenia. *Neuropharmacology* 62, 1342-1348.

Grace, A.A., and Bunney, B.S. (1984). The control of firing pattern in nigral dopamine neurons: burst firing. *J Neurosci* 4, 2877-2890.

Grace, A.A., Floresco, S.B., Goto, Y., and Lodge, D.J. (2007). Regulation of firing of dopaminergic neurons and control of goal-directed behaviors. *Trends Neurosci* 30, 220-227.

Guateteo, E., Chung, K.K., Bowala, T.K., Bernardi, G., Mercuri, N.B., and Lipski, J. (2005). Temperature sensitivity of dopaminergic neurons of the substantia nigra pars compacta: involvement of transient receptor potential channels. *J Neurophysiol* 94, 3069-3080.

Guzman, J.N., Sanchez-Padilla, J., Chan, C.S., and Surmeier, D.J. (2009). Robust pacemaking in substantia nigra dopaminergic neurons. *J Neurosci* 29, 11011-11019.

Guzman, J.N., Sanchez-Padilla, J., Wokosin, D., Kondapalli, J., Ilijic, E., Schumacker, P.T., and Surmeier, D.J. (2010). Oxidant stress evoked by pacemaking in dopaminergic neurons is attenuated by DJ-1. *Nature* 468, 696-700.

HEKAManuals EPC 10 Patch Clamp Amplifier - Manual 2.0; 8.52 PULSE+PULSEFIT Manual (HEKA Elektronik, Dr. Schulze GmbH, Deutschland).

Helton, T.D., Xu, W., and Lipscombe, D. (2005). Neuronal L-type calcium channels open quickly and are inhibited slowly. *J Neurosci* 25, 10247-10251.

- Hille, B. (2001). *Ion Channels of Excitable Membranes*, Third edn (Sunderland, MA: Sinauer Associates).
- Hindle, J.V. (2010). Ageing, neurodegeneration and Parkinson's disease. *Age Ageing* 39, 156-161.
- Hobom, M., Dai, S., Marais, E., Lacinova, L., Hofmann, F., and Klugbauer, N. (2000). Neuronal distribution and functional characterization of the calcium channel $\alpha_2\delta_2$ subunit. *Eur J Neurosci* 12, 1217-1226.
- Huang, H., Tan, B.Z., Shen, Y., Tao, J., Jiang, F., Sung, Y.Y., Ng, C.K., Raida, M., Kohr, G., Higuchi, M., *et al.* (2012). RNA editing of the IQ domain in $\text{Ca}_v1.3$ channels modulates their Ca^{2+} -dependent inactivation. *Neuron* 73, 304-316.
- Hurley, M.J., Brandon, B., Gentleman, S.M., and Dexter, D.T. (2013). Parkinson's disease is associated with altered expression of $\text{Cav}1$ channels and calcium-binding proteins. *Brain* 136, 2077-2097.
- Ihara, Y., Yamada, Y., Fujii, Y., Gono, T., Yano, H., Yasuda, K., Inagaki, N., Seino, Y., and Seino, S. (1995). Molecular diversity and functional characterization of voltage-dependent calcium channels ($\text{CACN}4$) expressed in pancreatic beta-cells. *Mol Endocrinol* 9, 121-130.
- Ilijic, E., Guzman, J.N., and Surmeier, D.J. (2011). The L-type channel antagonist isradipine is neuroprotective in a mouse model of Parkinson's disease. *Neurobiol Dis* 43, 364-371.
- Johnson, S.L., and Marcotti, W. (2008). Biophysical properties of $\text{Cav}1.3$ calcium channels in gerbil inner hair cells. *J Physiol* 586, 1029-1042.
- Kabbani, N., Negyessy, L., Lin, R., Goldman-Rakic, P., and Levenson, R. (2002). Interaction with neuronal calcium sensor NCS-1 mediates desensitization of the D2 dopamine receptor. *J Neurosci* 22, 8476-8486.
- Kang, S., Cooper, G., Dunne, S.F., Luan, C.H., Surmeier, D.J., and Silverman, R.B. (2013). Structure-activity relationship of N,N'-disubstituted pyrimidinetriones as $\text{Ca}_v1.3$ calcium channel-selective antagonists for Parkinson's disease. *J Med Chem* 56, 4786-4797.
- Kemmler, R. (2009). Analyse der Wirkung des Calciumkanalblockers Isradipin auf die elektrophysiologischen Eigenschaften von dopaminergen Neuronen der Substantia nigra mittels Ganzzell-Patch-Clamp Ableitungen von *in vitro* Hirnschnittpräparaten der Maus. (Bachelorarbeit Molekulare Medizin, Universität Ulm).
- Klugbauer, N., Welling, A., Specht, V., Seisenberger, C., and Hofmann, F. (2002). L-type Ca^{2+} channels of the embryonic mouse heart. *Eur J Pharmacol* 447, 279-284.
- Koschak, A., Reimer, D., Huber, I., Grabner, M., Glossmann, H., Engel, J., and Striessnig, J. (2001). $\alpha_1\text{D}$ ($\text{Cav}1.3$) subunits can form L-type Ca^{2+} channels activating at negative voltages. *J Biol Chem* 276, 22100-22106.
- Kuznetsova, A.Y., Huertas, M.A., Kuznetsov, A.S., Paladini, C.A., and Canavier, C.C. (2010). Regulation of firing frequency in a computational model of a midbrain dopaminergic neuron. *Journal of computational neuroscience* 28, 389-403.
- Lambert, R.C., Bessaih, T., Crunelli, V., and Leresche, N. (2013). The many faces of T-type calcium channels. *Pflügers Arch*.
- Lammel, S., Hetzel, A., Hackel, O., Jones, I., Liss, B., and Roeper, J. (2008). Unique properties of mesoprefrontal neurons within a dual mesocorticolimbic dopamine system. *Neuron* 57, 760-773.
- Liao, P., Yong, T.F., Liang, M.C., Yue, D.T., and Soong, T.W. (2005). Splicing for alternative structures of $\text{Cav}1.2$ Ca^{2+} channels in cardiac and smooth muscles. *Cardiovasc Res* 68, 197-203.
- Lieb, A., Scharinger, A., Sartori, S., Sinnegger-Brauns, M.J., and Striessnig, J. (2012). Structural determinants of $\text{Cav}1.3$ L-type calcium channel gating. *Channels (Austin)* 6, 197-205.

- Lipscombe, D., Helton, T.D., and Xu, W. (2004). L-type calcium channels: the low down. *J Neurophysiol* 92, 2633-2641.
- Liss, B., Franz, O., Sewing, S., Bruns, R., Neuhoﬀ, H., and Roeper, J. (2001). Tuning pacemaker frequency of individual dopaminergic neurons by Kv4.3L and KChip3.1 transcription. *Embo J* 20, 5715-5724.
- Liss, B., Haeckel, O., Wildmann, J., Miki, T., Seino, S., and Roeper, J. (2005). K-ATP channels promote the differential degeneration of dopaminergic midbrain neurons. *Nat Neurosci* 8, 1742-1751.
- Liss, B., Neu, A., and Roeper, J. (1999). The weaver mouse gain-of-function phenotype of dopaminergic midbrain neurons is determined by coactivation of wvGirk2 and K-ATP channels. *J Neurosci* 19, 8839-8848.
- Liss, B., and Roeper, J. (2008). Individual dopamine midbrain neurons: functional diversity and flexibility in health and disease. *Brain Res Rev* 58, 314-321.
- Liss, B., and Roeper, J. (2010). Ion Channels and Regulation of Dopamine Neuron Activity. In *Dopamine Handbook*, S.D.I. Leslie L. Iversen, Stephen B. Dunnett, Anders Björklund, ed. (OXFORD, University press), pp. 118-138.
- Luscher, C., and Slesinger, P.A. (2010). Emerging roles for G protein-gated inwardly rectifying potassium (GIRK) channels in health and disease. *Nat Rev Neurosci* 11, 301-315.
- Mai, J.K., and Paxinos, G. (2011). *The Human Nervous System*, 3rd edn (Academic Press).
- Maia, T.V., and Frank, M.J. (2011). From reinforcement learning models to psychiatric and neurological disorders. *Nat Neurosci* 14, 154-162.
- Marcantoni, A., Vandael, D.H., Mahapatra, S., Carabelli, V., Sinnegger-Brauns, M.J., Striessnig, J., and Carbone, E. (2010). Loss of Cav1.3 channels reveals the critical role of L-type and BK channel coupling in pacemaking mouse adrenal chromaffin cells. *J Neurosci* 30, 491-504.
- Marcellino, D., Kehr, J., Agnati, L.F., and Fuxe, K. (2012). Increased affinity of dopamine for D(2) -like versus D(1) -like receptors. Relevance for volume transmission in interpreting PET findings. *Synapse* 66, 196-203.
- Matulef, K., and Zagotta, W.N. (2003). Cyclic nucleotide-gated ion channels. *Annual review of cell and developmental biology* 19, 23-44.
- Mosharov, E.V., Larsen, K.E., Kanter, E., Phillips, K.A., Wilson, K., Schmitz, Y., Krantz, D.E., Kobayashi, K., Edwards, R.H., and Sulzer, D. (2009). Interplay between cytosolic dopamine, calcium, and alpha-synuclein causes selective death of substantia nigra neurons. *Neuron* 62, 218-229.
- Neuhoﬀ, H., Neu, A., Liss, B., and Roeper, J. (2002). I(h) channels contribute to the different functional properties of identified dopaminergic subpopulations in the midbrain. *J Neurosci* 22, 1290-1302.
- Ng, M.C., Iacopino, A.M., Quintero, E.M., Marches, F., Sonsalla, P.K., Liang, C.L., Speciale, S.G., and German, D.C. (1996). The neurotoxin MPTP increases calbindin-D28k levels in mouse midbrain dopaminergic neurons. *Brain Res Mol Brain Res* 36, 329-336.
- Nilius, B., Talavera, K., and Verkhatsky, A. (2006). T-type calcium channels: the never ending story. *Cell Calcium* 40, 81-88.
- Obeso, J.A., and Lanciego, J.L. (2011). Past, present, and future of the pathophysiological model of the Basal Ganglia. *Front Neuroanat* 5, 39.
- Olson, P.A., Tkatch, T., Hernandez-Lopez, S., Ulrich, S., Ilijic, E., Mugnaini, E., Zhang, H., Bezprozvanny, I., and Surmeier, D.J. (2005). G-protein-coupled receptor modulation of striatal Cav1.3 L-type Ca²⁺ channels is dependent on a Shank-binding domain. *J Neurosci* 25, 1050-1062.

- Parkinson Study, G. (2013). Phase II safety, tolerability, and dose selection study of isradipine as a potential disease-modifying intervention in early Parkinson's disease (STEADY-PD). *Mov Disord* 28, 1823-1831.
- Peloquin, J.B., Doering, C.J., Rehak, R., and McRory, J.E. (2008). Temperature dependence of Cav1.4 calcium channel gating. *Neuroscience* 151, 1066-1083.
- Perez-Reyes, E. (2003). Molecular physiology of low-voltage-activated t-type calcium channels. *Physiol Rev* 83, 117-161.
- Perez-Reyes, E. (2006). Molecular characterization of T-type calcium channels. *Cell Calcium* 40, 89-96.
- Picciotto, M.R., and Wickman, K. (1998). Using knockout and transgenic mice to study neurophysiology and behavior. *Physiol Rev* 78, 1131-1163.
- Platzer, J., Engel, J., Schrott-Fischer, A., Stephan, K., Bova, S., Chen, H., Zheng, H., and Striessnig, J. (2000). Congenital deafness and sinoatrial node dysfunction in mice lacking class D L-type Ca²⁺ channels. *Cell* 102, 89-97.
- Pötschke, C. (2008). Analyse der Pacemaker-Aktivität unterschiedlicher Typen von dopaminergen Mittelhirnneuronen mittels Ganzzell Patch-Clamp Ableitungen von *in vitro* Hirnschnittpräparaten der Maus. (Bachelorarbeit Molekulare Medizin, Universität Ulm).
- Pötschke, C. (2010). Electrophysiological *in vitro* characterisation of dopamine midbrain neurons from Cav1.3 KO mice. (Master's thesis, Molecular Medicine, Universität Ulm).
- Puopolo, M., Raviola, E., and Bean, B.P. (2007). Roles of subthreshold calcium current and sodium current in spontaneous firing of mouse midbrain dopamine neurons. *J Neurosci* 27, 645-656.
- Putzier, I., Kullmann, P.H., Horn, J.P., and Levitan, E.S. (2009). Cav1.3 channel voltage dependence, not Ca²⁺ selectivity, drives pacemaker activity and amplifies bursts in nigral dopamine neurons. *J Neurosci* 29, 15414-15419.
- R-Development-Core-Team (2009). R: A Language and Environment for Statistical Computing. (Vienna, Austria, R Foundation for Statistical Computing).
- Rice, M.E., Patel, J.C., and Cragg, S.J. (2011). Dopamine release in the basal ganglia. *Neuroscience* 198, 112-137.
- Ritz, B., Rhodes, S.L., Qian, L., Schernhammer, E., Olsen, J.H., and Friis, S. (2010). L-type calcium channel blockers and Parkinson disease in Denmark. *Ann Neurol* 67, 600-606.
- Saab, B.J., Georgiou, J., Nath, A., Lee, F.J., Wang, M., Michalon, A., Liu, F., Mansuy, I.M., and Roder, J.C. (2009). NCS-1 in the dentate gyrus promotes exploration, synaptic plasticity, and rapid acquisition of spatial memory. *Neuron* 63, 643-656.
- Salimpoor, V.N., Benovoy, M., Larcher, K., Dagher, A., and Zatorre, R.J. (2011). Anatomically distinct dopamine release during anticipation and experience of peak emotion to music. *Nat Neurosci* 14, 257-262.
- Salomone, J.D. (2010). Involvement of Nucleus Accumbens Dopamine in Behavioral Activation and Effort-Related Functions. In *Dopamine Handbook*, S.D.I. Leslie L. Iversen, Stephen B. Dunnett, Anders Björklund, ed. (OXFORD, University press), pp. 286-300.
- Santi, C.M., Cayabyab, F.S., Sutton, K.G., McRory, J.E., Mezeyova, J., Hamming, K.S., Parker, D., Stea, A., and Snutch, T.P. (2002). Differential inhibition of T-type calcium channels by neuroleptics. *J Neurosci* 22, 396-403.
- Schiemann, J., Schlaudraff, F., Klose, V., Bingmer, M., Seino, S., Magill, P.J., Zaghloul, K.A., Schneider, G., Liss, B., and Roeper, J. (2012). K-ATP channels in dopamine substantia nigra neurons control bursting and novelty-induced exploration. *Nat Neurosci* 15, 1272-1280.
- Schultz, W. (1998). Predictive reward signal of dopamine neurons. *J Neurophysiol* 80, 1-27.
- Schultz, W. (2002). Getting formal with dopamine and reward. *Neuron* 36, 241-263.
- Schultz, W. (2007). Behavioral dopamine signals. *Trends Neurosci* 30, 203-210.

- Schultz, W. (2010). Dopamine signals for reward value and risk: basic and recent data. *Behav Brain Funct* 6, 24.
- Shen, Y., Yu, D., Hiel, H., Liao, P., Yue, D.T., Fuchs, P.A., and Soong, T.W. (2006). Alternative splicing of the Ca(v)1.3 channel IQ domain, a molecular switch for Ca²⁺-dependent inactivation within auditory hair cells. *J Neurosci* 26, 10690-10699.
- Shipe, W.D., Barrow, J.C., Yang, Z.Q., Lindsley, C.W., Yang, F.V., Schlegel, K.A., Shu, Y., Rittle, K.E., Bock, M.G., Hartman, G.D., *et al.* (2008). Design, synthesis, and evaluation of a novel 4-aminomethyl-4-fluoropiperidine as a T-type Ca²⁺ channel antagonist. *J Med Chem* 51, 3692-3695.
- Simuni, T., Borushko, E., Avram, M.J., Miskevics, S., Martel, A., Zadikoff, C., Videnovic, A., Weaver, F.M., Williams, K., and Surmeier, D.J. (2010). Tolerability of isradipine in early Parkinson's disease: a pilot dose escalation study. *Mov Disord* 25, 2863-2866.
- Singh, A., Gebhart, M., Fritsch, R., Sinnegger-Brauns, M.J., Poggiani, C., Hoda, J.C., Engel, J., Romanin, C., Striessnig, J., and Koschak, A. (2008). Modulation of voltage- and Ca²⁺-dependent gating of Ca_v1.3 L-type calcium channels by alternative splicing of a C-terminal regulatory domain. *J Biol Chem* 283, 20733-20744.
- Smidt, M.P., and Burbach, J.P. (2007). How to make a mesodiencephalic dopaminergic neuron. *Nat Rev Neurosci* 8, 21-32.
- Soldatov, N.M. (1994). Genomic structure of human L-type Ca²⁺ channel. *Genomics* 22, 77-87.
- Staruschenko, A., Dorofeeva, N.A., Bolshakov, K.V., and Stockand, J.D. (2007). Subunit-dependent cadmium and nickel inhibition of acid-sensing ion channels. *Developmental neurobiology* 67, 97-107.
- Striessnig, J., and Koschak, A. (2008). Exploring the function and pharmacotherapeutic potential of voltage-gated Ca²⁺ channels with gene knockout models. *Channels (Austin)* 2, 233-251.
- Striessnig, J., Koschak, A., Sinnegger-Brauns, M.J., Hetzenauer, A., Nguyen, N.K., Busquet, P., Pelster, G., and Singewald, N. (2006). Role of voltage-gated L-type Ca²⁺ channel isoforms for brain function. *Biochem Soc Trans* 34, 903-909.
- Sulzer, D. (2007). Multiple hit hypotheses for dopamine neuron loss in Parkinson's disease. *Trends Neurosci* 30, 244-250.
- Sulzer, D., and Surmeier, D.J. (2013). Neuronal vulnerability, pathogenesis, and Parkinson's disease. *Mov Disord* 28, 41-50.
- Surmeier, D.J. (2007a). Calcium, ageing, and neuronal vulnerability in Parkinson's disease. *Lancet Neurol* 6, 933-938.
- Surmeier, D.J. (2007b). Dopamine and working memory mechanisms in prefrontal cortex. *J Physiol* 581, 885.
- Surmeier, D.J., Guzman, J.N., Sanchez-Padilla, J., and Goldberg, J.A. (2011a). The origins of oxidant stress in Parkinson's disease and therapeutic strategies. *Antioxid Redox Signal* 14, 1289-1301.
- Surmeier, D.J., Guzman, J.N., Sanchez-Padilla, J., and Schumacker, P.T. (2011b). The role of calcium and mitochondrial oxidant stress in the loss of substantia nigra pars compacta dopaminergic neurons in Parkinson's disease. *Neuroscience*.
- Surmeier, D.J., and Schumacker, P.T. (2013). Calcium, bioenergetics, and neuronal vulnerability in Parkinson's disease. *J Biol Chem* 288, 10736-10741.
- Talley, E.M., Cribbs, L.L., Lee, J.H., Daud, A., Perez-Reyes, E., and Bayliss, D.A. (1999). Differential distribution of three members of a gene family encoding low voltage-activated (T-type) calcium channels. *J Neurosci* 19, 1895-1911.

- Tang, Z.Z., Liang, M.C., Lu, S., Yu, D., Yu, C.Y., Yue, D.T., and Soong, T.W. (2004). Transcript scanning reveals novel and extensive splice variations in human L-type voltage-gated calcium channel, Cav1.2 α_1 subunit. *J Biol Chem* 279, 44335-44343.
- Tobler, P.N. (2010). Behavioral Functions of Dopamine Neurons. In *Dopamine Handbook*, S.D.I. Leslie L. Iversen, Stephen B. Dunnett, Anders Björklund, ed. (OXFORD, University press).
- Tong, Y., Pisani, A., Martella, G., Karouani, M., Yamaguchi, H., Pothos, E.N., and Shen, J. (2009). R1441C mutation in LRRK2 impairs dopaminergic neurotransmission in mice. *Proc Natl Acad Sci U S A* 106, 14622-14627.
- Toulorge, D., Guerreiro, S., Hild, A., Maskos, U., Hirsch, E.C., and Michel, P.P. (2011). Neuroprotection of midbrain dopamine neurons by nicotine is gated by cytoplasmic Ca^{2+} . *FASEB J* 25, 2563-2573.
- Tringham, E., Powell, K.L., Cain, S.M., Kuplast, K., Mezeyova, J., Weerapura, M., Eduljee, C., Jiang, X., Smith, P., Morrison, J.L., *et al.* (2012). T-type calcium channel blockers that attenuate thalamic burst firing and suppress absence seizures. *Sci Transl Med* 4, 121ra119.
- Tucker, K.R., Huertas, M.A., Horn, J.P., Canavier, C.C., and Levitan, E.S. (2012). Pacemaker rate and depolarization block in nigral dopamine neurons: a somatic sodium channel balancing act. *J Neurosci* 32, 14519-14531.
- Turner, R.W., and Zamponi, G.W. (2014). T-type channels buddy up. *Pflugers Arch* 466, 661-675.
- Wahl-Schott, C., and Biel, M. (2009). HCN channels: structure, cellular regulation and physiological function. *Cell Mol Life Sci* 66, 470-494.
- Wolfart, J., Neuheff, H., Franz, O., and Roeper, J. (2001). Differential expression of the small-conductance, calcium-activated potassium channel SK3 is critical for pacemaker control in dopaminergic midbrain neurons. *J Neurosci* 21, 3443-3456.
- Wolfart, J., and Roeper, J. (2002). Selective coupling of T-type calcium channels to SK potassium channels prevents intrinsic bursting in dopaminergic midbrain neurons. *J Neurosci* 22, 3404-3413.
- Xu, M., Welling, A., Paparisto, S., Hofmann, F., and Klugbauer, N. (2003). Enhanced expression of L-type Cav1.3 calcium channels in murine embryonic hearts from Cav1.2-deficient mice. *J Biol Chem* 278, 40837-40841.
- Xu, W., and Lipscombe, D. (2001). Neuronal Cav1.3 α_1 L-type channels activate at relatively hyperpolarized membrane potentials and are incompletely inhibited by dihydropyridines. *J Neurosci* 21, 5944-5951.
- Yang, Y.C., Tai, C.H., Pan, M.K., and Kuo, C.C. (2014). The T-type calcium channel as a new therapeutic target for Parkinson's disease. *Pflugers Arch* 466, 747-755.
- Zhang, Y., Jiang, X., Snutch, T.P., and Tao, J. (2013). Modulation of low-voltage-activated T-type Ca^{2+} channels. *Biochimica et biophysica acta* 1828, 1550-1559.

APPENDIX

Supplemental tables

A)

	pacemaker	irregular	sporadic spikes	inactive	n (complete)
juvenile WT	92.8 %	7.2 %			69 [‡]
juvenile Cav1.3 KO	77.5 %	20 %	2.5 %		40
juvenile WT 36°C	86.7 %	13.3 %			15
juvenile Cav1.3 KO 36°C	88.9 %	11.1 %			18
juvenile WT high EGTA	73.3 %	26.7 %			15
juvenile Cav1.3 KO high EGTA	60 %	25 %	10 %	5 %	20
juvenile WT israd	92.9 %	7.1 %			14
juvenile Cav1.3 KO israd	78.6 %	21.4 %			14
juvenile Cav1.3WT Z941	70.6 %	29.4 %			17
juvenile Cav1.3 KO Z941	71.4 %	28.6 %			14
juvenile WT ZD7288	20 %	20 %	26.7 %	33.3 %	15
juvenile Cav1.3 KO ZD7288	4 %	16 %	8 %	72 %	25
juvenile WT israd + ZD7288	9.5 %	9.5 %	38.1 %	42.9 %	21
adult WT	71.7 %	26.1 %	2.2 %		46 [†]
adult Cav1.3 KO	68.2 %	31.8 %			22
adult WT israd	69.2 %	15.4 %	7.7 %	7.7 %	13
adult Cav1.3 KO israd	18.75 %	25 %	25 %	31.25 %	16
adult WT ZD7288	10 %		10 %	80 %	10
adult Cav1.3 KO ZD7288				100 %	7

B)

	pacemaker	irregular	sporadic spikes	inactive
juvenile C57BL/6	45	2		
juvenile Cav1.3 ^{+/+}	19	3		
juvenile Cav1.3 KO	31	8	1	
juvenile C57BL/6 36°C	13	2		
juvenile Cav1.3 36°C	16	2		
juvenile WT high EGTA	11	4		
juvenile Cav1.3 KO high EGTA	12	5	2	1
juvenile WT israd	13	1		
juvenile Cav1.3 KO israd	11	3		
juvenile Cav1.3 ^{+/+} Z941	12	5		
juvenile Cav1.3 KO Z941	10	4		
juvenile WT ZD7288	3	3	4	5
juvenile Cav1.3 KO ZD7288	1	4	2	18
juvenile WT israd + ZD7288	2	2	8	9
adult C57BL/6	25	8	1	
adult Cav1.3 ^{+/+}	8	4		
adult Cav1.3 KO	15	7		
adult WT israd	9	2	1	1
adult Cav1.3 KO israd	3	4	4	5
adult WT ZD7288	1		1	8
adult Cav1.3 KO ZD7288				7

Supplemental Table 1: Spontaneous activity overview of all analysed neurons for basal electrophysiological characterisation

A: Shows percentage of neurons from 3.1 in their respective activity groups. [‡] includes 23 Cav1.3 WT mice; [†] includes 12 Cav1.3^{+/+} mice. **B:** Detailed listing of all neurons included in 3.1 (absolute numbers).

Supplemental Table 2: Overview over data from juvenile and adult C57BL/6, Cav1.3^{+/+} and Cav1.3 KO mice

A) control conditions:

	juvenile C57BL/6	n	juvenile Cav1.3 KO	n	juvenile Cav1.3 ^{+/+}	n	adult C57BL/6	n	adult Cav1.3 KO	n	adult Cav1.3 ^{+/+}	n
capacitance [pF]	54.51 ± 1.9	47	51.17 ± 2.1	40	60.72 ± 3.6	22	33.08 ± 1.6	34	37.27 ± 1.8	22	37.61 ± 2.2	12
input resistance [GΩ]	1.41 ± 0.03	46	1.4 ± 0.03	36	1.38 ± 0.04	20	1.3 ± 0.03	30	1.49 ± 0.06	19	1.26 ± 0.1	11
mean membrane potential [mV]	-46.15 ± 0.4	47	-41.54 ± 0.6	40	-46.92 ± 0.7	12	-42.06 ± 0.8	34	-44.46 ± 0.9	21	-41.47 ± 1.1	12
frequency [Hz]	2.23 ± 0.1	46	2.16 ± 0.1	33	1.97 ± 0.2	20	2.37 ± 0.1	26	1.97 ± 0.2	14	2.05 ± 0.3	8
maximal frequency [Hz]	13.76 ± 0.4	45	12.78 ± 0.6	36	13.92 ± 0.8	20	12.5 ± 0.6	31	13.55 ± 0.9	20	11.15 ± 0.6	11
AP threshold [mV]	-28.55 ± 0.4	47	-25.81 ± 0.6	39	-29.3 ± 0.8	12	-24.45 ± 0.7	25	-25.76 ± 1.1	16	-22.65 ± 1	11
AP overshoot [mV]	37.23 ± 0.7	47	38.07 ± 1	40	33.63 ± 2.3	12	37.61 ± 1.4	34	36.43 ± 1.3	22	33.83 ± 2	12
AP width [ms]	3.27 ± 0.09	47	3.39 ± 0.1	39	3.13 ± 0.1	12	2.04 ± 0.07	23	2.33 ± 2.1	14	2.21 ± 0.1	11
afterhyperpolarisation [mV]	-59.27 ± 0.6	47	-55.25 ± 0.9	40	-59.09 ± 1.2	12	-56.59 ± 1	34	-59.75 ± 1.1	22	-56.32 ± 1.05	12
sag component [mV]	59.12 ± 0.8	47	61.81 ± 1.2	39	57.86 ± 1.5	22	61.1 ± 1.3	34	58.7 ± 1.4	22	62.44 ± 1.1	12
current to sag [pA]	-438 ± 18	47	-435 ± 18	39	-506.8 ± 29	22	-447 ± 25	33	-407 ± 34	22	-492 ± 56	12
I _h amplitude [pA]	-592 ± 37	25	-605 ± 40	24	-694.9 ± 145	5	-533 ± 39	20	-482 ± 73	8	-395.9 ±	1
area _h [pAs]	-969 ± 58	25	-999 ± 65	24	-1116 ± 264	5	-901 ± 59	20	817 ± 126	11	-617.7 ±	1
basal frequency (five minutes) [Hz]	1.91 ± 0.1	8	1.89 ± 0.2	8								
CV ISI [%]	9.14 ± 1.2	8	5.63 ± 0.7	8								
activity at min. 15 of dopamine [%]	10.84 ± 4.4	7	48.95 ± 14.2	7								
basal frequency (five minutes, perforated patch) [Hz]	2.67 ± 0.3	7	2.07 ± 0.3	9	2.31 ± 0.1	21	3.18 ± 0.2	9	3.34 ± 0.3	13		
CV ISI (perforated patch) [%]	7.71 ± 0.8	7	16.77 ± 4	9	8.36 ± 1.2	11	7.13 ± 2	5	12.58 ± 2.3	5		
activity at min. 15 of dopamine (perforated patch) [%]	43.11 ± 11.9	5	11.55 ± 7.6	9	19.8 ± 6.6	16	12.13 ± 6.1	7	12.59 ± 5.4	12		

B) 36°C (low EGTA)

	juvenile C57BL/6		n	juvenile Cav1.3 KO		n	C) after at least 30 minutes of incubation in isradipine						adult C57BL/6		n	adult Cav1.3 KO		n
capacitance [pF]	53.03	± 3.3	15	61.51	± 1.6	18	53.15	± 3.3	14	55.15	± 2.9	14	35.09	± 3.9	13	30.68	± 2.5	16
input resistance [GΩ]	1.39	± 0.05	13	1.49	± 0.03	17	1.36	± 0.03	14	1.27	± 0.05	11	1.4	± 0.06	12	1.39	± 0.06	16
mean membrane potential [mV]	-44.07	± 0.9	15	-45.49	± 1.1	18	-43.86	± 0.6	14	-41.69	± 0.8	14	-43.9	± 0.9	13	-40.75	± 1.3	16
frequency [Hz]	2.88	± 0.4	13	2.28	± 0.2	16	1.79	± 0.2	13	1.78	± 0.2	11	2.14	± 0.3	9	2.13	± 0.2	5
maximal frequency [Hz]	18.82	± 1.5	14	15.47	± 1	17	16.98	± 1.8	14	11.49	± 0.5	14	10.78	± 1	13	10.5	± 0.8	13
AP threshold [mV]	-27.52	± 0.8	14	-25.95	± 0.7	17	-25.99	± 0.5	12	-26.14	± 1.1	14	-24.47	± 0.7	10	-28.65	± 2.1	8
AP overshoot [mV]	34.05	± 1.7	15	37.48	± 1.4	17	38.95	± 4.3	14	38.48	± 2.1	14	37.12	± 2.4	12	37.92	± 1.7	11
AP width [ms]	3.12	± 0.1	15	3.35	± 0.1	17	2.77	± 0.1	12	3.35	± 0.2	14	2.18	± 0.2	10	2.38	± 0.2	8
afterhyperpolarisation [mV]	-57.78	± 1.5	15	-58.65	± 0.7	18	-56.94	± 1.2	14	-56.94	± 1.2	14	-59.81	± 1.3	12	-59.28	± 1.5	11
sag component [mV]	66.02	± 1.2	15	63.42	± 1.2	18	59.96	± 1.9	14	59.72	± 2.4	14	59.57	± 1.5	13	57.93	± 1.7	16
current to sag [pA]	-482	± 28	14	-431	± 30	18	-460.7	± 30	14	-504	± 38	14	-458	± 47	13	-422	± 35	16
I _h amplitude [pA]	-809	± 58	13	-653	± 57	17	-632.8	± 63	13	-633	± 63	13	-463.7	± 83	7	-441.5	± 81	5
area _h [pAs]	-1368	± 100	13	-1095	± 103	17	-1065	± 106	13	-1051	± 154	9	-907	± 69	7	-726.4	± 142	5
basal frequency (five minutes) [Hz]																		
CV ISI [%]																		
activity at min. 15 of dopamine [%]																		
basal frequency (five minutes, perforated patch) [Hz]	3.57	± 0.3	10	3.02	± 0.1	18	2.57	± 0.04	7	1.96	± 0.1	9						
CV ISI (perforated patch) [%]	7.87	± 1	9	11.63	± 1.6	18	8.85	± 1.5	8	15.53	± 3.5	8						
activity at min. 15 of dopamine (perforated patch) [%]	58.61	± 10.3	9	56.14	± 8.9	15	34.29	± 9.9	7	5.39	± 2.5	9						

D) 10 mM EGTA (high EGTA)

	juvenile C57BL/6				juvenile Cav1.3 KO				E) WT (C57BL/6 & Cav1.3 ^{+/+}) control conditions				F) after at least 30 minutes incubation in Z941			
	juvenile C57BL/6	n	juvenile Cav1.3 KO	n	juvenile WT	n	adult WT	n	juvenile Cav1.3 ^{+/+}	n	juvenile Cav1.3 KO	n	juvenile Cav1.3 ^{+/+}	n	juvenile Cav1.3 KO	n
capacitance [pF]	40.79 ± 2.4	14	51.36 ± 2.8	20	56.49 ± 1.8	69	34.26 ± 1.4	46	51.71 ± 3.1	17	53.94 ± 4.1	14	51.71 ± 3.1	17	53.94 ± 4.1	14
input resistance [GΩ]	1.62 ± 0.5	11	1.43 ± 0.4	20	1.4 ± 0.02	66	1.29 ± 0.04	41	1.44 ± 0.05	16	1.36 ± 0.06	13	1.44 ± 0.05	16	1.36 ± 0.06	13
mean membrane potential [mV]	-44.37 ± 0.7	15	-45 ± 0.8	20	-46.31 ± 0.3	59	-41.54 ± 0.6	40	-46.12 ± 0.6	17	-44.18 ± 1.1	14	-46.12 ± 0.6	17	-44.18 ± 1.1	14
frequency [Hz]	2.04 ± 0.2	15	1.81 ± 0.1	14	2.15 ± 0.1	66	2.29 ± 0.1	34	1.63 ± 0.1	15	1.79 ± 0.2	11	1.63 ± 0.1	15	1.79 ± 0.2	11
maximal frequency [Hz]	47.13 ± 4	14	61.02 ± 5.7	16	13.81 ± 0.4	65	12.15 ± 0.5	42	13.44 ± 0.7	16	11.5 ± 0.6	12	13.44 ± 0.7	16	11.5 ± 0.6	12
AP threshold [mV]	-26.96 ± 0.9	14	-28.41 ± 0.7	19	-28.71 ± 0.4	59	-23.9 ± 0.6	36	-28.34 ± 0.9	16	-27.29 ± 1.3	13	-28.34 ± 0.9	16	-27.29 ± 1.3	13
AP overshoot [mV]	32.55 ± 1.6	14	36.99 ± 1.5	19	36.5 ± 0.8	59	36.63 ± 1.2	46	33.79 ± 1.5	17	32.78 ± 1.3	14	33.79 ± 1.5	17	32.78 ± 1.3	14
AP width [ms]	3.34 ± 0.2	14	3.21 ± 0.2	19	3.2 ± 0.07	59	2.1 ± 0.07	34	3.4 ± 0.2	16	3.66 ± 0.2	13	3.4 ± 0.2	16	3.66 ± 0.2	13
afterhyperpolarisation [mV]	-56.25 ± 0.7	15	-56.99 ± 0.8	19	-59.23 ± 0.6	59	-55.26 ± 0.9	46	-59.06 ± 0.8	17	-58.35 ± 1.6	14	-59.06 ± 0.8	17	-58.35 ± 1.6	14
sag component [mV]	60.57 ± 1.7	14	60.8 ± 2.1	20	58.72 ± 0.7	69	61.45 ± 1	46	60.3 ± 1.5	17	62.58 ± 1.1	14	60.3 ± 1.5	17	62.58 ± 1.1	14
current to sag [pA]	-337 ± 32	15	-474 ± 42	19	-460 ± 15	69	-459 ± 23	45	-427 ± 28	17	-510.7 ± 50	14	-427 ± 28	17	-510.7 ± 50	14
I _h amplitude [pA]	-482 ± 73	8	-614 ± 62	16	-609 ± 38	30	-527 ± 37	21								
area _h [pAs]	-775 ± 117	8	-979 ± 99	16	-955 ± 52	29	-887 ± 58	21								
basal frequency (five minutes) [Hz]	1.97 ± 0.2	6	2.1 ± 0.2	7												
CV ISI [%]	11.21 ± 1.1	6	11.31 ± 2	7												
activity at min. 15 of dopamine [%]	65.2 ± 18.1	6	66.63 ± 13.5	7												
basal frequency (five minutes, perforated patch) [Hz]					2.33 ± 0.09	27			2.19 ± 0.3	10	2.41 ± 0.3	8				
CV ISI (perforated patch) [%]					8.1 ± 0.8	18			12.44 ± 1.3	7	12.25 ± 1.4	7				
activity at min. 15 of dopamine (perforated patch) [%]					25.35 ± 6.02	21			43.11 ± 14.3	8	42.6 ± 12.1	8				

G) after at least 30 minutes in**10 μM DNIP****10 μM srDNIP**

	juvenile Cav1.3 KO		juvenile Cav1.3 KO	
	juvenile Cav1.3 KO	n	juvenile Cav1.3 KO	n
basal frequency (five minutes, perforated patch) [Hz]	2.6 ± 0.3	11	2.49 ± 0.4	10
CV ISI (perforated patch) [%]	12.51 ± 1.7	8	9.12 ± 1.6	4
activity at min. 15 of dopamine (perforated patch) [%]	28.95 ± 11.1	6	8.43 ± 8.4	7

Supplemental Table 2: Overview over data from juvenile and adult C57BL/6, Cav1.3^{+/-} and Cav1.3 KO mice

Values are given as mean \pm SEM. AP: action potential. If not stated explicitly in () behind the parameter, data from whole-cell recordings. **A:** Data for juvenile and adult C57BL/6, Cav1.3^{+/-} and Cav1.3 KO mice recorded under control conditions. **B:** Data for juvenile C57BL/6 and Cav1.3 KO mice recorded at 36°C. **C:** Data for juvenile and adult C57BL/6 and Cav1.3 KO mice recorded in 300 nM isradipine. **D:** Data for juvenile C57BL/6 and Cav1.3 KO mice recorded with 10 mM EGTA. **E:** Data for pooled (C57BL/6 and Cav1.3^{+/-}) WT recorded under control conditions. **F:** Data for juvenile Cav1.3^{+/-} and Cav1.3 KO recorded in 10 mM Z941. **G:** Data for juvenile Cav1.3 KO in 10 μ M DNIP (includes perforated-patch and on-cell recordings) and or srDNIP.

Supplemental Table 3: Comparison matrixes for parameters from whole-cell recordings

capacitance [pF]	juvenile C57BL/6	juvenile WT (pooled)	juvenile Cav1.3 KO	juvenile Cav1.3 ^{+/+}	juvenile C57BL/6 36°C	juvenile Cav1.3 KO 36°C	juvenile C57BL/6 isradipine	juvenile Cav1.3 KO isradipine	juvenile C57BL/6 high EGTA	juvenile Cav1.3 KO high EGTA	juvenile Cav1.3 ^{+/+} Z941	juvenile Cav1.3 KO Z941	adult C57BL/6	adult WT (pooled)	adult Cav1.3 KO	adult Cav1.3 ^{+/+}	adult C57BL/6 isradipine	adult C57BL/6 isradipine
juvenile C57BL/6																		
juvenile WT (pooled)																		
juvenile Cav1.3 KO	n.s.	n.s.																
juvenile Cav1.3 ^{+/+}	n.s.		0.02															
juvenile C57BL/6 36°C	n.s.	n.s.																
juvenile Cav1.3 KO 36°C			n.s.		n.s.													
juvenile C57BL/6 isradipine	n.s.	n.s.																
juvenile Cav1.3 KO isradipine			n.s.				n.s.											
juvenile C57BL/6 high EGTA	0.0003	0.000061																
juvenile Cav1.3 high EGTA			n.s.						0.02									
juvenile Cav1.3 ^{+/+} Z941		n.s.		n.s.														
juvenile Cav1.3 KO Z941			n.s.								n.s.							
adult C57BL/6	8.30E-12																	
adult WT (pooled)		2.90E-16																
adult Cav1.3 KO			0.00004										n.s.	n.s.				
adult Cav1.3 ^{+/+}				0.00002											n.s.			
adult C57BL/6 isradipine							0.001							n.s.	n.s.			
adult Cav1.3 KO isradipine								0.0000035								0.03	n.s.	

input resistance [GΩ]	juvenile C57BL/6	juvenile WT (pooled)	juvenile Cav1.3 KO	juvenile Cav1.3 ^{+/+}	juvenile C57BL/6 36°C	juvenile Cav1.3 KO 36°C	juvenile C57BL/6 isradipine	juvenile Cav1.3 KO isradipine	juvenile C57BL/6 high EGTA	juvenile Cav1.3 KO high EGTA	juvenile Cav1.3 ^{+/+} Z941	juvenile Cav1.3 KO Z941	adult C57BL/6	adult WT (pooled)	adult Cav1.3 KO	adult Cav1.3 ^{+/+}	adult C57BL/6 isradipine	adult C57BL/6 isradipine
juvenile C57BL/6																		
juvenile WT (pooled)																		
juvenile Cav1.3 KO	n.s.	n.s.																
juvenile Cav1.3 ^{+/+}	n.s.		n.s.															
juvenile C57BL/6 36°C	n.s.	n.s.																
juvenile Cav1.3 KO 36°C			n.s.		n.s.													
juvenile C57BL/6 isradipine	n.s.	n.s.																
juvenile Cav1.3 KO isradipine			0.0498				n.s.											
juvenile C57BL/6 high EGTA	0.0008	0.0003																
juvenile Cav1.3 high EGTA			n.s.						0.003									
juvenile Cav1.3 ^{+/+} Z941		n.s.		n.s.														
juvenile Cav1.3 KO Z941			n.s.								n.s.							
adult C57BL/6	0.009																	
adult WT (pooled)		0.003																
adult Cav1.3 KO			n.s.											0.007	0.004			
adult Cav1.3 ^{+/+}				n.s.												0.04		
adult C57BL/6 isradipine							n.s.						n.s.	n.s.				
adult Cav1.3 KO isradipine								n.s.							n.s.		n.s.	

mean membrane potential [mV]	juvenile C57BL/6	juvenile WT (pooled)	juvenile Cav1.3 KO	juvenile Cav1.3 ^{+/+}	juvenile C57BL/6 36°C	juvenile Cav1.3 KO 36°C	juvenile C57BL/6 isradipine	juvenile Cav1.3 KO isradipine	juvenile C57BL/6 high EGTA	juvenile Cav1.3 KO high EGTA	juvenile Cav1.3 ^{+/+} Z941	juvenile Cav1.3 KO Z941	adult C57BL/6	adult WT (pooled)	adult Cav1.3 KO	adult Cav1.3 ^{+/+}	adult C57BL/6 isradipine	adult C57BL/6 isradipine
juvenile C57BL/6																		
juvenile WT (pooled)																		
juvenile Cav1.3 KO	5.60E-09	2.70E-10																
juvenile Cav1.3 ^{+/+}	n.s.		0.000016															
juvenile C57BL/6 36°C	n.s.	0.03																
juvenile Cav1.3 KO 36°C			0.0008		n.s.													
juvenile C57BL/6 isradipine	0.004	0.002																
juvenile Cav1.3 KO isradipine			n.s.					0.02										
juvenile C57BL/6 high EGTA	0.04	0.02																
juvenile Cav1.3 high EGTA			0.002						n.s.									
juvenile Cav1.3 ^{+/+} Z941		n.s.		n.s.														
juvenile Cav1.3 KO Z941			0.02									n.s.						
adult C57BL/6	0.000018																	
adult WT (pooled)		2.40E-08																
adult Cav1.3 KO			0.01										n.s.		0.04			
adult Cav1.3 ^{+/+}				0.0002									n.s.		n.s.			
adult C57BL/6 isradipine							n.s.						n.s.	n.s.				
adult Cav1.3 KO isradipine								n.s.							0.03		n.s.	

frequency [Hz]	juvenile C57BL/6	juvenile WT (pooled)	juvenile Cav1.3 KO	juvenile Cav1.3 ^{+/+}	juvenile C57BL/6 36°C	juvenile Cav1.3 KO 36°C	juvenile C57BL/6 isradipine	juvenile Cav1.3 KO isradipine	juvenile C57BL/6 high EGTA	juvenile Cav1.3 KO high EGTA	juvenile Cav1.3 ^{+/+} Z941	juvenile Cav1.3 KO Z941	adult C57BL/6	adult WT (pooled)	adult Cav1.3 KO	adult Cav1.3 ^{+/+}	adult C57BL/6 isradipine	adult C57BL/6 isradipine
juvenile C57BL/6																		
juvenile WT (pooled)																		
juvenile Cav1.3 KO	n.s.	n.s.																
juvenile Cav1.3 ^{+/+}	n.s.		n.s.															
juvenile C57BL/6 36°C	n.s.	0.04																
juvenile Cav1.3 KO 36°C			n.s.		n.s.													
juvenile C57BL/6 isradipine	n.s.	n.s.																
juvenile Cav1.3 KO isradipine			n.s.				n.s.											
juvenile C57BL/6 high EGTA	n.s.	n.s.																
juvenile Cav1.3 high EGTA			n.s.						n.s.									
juvenile Cav1.3 ^{+/+} Z941		0.02		n.s.														
juvenile Cav1.3 KO Z941			n.s.									n.s.						
adult C57BL/6	n.s.																	
adult WT (pooled)		n.s.																
adult Cav1.3 KO			n.s.										n.s.	n.s.				
adult Cav1.3 ^{+/+}				n.s.									n.s.		n.s.			
adult C57BL/6 isradipine							n.s.						n.s.	n.s.				
adult Cav1.3 KO isradipine								n.s.							n.s.		n.s.	

maximal frequency [Hz]	juvenile C57BL/6	juvenile WT (pooled)	juvenile Cav1.3 KO	juvenile Cav1.3 ^{+/+}	juvenile C57BL/6 36°C	juvenile Cav1.3 KO 36°C	juvenile C57BL/6 isradipine	juvenile Cav1.3 KO isradipine	juvenile C57BL/6 high EGTA	juvenile Cav1.3 KO high EGTA	juvenile Cav1.3 ^{+/+} Z941	juvenile Cav1.3 KO Z941	adult C57BL/6	adult WT (pooled)	adult Cav1.3 KO	adult Cav1.3 ^{+/+}	adult C57BL/6 isradipine	adult C57BL/6 isradipine
juvenile C57BL/6																		
juvenile WT (pooled)																		
juvenile Cav1.3 KO	0.07	n.s.																
juvenile Cav1.3 ^{+/+}	n.s.		n.s.															
juvenile C57BL/6 36°C	0.003	0.003																
juvenile Cav1.3 KO 36°C			0.02		n.s.													
juvenile C57BL/6 isradipine	n.s.	n.s.																
juvenile Cav1.3 KO isradipine			n.s.				0.003											
juvenile C57BL/6 high EGTA	3.00E-13	5.60E-15																
juvenile Cav1.3 high EGTA			2.00E-13						n.s.									
juvenile Cav1.3 ^{+/+} Z941		n.s.		n.s.														
juvenile Cav1.3 KO Z941			n.s.								n.s.							
adult C57BL/6	n.s.																	
adult WT (pooled)		0.003																
adult Cav1.3 KO			n.s.										n.s.	n.s.				
adult Cav1.3 ^{+/+}				0.008									n.s.		n.s.			
adult C57BL/6 isradipine							0.002							0.04	n.s.			
adult Cav1.3 KO isradipine								n.s.								0.03	n.s.	

action potential threshold [ms]	juvenile C57BL/6	juvenile WT (pooled)	juvenile Cav1.3 KO	juvenile Cav1.3 ^{+/+}	juvenile C57BL/6 36°C	juvenile Cav1.3 KO 36°C	juvenile C57BL/6 isradipine	juvenile Cav1.3 KO isradipine	juvenile C57BL/6 high EGTA	juvenile Cav1.3 KO high EGTA	juvenile Cav1.3 ^{+/+} Z941	juvenile Cav1.3 KO Z941	adult C57BL/6	adult WT (pooled)	adult Cav1.3 KO	adult Cav1.3 ^{+/+}	adult C57BL/6 isradipine	adult C57BL/6 isradipine
juvenile C57BL/6																		
juvenile WT (pooled)																		
juvenile Cav1.3 KO	0.0002	0.000035																
juvenile Cav1.3 ^{+/+}	n.s.		0.003															
juvenile C57BL/6 36°C	n.s.	n.s.																
juvenile Cav1.3 KO 36°C			n.s.		n.s.													
juvenile C57BL/6 isradipine	0.001	0.0006																
juvenile Cav1.3 KO isradipine			n.s.				n.s.											
juvenile C57BL/6 high EGTA	n.s.	n.s.																
juvenile Cav1.3 high EGTA			0.006						n.s.									
juvenile Cav1.3 ^{+/+} Z941		n.s.		n.s.														
juvenile Cav1.3 KO Z941			n.s.								n.s.							
adult C57BL/6	0.0000078																	
adult WT (pooled)		9.00E-10																
adult Cav1.3 KO			n.s.										n.s.	n.s.				
adult Cav1.3 ^{+/+}				0.000067									n.s.		n.s.			
adult C57BL/6 isradipine							n.s.						n.s.	n.s.				
adult Cav1.3 KO isradipine								n.s.							n.s.		0.02	

action potential overshoot [mV]	juvenile C57BL/6	juvenile WT (pooled)	juvenile Cav1.3 KO	juvenile Cav1.3 ^{+/+}	juvenile C57BL/6 36°C	juvenile Cav1.3 KO 36°C	juvenile C57BL/6 isradipine	juvenile Cav1.3 KO isradipine	juvenile C57BL/6 high EGTA	juvenile Cav1.3 KO high EGTA	juvenile Cav1.3 ^{+/+} Z941	juvenile Cav1.3 KO Z941	adult C57BL/6	adult WT (pooled)	adult Cav1.3 KO	adult Cav1.3 ^{+/+}	adult C57BL/6 isradipine	adult C57BL/6 isradipine
juvenile C57BL/6																		
juvenile WT (pooled)																		
juvenile Cav1.3 KO	n.s.	n.s.																
juvenile Cav1.3 ^{+/+}	n.s.		n.s.															
juvenile C57BL/6 36°C	n.s.	n.s.																
juvenile Cav1.3 KO 36°C			n.s.		n.s.													
juvenile C57BL/6 isradipine	n.s.	n.s.					n.s.											
juvenile Cav1.3 KO isradipine			n.s.					n.s.										
juvenile C57BL/6 high EGTA	0.02	0.04																
juvenile Cav1.3 high EGTA			n.s.						n.s.									
juvenile Cav1.3 ^{+/+} Z941		n.s.		n.s.														
juvenile Cav1.3 KO Z941				0.005							n.s.							
adult C57BL/6	n.s.																	
adult WT (pooled)		n.s.																
adult Cav1.3 KO			n.s.										n.s.	n.s.				
adult Cav1.3 ^{+/+}				n.s.									n.s.		n.s.			
adult C57BL/6 isradipine							n.s.						n.s.	n.s.				
adult Cav1.3 KO isradipine								n.s.							n.s.		n.s.	

action potential width [ms]	juvenile C57BL/6	juvenile WT (pooled)	juvenile Cav1.3 KO	juvenile Cav1.3 ^{+/+}	juvenile C57BL/6 36°C	juvenile Cav1.3 KO 36°C	juvenile C57BL/6 isradipine	juvenile Cav1.3 KO isradipine	juvenile C57BL/6 high EGTA	juvenile Cav1.3 KO high EGTA	juvenile Cav1.3 ^{+/+} Z941	juvenile Cav1.3 KO Z941	adult C57BL/6	adult WT (pooled)	adult Cav1.3 KO	adult Cav1.3 ^{+/+}	adult C57BL/6 isradipine	adult C57BL/6 isradipine
juvenile C57BL/6																		
juvenile WT (pooled)																		
juvenile Cav1.3 KO	n.s.	n.s.																
juvenile Cav1.3 ^{+/+}	n.s.		n.s.															
juvenile C57BL/6 36°C	n.s.	n.s.																
juvenile Cav1.3 KO 36°C			n.s.		n.s.													
juvenile C57BL/6 isradipine	0.002	0.002						0.01										
juvenile Cav1.3 KO isradipine			n.s.															
juvenile C57BL/6 high EGTA	n.s.	n.s.								n.s.								
juvenile Cav1.3 high EGTA			n.s.															
juvenile Cav1.3 ^{+/+} Z941		n.s.		n.s.														
juvenile Cav1.3 KO Z941			n.s.								n.s.							
adult C57BL/6	4.20E-13																	
adult WT (pooled)		2.20E-16																
adult Cav1.3 KO			9.10E-08										0.01	0.02				
adult Cav1.3 ^{+/+}				0.0002									n.s.		n.s.			
adult C57BL/6 isradipine							0.004						n.s.	n.s.				
adult Cav1.3 KO isradipine								0.004							n.s.		n.s.	

after hyperpolarisation [mV]	juvenile C57BL/6	juvenile WT (pooled)	juvenile Cav1.3 KO	juvenile Cav1.3 ^{+/+}	juvenile C57BL/6 36°C	juvenile Cav1.3 KO 36°C	juvenile C57BL/6 isradipine	juvenile Cav1.3 KO isradipine	juvenile C57BL/6 high EGTA	juvenile Cav1.3 KO high EGTA	juvenile Cav1.3 ^{+/+} Z941	juvenile Cav1.3 KO Z941	adult C57BL/6	adult WT (pooled)	adult Cav1.3 KO	adult Cav1.3 ^{+/+}	adult C57BL/6 isradipine	adult C57BL/6 isradipine
juvenile C57BL/6																		
juvenile WT (pooled)																		
juvenile Cav1.3 KO	0.001	0.0008																
juvenile Cav1.3 ^{+/+}	n.s.		n.s.															
juvenile C57BL/6 36°C	n.s.	n.s.																
juvenile Cav1.3 KO 36°C			0.04		n.s.													
juvenile C57BL/6 isradipine	n.s.	n.s.																
juvenile Cav1.3 KO isradipine			n.s.				n.s.											
juvenile C57BL/6 high EGTA	0.006	0.004																
juvenile Cav1.3 high EGTA			n.s.						n.s.									
juvenile Cav1.3 ^{+/+} Z941		n.s.		n.s.														
juvenile Cav1.3 KO Z941			n.s.								n.s.							
adult C57BL/6	n.s.																	
adult WT (pooled)		0.01																
adult Cav1.3 KO			0.003											0.03	0.02			
adult Cav1.3 ^{+/+}				n.s.									n.s.		n.s.			
adult C57BL/6 isradipine							n.s.						n.s.		0.04			
adult Cav1.3 KO isradipine								n.s.							n.s.		n.s.	

sag-component [mV]	juvenile C57BL/6	juvenile WT (pooled)	juvenile Cav1.3 KO	juvenile Cav1.3 ^{+/+}	juvenile C57BL/6 36°C	juvenile Cav1.3 KO 36°C	juvenile C57BL/6 isradipine	juvenile Cav1.3 KO isradipine	juvenile C57BL/6 high EGTA	juvenile Cav1.3 KO high EGTA	juvenile Cav1.3 ^{+/+} Z941	juvenile Cav1.3 KO Z941	adult C57BL/6	adult WT (pooled)	adult Cav1.3 KO	adult Cav1.3 ^{+/+}	adult C57BL/6 isradipine	adult C57BL/6 isradipine
juvenile C57BL/6																		
juvenile WT (pooled)																		
juvenile Cav1.3 KO	0.046	0.02																
juvenile Cav1.3 ^{+/+}	n.s.		n.s.															
juvenile C57BL/6 36°C	0.000049	0.000028																
juvenile Cav1.3 KO 36°C			n.s.		n.s.													
juvenile C57BL/6 isradipine	n.s.	n.s.																
juvenile Cav1.3 KO isradipine			n.s.				n.s.											
juvenile C57BL/6 high EGTA	n.s.	n.s.																
juvenile Cav1.3 high EGTA			n.s.						n.s.									
juvenile Cav1.3 ^{+/+} Z941		n.s.		n.s.														
juvenile Cav1.3 KO Z941			n.s.								n.s.							
adult C57BL/6	n.s.																	
adult WT (pooled)		0.03																
adult Cav1.3 KO			n.s.										n.s.	n.s.				
adult Cav1.3 ^{+/+}				n.s.									n.s.		n.s.			
adult C57BL/6 isradipine							n.s.						n.s.	n.s.				
adult Cav1.3 KO isradipine								n.s.							n.s.		n.s.	

current to sag [pA]	juvenile C57BL/6	juvenile WT (pooled)	juvenile Cav1.3 KO	juvenile Cav1.3 ^{+/+}	juvenile C57BL/6 36°C	juvenile Cav1.3 KO 36°C	juvenile C57BL/6 isradipine	juvenile Cav1.3 KO isradipine	juvenile C57BL/6 high EGTA	juvenile Cav1.3 KO high EGTA	juvenile Cav1.3 ^{+/+} Z941	juvenile Cav1.3 KO Z941	adult C57BL/6	adult WT (pooled)	adult Cav1.3 KO	adult Cav1.3 ^{+/+}	adult C57BL/6 isradipine	adult C57BL/6 isradipine
juvenile C57BL/6																		
juvenile WT (pooled)																		
juvenile Cav1.3 KO	n.s.	n.s.																
juvenile Cav1.3 ^{+/+}	0.049		0.04															
juvenile C57BL/6 36°C	n.s.	n.s.																
juvenile Cav1.3 KO 36°C			n.s.		n.s.													
juvenile C57BL/6 isradipine	n.s.	n.s.					n.s.											
juvenile Cav1.3 KO isradipine			n.s.															
juvenile C57BL/6 high EGTA	0.005	0.0008																
juvenile Cav1.3 high EGTA			n.s.						0.01									
juvenile Cav1.3 ^{+/+} Z941		n.s.		n.s.														
juvenile Cav1.3 KO Z941			n.s.								n.s.							
adult C57BL/6	n.s.																	
adult WT (pooled)		n.s.																
adult Cav1.3 KO			n.s.										n.s.	n.s.				
adult Cav1.3 ^{+/+}				n.s.									n.s.		n.s.			
adult C57BL/6 isradipine							n.s.						n.s.	n.s.				
adult Cav1.3 KO isradipine								n.s.							n.s.		n.s.	

I _a amplitude [pA]	juvenile C57BL/6	juvenile WT (pooled)	juvenile Cav1.3 KO	juvenile Cav1.3 ^{+/+}	juvenile C57BL/6 36°C	juvenile Cav1.3 KO 36°C	juvenile C57BL/6 isradipine	juvenile Cav1.3 KO isradipine	juvenile C57BL/6 high EGTA	juvenile Cav1.3 KO high EGTA	juvenile Cav1.3 ^{+/+} Z941	juvenile Cav1.3 KO Z941	adult C57BL/6	adult WT (pooled)	adult Cav1.3 KO	adult Cav1.3 ^{+/+}	adult C57BL/6 isradipine	adult C57BL/6 isradipine
juvenile C57BL/6																		
juvenile WT (pooled)																		
juvenile Cav1.3 KO	n.s.	n.s.																
juvenile Cav1.3 ^{+/+}	n.s.		n.s.															
juvenile C57BL/6 36°C	0.004	0.006																
juvenile Cav1.3 KO 36°C			n.s.		n.s.													
juvenile C57BL/6 isradipine	n.s.	n.s.																
juvenile Cav1.3 KO isradipine			n.s.				n.s.											
juvenile C57BL/6 high EGTA	n.s.	n.s.																
juvenile Cav1.3 high EGTA			n.s.						n.s.									
juvenile Cav1.3 ^{+/+} Z941																		
juvenile Cav1.3 KO Z941																		
adult C57BL/6	n.s.																	
adult WT (pooled)		n.s.																
adult Cav1.3 KO			n.s.										n.s.	n.s.				
adult Cav1.3 ^{+/+}				n.s.									n.s.		n.s.			
adult C57BL/6 isradipine							n.s.						n.s.	n.s.				
adult Cav1.3 KO isradipine								n.s.							n.s.		n.s.	

area I_h [pAs]	juvenile C57BL/6	juvenile WT (pooled)	juvenile Cav1.3 KO	juvenile Cav1.3 ^{+/+}	juvenile C57BL/6 36°C	juvenile Cav1.3 KO 36°C	juvenile C57BL/6 isradipine	juvenile Cav1.3 KO isradipine	juvenile C57BL/6 high EGTA	juvenile Cav1.3 KO high EGTA	juvenile Cav1.3 ^{+/+} Z941	juvenile Cav1.3 KO Z941	adult C57BL/6	adult WT (pooled)	adult Cav1.3 KO	adult Cav1.3 ^{+/+}	adult C57BL/6 isradipine	adult C57BL/6 isradipine
juvenile C57BL/6																		
juvenile WT (pooled)																		
juvenile Cav1.3 KO	n.s.	n.s.																
juvenile Cav1.3 ^{+/+}	n.s.		n.s.															
juvenile C57BL/6 36°C	0.001	0.0005																
juvenile Cav1.3 KO 36°C			n.s.		n.s.													
juvenile C57BL/6 isradipine	n.s.	n.s.																
juvenile Cav1.3 KO isradipine			n.s.				n.s.											
juvenile C57BL/6 high EGTA	n.s.	n.s.																
juvenile Cav1.3 high EGTA			n.s.						n.s.									
juvenile Cav1.3 ^{+/+} Z941																		
juvenile Cav1.3 KO Z941																		
adult C57BL/6	n.s.																	
adult WT (pooled)		n.s.																
adult Cav1.3 KO			n.s.											n.s.	n.s.			
adult Cav1.3 ^{+/+}				n.s.										n.s.		n.s.		
adult C57BL/6 isradipine							n.s.							n.s.	n.s.			
adult Cav1.3 KO isradipine								n.s.							n.s.		n.s.	

Supplemental Table 3: Comparison matrixes for parameters from whole-cell recordings

Shown are p-values in red (or n.s. in black in case the difference was not significant) from wilcoxon-rank-u-tests (see 2.2.4.2 for details). Juvenile and adult C57BL/6, juvenile and adult WT (pooled), juvenile and adult Cav1.3 KO, and juvenile and adult Cav1.3^{+/+} are recordings under control conditions (0.1 mM EGTA); juvenile C57BL/6 36°C and juvenile Cav1.3 KO 36°C are recordings at 36°C; juvenile and adult C57BL/6 isradipine and juvenile and adult Cav1.3 KO isradipine are recordings in 300 nM isradipine; juvenile C57BL/6 high EGTA and juvenile Cav1.3 KO high EGTA are recordings with 10 mM EGTA in the pipette solution; juvenile Cav1.3^{+/+} Z941 and juvenile Cav1.3 KO Z941 are recordings in 10 μ M Z941.

Supplemental Table 4: Comparison matrixes for parameters from 40 minute recordings

mean basal frequency [Hz]	juvenile Cav1.3 ^{+/+}	juvenile C57BL/6	juvenile WT (pooled)	juvenile Cav1.3 KO	juvenile C57BL/6 36°C	juvenile Cav1.3 KO 36°C	juvenile C57BL/6 isradipine	juvenile Cav1.3 KO isradipine	juvenile C57BL/6 high EGTA	juvenile Cav1.3 KO high EGTA	juvenile Cav1.3 KO DNIP	juvenile Cav1.3 KO srDNIP	juvenile Cav1.3 ^{+/+} Z941	juvenile Cav1.3 KO Z941	adult C57BL/6	adult Cav1.3 KO
juvenile Cav1.3 ^{+/+}																
juvenile C57BL/6	n.s.															
juvenile WT (pooled)	n.s.	n.s.														
juvenile Cav1.3 KO	n.s.	n.s.	n.s.													
juvenile C57BL/6 36°C		n.s.	0.0009													
juvenile Cav1.3 KO 36°C				0.003	0.0496											
juvenile C57BL/6 isradipine		n.s.	n.s.													
juvenile Cav1.3 KO isradipine				n.s.			n.s.									
juvenile C57BL/6 high EGTA		n.s.	n.s.													
juvenile Cav1.3 KO high EGTA				n.s.				n.s.								
juvenile Cav1.3 KO DNIP	n.s.	n.s.	n.s.	n.s.												
juvenile Cav1.3 KO srDNIP	n.s.	n.s.	n.s.	n.s.						n.s.						
juvenile Cav1.3 ^{+/+} Z941	n.s.															
juvenile Cav1.3 KO Z941				n.s.									n.s.			
adult C57BL/6		n.s.	0.004													
adult Cav1.3 KO				0.01											n.s.	

CV ISI [%]	juvenile Cav1.3 ^{+/+}	juvenile C57BL/6	juvenile WT (pooled)	juvenile Cav1.3 KO	juvenile C57BL/6 36°C	juvenile Cav1.3 KO 36°C	juvenile C57BL/6 isradipine	juvenile Cav1.3 KO isradipine	juvenile C57BL/6 high EGTA	juvenile Cav1.3 KO high EGTA	juvenile Cav1.3 KO DNIP	juvenile Cav1.3 KO srDNIP	juvenile Cav1.3 ^{+/+} Z941	juvenile Cav1.3 KO Z941	adult C57BL/6	adult Cav1.3 KO
juvenile Cav1.3 ^{+/+}																
juvenile C57BL/6	n.s.															
juvenile WT (pooled)	n.s.	n.s.														
juvenile Cav1.3 KO	0.02	n.s.	0.01													
juvenile C57BL/6 36°C		n.s.	n.s.													
juvenile Cav1.3 KO 36°C				n.s.	n.s.											
juvenile C57BL/6 isradipine		n.s.	n.s.													
juvenile Cav1.3 KO isradipine				n.s.			n.s.									
juvenile C57BL/6 high EGTA		n.s.	0.047													
juvenile Cav1.3 KO high EGTA				n.s.				n.s.								
juvenile Cav1.3 KO DNIP	0.03	0.04	0.01	n.s.												
juvenile Cav1.3 KO srDNIP	n.s.	n.s.	n.s.	n.s.						n.s.						
juvenile Cav1.3 ^{+/+} Z941	0.04	0.007														
juvenile Cav1.3 KO Z941				n.s.									n.s.			
adult C57BL/6		n.s.	n.s.													
adult Cav1.3 KO				n.s.											n.s.	

[illegible]

Supplemental Table 4: Comparison matrixes for parameters from 40 minute recordings

Shown are p-values in red (or n.s. in black in case the difference was not significant) from wilcoxon-rank-u-tests (see 2.2.4.2 for details). Juvenile and adult C57BL/6, juvenile WT (pooled), juvenile and adult Cav1.3 KO, and juvenile and adult Cav1.3^{+/+} are recordings under control conditions (perforated-patch); juvenile C57BL/6 36°C and juvenile Cav1.3 KO are recordings at 36°C (perforated-patch); juvenile C57BL/6 isradipine and juvenile Cav1.3 KO isradipine are recordings in 300 nM isradipine (perforated-patch); juvenile C57BL/6 high EGTA and juvenile Cav1.3 KO high EGTA are recordings with 10 mM EGTA in the pipette solution (whole-cell); juvenile Cav1.3^{+/+} Z941 and juvenile Cav1.3 KO Z941 are recordings in 10 μM Z941 (perforated-patch); juvenile Cav1.3 KO DNIP is a recording with 10 μM DNIP (perforated-patch and on-cell) and Cav1.3 KO srDNIP is a recording with 10 μM srDNIP (perforated-patch).

ACKNOWLEDGEMENT/DANKSAGUNG

Die Danksagung wurde aus Gründen des Datenschutzes für die online Veröffentlichung entfernt.

The acknowledgement was removed for online publication due to privacy protection.

STATUTORY DECLARATION

I hereby declare that I wrote the present dissertation

„Compensatory T-type calcium channel activity alters the dopamine D2-autoreceptor response of dopaminergic substantia nigra neurons from juvenile Cav1.3 KO mice“

independently and used no other aids than those cited. In each individual case, I have clearly identified the source of the passages that are taken word for word or paraphrased from other works.

I also hereby declare that I have carried out my scientific work according to the principles of good scientific practice in accordance with the current “Satzung der Universität Ulm zur Sicherung guter wissenschaftlicher Praxis” (Rules of the University of Ulm for Assuring Good Scientific Practice).

Ulm,

.

(Christina Pötschke)

CURRICULUM VITAE

Ein Teil der persönlichen Informationen wurden aus Datenschutzgründen für die online Veröffentlichung entfernt.

Part of the personal information have been removed for online publication due to privacy protection.

Personal Information

Last Name:	Pötschke
First Name:	Christina
Date of Birth:	22.04.1986
Place of Birth:	Bautzen

Studies

01.10.2010 – now	PhD studies in the Institute of Applied Physiology under the supervision of Prof. Birgit Liss; title of thesis: “Compensatory T-type calcium channel activity alters the dopamine D2-autoreceptor response of dopaminergic substantia nigra neurons from juvenile Cav1.3 KO mice”
01.10.2009 – 31.03.2014	Member of the Graduate School for Molecular Medicine of Ulm University (Master–PhD–Programme – already joined during Master’s thesis)
23.07.2010	Master of Science in Molecular Medicine, grade: 1.2 (thesis: Electrophysiological <i>in vitro</i> characterisation of dopamine midbrain neurons from Cav1.3 KO mice; grade: 1.0)
01.10.2008	Enrolment in Master Studies “Molecular Medicine” at Ulm University
04.08.2008	Bachelor of Science in Molecular Medicine, grade: 2.2 (thesis: Analyse der Pacemaker–Aktivität unterschiedlicher Typen von dopaminergen Mittelhirnneuronen mittels Ganzzell Patch-Clamp Ableitungen von <i>in vitro</i> Hirnschnittpräparaten der Maus; grade: 1.1)

01.10.2005	Enrolment in Bachelor Studies “Molecular Medicine” at Ulm University
------------	--

Education

1998–2005	Secondary School: Heinrich-Heine-Gymnasium Cottbus 18.06.2005: Abitur (A-levels); grade: 1.4
1992–1998	Primary School: 5. Primary School in Cottbus

Conferences, visits and presentations

April 2014	Talk at “Neurobiologisches Oberseminar” at Ulm University; title: Adult-like dopamine D2-autoreceptor responses in SN DA neurons from juvenile Cav1.3 KO mice due to altered T-type channel activity
April 2012	Poster presentation at Neuroscience Day 2012, Innsbruck University (Austria); title: Defining the role of L-type Ca ²⁺ channels in substantia nigra dopaminergic midbrain neurons
January 2012	Talk “3 rd progress report” for the International Graduate School of Molecular Medicine, Ulm University; title: Defining role of L-type calcium channels in substantia nigra dopaminergic midbrain neurons
Oktober 2011	Talk and poster presentation at the Fall Meeting of the International Graduate School in Molecular Medicine, Ulm University; title: Defining the role of L-type calcium channels in substantia nigra dopaminergic midbrain neurons
September 2011	Poster presentation at OXION Day 2011, University of Oxford (UK); title: Defining the role of L-type calcium channels in substantia nigra dopaminergic midbrain neurons
May 2011	Poster presentation at Neuroscience Day 2011, Innsbruck University (Austria); title: Selective vulnerability of dopaminergic midbrain neurons in Parkinsons’s disease: focus on ion channels and genomic integrity
April 2011	Talk “2 nd progress report” for the Internation Graduate School of Molecular Medicine, Ulm University; title: Defining the functional roles of L-type calcium channels in dopaminergic neurons in health and disease states
March 2011	Poster presentation at the Alfried Krupp Symposium “Role of ion channels in chonric disease”, University of Regensburg; title: Selective vulnerability of dopaminergic

- midbrain neurons in Parkinsons's disease: focus on ion channels and genomic integrity
- 9.–15.07.2009 2009 PENS Summer School: "Metabolic Aspects of Chronic Brain Diseases", Günzburg; poster presentation: Analysing the pacemaker activity of dopaminergic midbrain neurons – role of calcium channels
- April 2009 Talk at the Symposium „Day of Molecular Medicine“, Ulm University; title: Analyse der Pacemaker Aktivität dopaminerger Mittelhirnneurone der Maus

Publications, abstracts and posters

Dragicevic E, **Poetschke C**, Duda J, Schlaudraff F, Lammel S, Schiemann J, Fauler M, Hetzel A, Watanabe M, Lujan R, Malenka R, Striessnig J, Liss B; "Cav1.3 channels control D2-autoreceptor responses via NCS-1 in Substantia Nigra dopamine neurons". Brain 2014.

Duda J, **Poetschke C**, Dragicevic E, Benkert J, Snutch TP, Striessnig J, Liss B; "Compensatory T-type calcium channel activity alters dopamine D2-autoreceptor responses of dopamine substantia nigra neurons from CaV1.3 L-type calcium channel deficient mice"; SfN Annual Meeting Abstract/Poster 2014

Dragicevic E, **Poetschke C**, Duda J, Schlaudraff F, Lammel S, Schiemann J, Duda J, Hetzel A, Watanabe M, Lujan R, Striessnig J, Malenka RC, Liss B; "Cav1.3 L-type calcium channels control age-dependent D2-autoreceptor responses via NCS-1 in substantia nigra dopamine neurons"; SfN Annual Meeting Abstract/Poster 2014

Duda J, **Poetschke C**, Dragicevic E, Benkert J, Striessnig J, Liss B; "Defining the role of Lt-type calcium channels in substantia nigra dopaminergic midbrain neurons"; Neuroscience Day Innsbruck University, Abstract/Poster 2014

Duda J, **Poetschke C**, Dragicevic E, Striessnig J, Liss B; "Function and expression of Cav1.3 L-type Ca²⁺ channels in substantia nigra dopamine midbrain neurons"; SfN Annual Meeting Abstract/Poster 2012

Dragicevic E, **Poetschke C**, Schiemann J, Schlaudraff F, Lammel S, Duda J, Hetzel A, Lujan R, Striessnig J, Malenka RC, Liss B; "L-type calcium channels control age-dependent desensitization and plasticity of D2-autoreceptor function in SN dopamine midbrain neurons via NCS-1"; SfN Annual Meeting Abstract/Poster 2012

Poetschke C, Duda J, Dragicevic E, Striessnig J, Liss B; "Defining the role of L-type calcium channels in substantia nigra dopaminergic midbrain neurons"; Neuroscience Day Innsbruck University, Abstract/Poster 2012

Dragicevic E, **Poetschke C**, Schiemann J, Duda J, Schlaudraff F, Lujan R, Striessnig J, Röper J, Liss B; "L-type calcium channels control age-dependent desensitisation and cocaine-induced plasticity of D2-autoreceptor function in substantia nigra dopamine midbrain neurons"; Neuroscience Day Innsbruck University, Abstract/Poster 2012

Poetschke C, Duda J, Dragicevic E, Striessnig J, Röper J, Liss B; “Defining the role of L-type calcium channels in substantia nigra dopaminergic midbrain neurons”; OXION day University of Oxford, Abstract/Poster 2011

Poetschke C, Duda J, Dragicevic E, Striessnig J, Röper J, Liss B; “Selective vulnerability of dopaminergic midbrain neurons in Parkinson’s disease: focus on ion channels and genomic integrity”; Neuroscience Day Innsbruck University, Abstract/Poster 2011

Dragicevic E, **Poetschke C**, Schiemann J, Duda J, Schlaudraff F, Lujan R, Striessnig J, Röper J, Liss B; “L-type calcium channels control age-dependent desensitisation and cocaine-induced plasticity of D2-autoreceptor function in substantia nigra dopamine midbrain neurons”; Neuroscience Day Innsbruck University, Abstract/Poster 2011

Dragicevic E, **Poetschke C**, Schiemann J, Schmidt K, Schlaudraff F, Lujan R, Striessnig J, Röper J, Liss B; “L-type calcium channels control age-dependent desensitization and cocaine-induced plasticity of D2-autoreceptor function in SN dopamine midbrain neurons”; SfN Annual Meeting Abstract/Poster 2010

Poetschke C, Kemmler R, Dragicevic E, Liss B; “Analysing the pacemaker activity of dopaminergic midbrain neurons in mice – role of calcium channels”; PENS Summer School Poster 2009

Skills

German	first language
English	fluent in spoken and written
French	fluent
Swedish	basics
Japanese	beginner
Software Skills	superior: MS Windows, MS Office good: Fitmaster, GraphPad Prism, Igor Pro, Neuroexplorer average: Linux OS, R, RExcel, LaTeX
Animal Care	„Versuchstierkundlicher Blockkurs entsprechend der Lehrinhalte der GV-SOLAS Kategorie B“ (FELASA B)

